TEKNISK RAPPORT · TECHNICAL REPORT 283 · 1993

ISSN 0908-3871

Estimation of transfer coefficients in models for coupled heat and moisture transfer in porous media.

Morten Hjorslev Hansen

LABORATORIET FOR BYGNINGSMATERIALER
Danmarks Tekniske Højskole

BUILDING MATERIALS LABORATORY
Technical University of Denmark

Estimation of transfer coefficients in models for coupled heat and moisture transfer in porous media.

Estimation of transfer coefficients
in models for
coupled heat and moisture transfer
in porous media

Building Materials Laboratory
Technical University of Denmark
Teknisk Rapport · Technical Report 283·1993
Lyngby December 1993
ISSN 0908-3871

Keywords
Heat and moisture transfer, sorption isotherms, diffusivity, estimation of transfer coefficients, inverse methods, sorptivity, capillary suction

Preface

This report serves as partial fulfilment of the requirements for the Ph.D. degree at the Technical University of Denmark. The study was carried out a the Building Materials Laboratory at the Technical University of Denmark.

Dr. A. Nielsen and Dr. K. K. Hansen, both at the Buildings Materials Laboratory, served as advisers. I gratefully acknowledge the support given to me by my advisers and the rest of the staff of the Building Materials Laboratory. A special thanks is given to Dr. C. B. Nielsen with whom I had many fruitful discussions.

During the study a one year leave was spent at the Civil Engineering Department of the Danish Engineering Academy. I wish to gratefully acknowledge the support from the staff at the Physics and Materials Section there. I especially wish to thank Professor P. Freiesleben Hansen, who made me feel much more comfortable in the world of thermodynamics and who encouraged me to work with the thermodynamics of adsorption.

I sincerely wish to acknowledge the constant interest in my work shown to me by Dr. C. Rode, formerly at the Thermal Insulation Laboratory, the Technical University of Denmark, presently at the Danish Building Research Institute.

The study was part of the project Moisture in Building Materials funded by the Danish Council for Scientific and Industrial Research under the Research and Technical Development programme.

December 1993

Morten Hjorslev Hansen

Table of Contents

Summary

The thermodynamic properties and the transport properties of water are presented. Empirical expressions for the description of these properties as functions of temperature are given.

A brief description of thermodynamic properties of moist porous materials and moist air is given. A part of this description is the thermodynamics of adsorption of porous media. Based on the thermodynamics of adsorption a model for the description of the sorption isotherm as a function of moisture content and temperature is presented.

The basic equations of diffusive moisture and heat transfer in porous media are presented. Luikov's model for heat and mass transfer in porous media is elucidated on basis of the transfer equations and thermodynamic properties of porous media and moist air.

Methods for the measurements of the material properties involved in models describing moisture and heat transfer in porous media are presented. Examples taken from literature of the variation of the material properties with moisture content and temperature is given. A least squares based method for the evaluation of the water vapour conductivity as a function of relative humidity from cup measurements is proposed. Two methods for the calculation of the isothermal liquid diffusivity from sorptivity measurements are presented.

A small presentation of inverse methods for the estimation of material properties is made. An inverse method for the estimation of transfer coefficients in the Luikov model for coupled heat and mass transfer in porous media is introduced. The objective of method is to estimate the moisture diffusivity, the thermogradient coefficient, the thermal conductivity and the condensation factor as functions of moisture content from moisture and temperature fields measured during non-stationary conditions. The inverse method is based on a least squares gradient method for the estimation of the coefficients in the functions describing of the transfer coefficients. The gradient method makes use of first derivatives calculated numerically. The Luikov equations are solved numerically with a finite difference method.

The use of the method is demonstrated on simulated moisture content and temperature fields. Also, the inverse method is used for the estimation of the isothermal moisture diffusivity of cellular concrete as a function of moisture content from measurements of the moisture content as a function of space coordinate and experimental time during drying.

The use of the inverse method for the estimation of all four transfer coefficients in the Luikov model from measurements of temperature and moisture content as functions of space coordinate and experimental time during condensation was only partly successful. Keeping the condensation factor at a fixed value it was possible to estimate the three remaining transfer coefficients as functions of moisture content.

The use of the Boltzmann transformation for the estimation of liquid diffusivity of brick as a function of moisture content is demonstrated.

Based on the thermodynamic properties and the transport properties of water approximations for the calculation of the temperature dependence of the water vapour diffusivity, the liquid diffusivity, the moisture diffusivity and the condensation factor are derived.

Resumé

Transportegenskaber og termodynamiske data for vand er beskrevet kort. Der er angivet empiriske udtryk til beregning af disse størrrelser som funktion af temperaturen.

De termodynamiske egenskaber af fugtige porøse materialer og af fugtig luft er beskrevet. En del af denne beskrivelse er termodynamikken for adsorption i porøse materialer. Med udgangspunkt i termodynamikken for adsorption præsenteres en model til beskrivelse af sorptionsisotermerne for et porøst materiale som funktion af fugtindhold og temperatur.

De grundlæggende ligninger for diffusiv fugt- og varmetransport i porøse materialer er beskrevet. Med udgangspunkt i disse ligninger og vands termodynamiske og transportmæssige egenskaber udledes Luikovs ligningssæt til beskrivelse af fugt- og varmetransport i porøse materialer.

En række metoder til måling af de materialeparametre, der indgår i modeller til beskrivelse af fugt- og varmetransport i porøse materialer bliver præsenteret. Fra literaturen gives der eksempler på, hvorledes disse parametre varierer med fugtindhold og temperatur. En metode til estimering af vanddamppermeabilitet ud fra kopmålinger som funktion af den relative fugtighed er udviklet. Metoden er baseret på mindste kvadraters metode. Endvidere er der udviklet to metoder til beregning af den isoterme væskediffusivitet ud fra kapillarsugningsforsøg.

Såkaldte inverse metoder til bestemmelse af materialeegenskaber beskrives kortfattet. Der er udviklet en invers metode til estimation af transportkoefficienterne i Luikovs model. Det er hensigten med metoden at gøre det muligt at bestemme fugtdiffusiviteten, termogradientkoefficienten, varmeledningsevnen og kondenseringsfaktoren som funktioner af fugtindholdet ud fra ikke-stationære målinger af fugt- og temperaturfelter. Metoden er en gradientmetode baseret på mindste kvadraters metode til at bestemme de konstanter, der indgår i de funktioner, der beskriver transportkoefficienterne. Gradientmetoden gør brug af første afledede fundet ved numerisk differentiation. Ligningerne i Luikovs model løses numerisk med en differensmetode.

Brugen af den inverse metode er demonstreret på simulerede fugt- og temperaturfelter. Endvidere er den inverse metode anvendt til at estimere fugtdiffusiviteten af gasbeton som funktion af fugtindholdet ud fra målinger af fugtindholdet under udtørring som funktion af tid og stedkoordinat.

Der er forsøgt at estimere alle fire transportkoefficienter i Luikovs model ud fra målinger af fugt og temperatur som funktion af tid og stedkoordinat, men uden succes. Derimod var det ved at holde kondenseringsfaktoren konstant muligt at bestemme de tre resterende transportkoefficienter som funktioner af fugtindholdet.

Det er vist, hvorledes man kan anvende Boltzmanntransformation til beregning af væskediffusiviteten for tegl som funktion af fugtindholdet.

Med udgangspunkt i transportegenskaber og termodynamiske egenskaber for vand er der udviklet tilnærmede udtryk til beskivelse af, hvorledes dampdiffusiviteten, væskediffusiviteten, fugtdiffusiviteten og kondenseringsfaktoren varierer med temperaturen.

Nomenclature

a	thermal diffusivity	m^2/s
a_m	moisture diffusivity	m^2/s
A	area	m^2
c	moisture concentration in air	kg/m^3
c_p	specific heat capacity at constant pressure	J/mole K or J/kg K
D	water vapour diffusivity in air	m^2/s
F	force	N
G	specific Gibbs free energy	J/mole
h	convective heat transfer coefficient	J/s m^2 K = W/m^2 K
H	specific enthalpy	J/mole or J/kg
I	mass source/sink	kg/m^3 s
$\vec{j}$	mass flux	kg/m^2 s
K	capillary conductivity	kg/s m Pa
m	mass	kg
$\dot{m}$	mass flow	kg/s
M	molecular weight	kg/mole
p	pressure	Pa
$\vec{q}$	heat flux	J/m^2 s = W/m^2
r	radius of capillary	m
R	gas constant	J/mole K
S	specific entropy	J/mole K
S	degree of saturation	-
S	sorptivity	$m/s^{1/2}$
t	temperature	°C
T	temperature	K
u	moisture content	kg/kg
V	volume	m^3
w	moisture content	kg/m^3
w	weight factor	-
x,y,z	space coordinates	m
x	moisture content of air	kg/kg
δ	thermogradient coefficient	K^{-1}
δ_a	water vapour conductivity in air	kg/s m Pa
δ_p	water vapour conductivity in porous material	kg/s m Pa
δ_φ	water vapour conductivity in porous material	kg/s m
ε	condensation factor	-
ε	emissivity	-
ζ	obstruction factor	-
θ	contact angle	°
λ	thermal conductivity	J/s m K = W/m K
λ	Boltzmann transformed	$m/s^{1/2}$
μ	dynamic viscosity	Pa s
ν	kinematic viscosity	m^2/s
ρ	mass concentration	kg/m^3
σ	surface tension	N/m
τ	time	s
φ	relative humidity	-
ψ	moisture content	m^3/m^3

Superscripts and subscripts

0	inert solid, reference
1	water vapour
2	liquid water
3	ice
4	dry air
a	adsorbed
b	barometric
c	critical
cap	capillary
f	freezing point
g	gaseous
l	liquid
m	mass, monolayer
s	solid
s	saturation
suc	suction
vac	vacuum
θ	standard state

1 Introduction

Temperature and moisture content play a major role for most of the material properties, which are of interest to us, when we are dealing with building materials and structures.

The temperature and the moisture content of a building component or structure is given by the environmental climate, the geometry of the component or structure dealt with and the heat and moisture transfer properties of the materials involved.

Durability and performance of building materials and constructions is to a large extent dependent on both their temperature and moisture content. Among others the following examples on moisture and temperature related topics can be given:

- Corrosion of steel is absent, when the relative humidity is below 0.60.
- Corrosion of the reinforcement in concrete caused by chloride ions is only possible in the presence of water through which, the chloride ions can diffuse towards the reinforcement.
- Frost damage to porous materials depends on the degree of moisture saturation, the temperature and the cooling rate.
- Decay of wood caused by rot and fungi is normally regarded as possible only, when the moisture content exceeds 20 percent on mass basis and the temperature is above 5 °C.
- Decay of porous materials due to mechanisms originating from various sorts of salt depends on the environmental humidity.
- Creep deformation and relaxation depends on temperature and moisture content.
- Shrinkage and swelling are moisture related deformations.
- Alkali silica reactions are only possible in the presence of water.
- Plastic shrinkage of concrete is, by definition, dependent on the transfer of water to the environment.
- Thermal loss from buildings is a function of moisture content and temperature.
- Compressive and tensile strength of porous materials decreases with increasing moisture content in the form of water in the liquid phase and increases with increasing moisture content in the form of ice.
- Fire endurance and the time dependent development of fires depend among other things on the heat and moisture transfer properties of the materials involved.
- The proper use of paint, adhesives, sealants and other processes in the building industry is dependent on the moisture content of the involved materials.

The use of mathematical models for the description of heat and moisture transfer in porous materials is a very useful tool in the design of structures, the research connected to above mentioned building physical topics and related material properties. Numerous more or less complex mathematical models have been advanced over the years, mostly in the form of

partial differential equations. Before the use of digital computers became customary in research laboratories and in engineering companies the main problem with the use of these mathematical models were, that there existed only a limited number of exact analytical solutions for restricted classes of problems. Alternatively, one had to perform the very time consuming task of making numerical solutions by hand. In addition, the heat and moisture transfer coefficients necessary for the solution were often not available.

Today computers perform the numerical solutions with relative ease, but there is still a lack of heat and moisture transfer coefficients. There exists a number of different methods for the determination of these data but, unfortunately, most of these methods are either very time consuming or experimentally difficult to perform. It was with the intention of the development of a method for a faster and easier determination of the heat and moisture transfer coefficients that this work was initiated.

2 Thermodynamic and transport properties of water

This section gives an overview of basic thermodynamic properties of water which are frequently used in calculations related to heat and moisture transfer in porous materials. It also gives some useful formulas for the interpolation between tabulated values.

2.1 Enthalpy

Standard enthalpy of water in the solid, liquid and the vapour phase is found in Table 2.1. Enthalpy can be considered independent of pressure. By definition the enthalpy as a function of temperature is found as

$$H(T) = H^{\theta}_{298} + \int_{298.15\,\mathrm{K}}^{T} \mathrm{d}H = H^{\theta}_{298} + \int_{298.15\,\mathrm{K}}^{T} \left(\frac{\partial H}{\partial T}\right)_p \mathrm{d}T = H^{\theta}_{298} + \int_{298.15\,\mathrm{K}}^{T} c_p \mathrm{d}T \tag{2.1}$$

2.2 Entropy

Standard entropy of water in the solid, liquid and the vapour phase is found in Table 2.1. Entropy as a function of temperature and pressure is found from the fundamental thermodynamic equation

$$\mathrm{d}H = T\mathrm{d}S + V\mathrm{d}p \tag{2.2}$$

which gives

$$S(T,p) = S^{\theta}_{298} + \int_{298.15\,\mathrm{K}}^{T} \frac{1}{T}\mathrm{d}H - \int_{p^{\theta}}^{p} \frac{V}{T}\mathrm{d}p = S^{\theta}_{298} + \int_{298.15\,\mathrm{K}}^{T} \frac{c_p}{T}\mathrm{d}T - \int_{p^{\theta}}^{p} \frac{V}{T}\mathrm{d}p \tag{2.3}$$

Considering the entropy of the solid and the liquid phase independent of pressure simplifies Eq. (2.3) to

$$S(T,p) = S^{\theta}_{298} + \int_{298.15\,\mathrm{K}}^{T} \frac{c_p}{T}\mathrm{d}T \tag{2.4}$$

Considering the vapour phase ideal turns Eq. (2.3) into

$$S(T,p) = S^{\theta}_{298} + \int_{298.15\,\mathrm{K}}^{T} \frac{c_p}{T}\mathrm{d}T - R\ln\left(\frac{p}{p^{\theta}}\right) \tag{2.5}$$

2.3 Gibbs free energy

Standard Gibbs free energy of water in the liquid and the vapour phase is found in Table 2.1. Gibbs free energy as a function of temperature and pressure is found from the fundamental thermodynamic equation

Table 2.1. **Standard thermochemical data of water. Enthalpy and entropy data of the solid phase was calculated from vapour pressure with the Clausius-Clapeyron equation. c_p of the solid phase was extrapolated with Eq. (2.10).** (Data of liquid and vapour from Barin [1], p. 649-650).

state	T K	c_p J/mole K	H_T^θ kJ/mole	S_T^θ J/mole K	G_T^θ kJ/mole
$H_2O(s)$	273.15	38.11	-293.7	44.24	
$H_2O(l)$	298.15	75.288	-285.830	69.590	-237.141
$H_2O(g)$	298.15	33.590	-241.826	188.959	-228.620

$$dG = -S\,dT + V\,dp \tag{2.6}$$

which gives

$$G(T,p) = G_{298}^\theta - \int_{298.15\,K}^{T} S\,dT + \int_{p^\theta}^{p} V\,dp \tag{2.7}$$

2.4 Specific heat capacity

This section describes the specific heat capacity at constant pressure of water in the ice, liquid and saturated vapour phase.

The specific heat capacity of saturated water vapour as a function of temperature is seen in Fig. 2.1. In the temperature range covered in Fig. 2.1 the specific heat capacity is very well described by the empirical expression

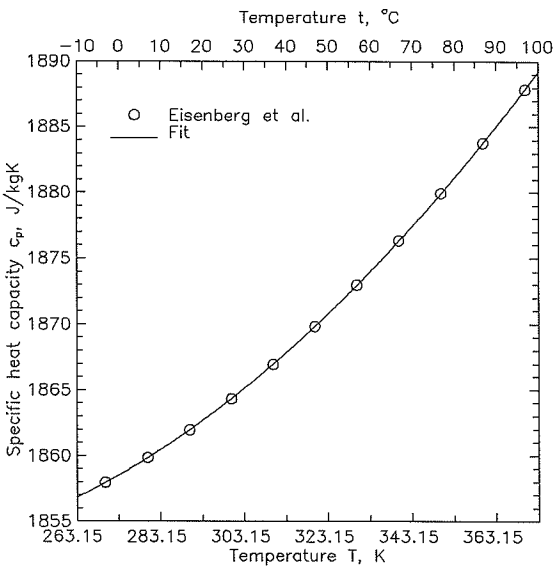

Figure 2.1. **Specific heat capacity at constant pressure of saturated water vapour as a function of temperature.** (Data from Eisenberg *et al.* [2], p. 67).

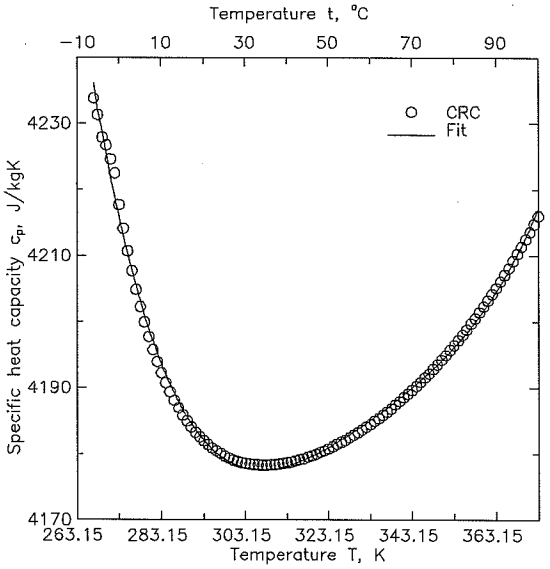

Figure 2.2. **Specific heat capacity of water as a function of temperature.** (Data from Handbook of Chemistry and Physics (CRC) [3], p. D-174).

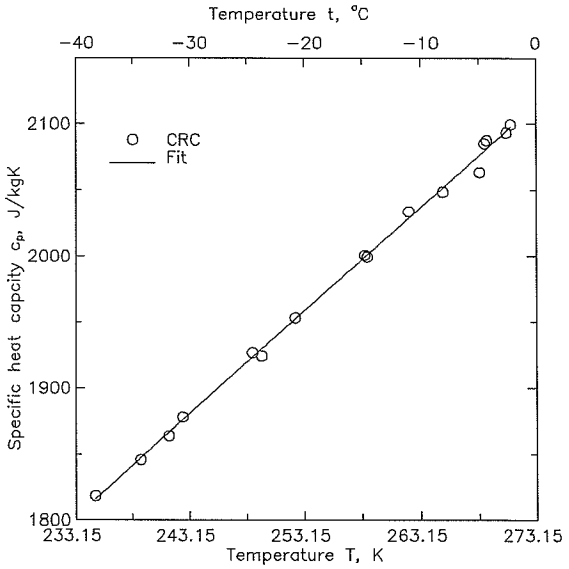

Figure 2.3. **Specific heat capacity of ice as a function of temperature.** (Data from Handbook of Chemistry and Physics (CRC) [3], p. D-175).

$$c_{p1} = c_0 + c_1 T + c_2 T^2 \tag{2.8}$$

with c_0 = 1899.84 J/kg K, c_1 = -0.48694 J/kg K^2 and c_2 = 1.22854 ·10^{-3} J/kg K^3. The increase with temperature is so small that for most building physical calculations it is appropriate to use a constant value.

The specific heat capacity of water in the liquid phase as a function of temperature is in Fig. 2.2 compared to the expression

$$c_{p2} = c_0 + c_1 T + c_2 T^2 + c_3 T^3 + c_4 T^4 \tag{2.9}$$

with c_0 = 44860.8 J/kg K, c_1 = -486.24 J/kg K^2, c_2 = 2.17947 J/kg K^3, c_3 = 4.34544 · 10^{-3} J/kg K^4 and c_4 = 3.25481 · 10^{-6} J/kg K^5. On the other hand the difference between minimum and maximum value in the regarded temperature range is only about 3%. This makes it just in the simulation of heat and mass transfer in building materials to use a constant value.

The specific heat capacity of ice, as is seen in Fig. 2.3, can be described empirically as a function of temperature by the linear relationship

$$c_{p3} = c_0 + c_1 T \tag{2.10}$$

with c_0 = -17.381 J/kg K and c_1 = 7.80756 J/kg K^2.

2.5 Saturation vapour pressure

The partial pressure of saturated water vapour over a free surface of liquid water is found by looking at the equilibrium

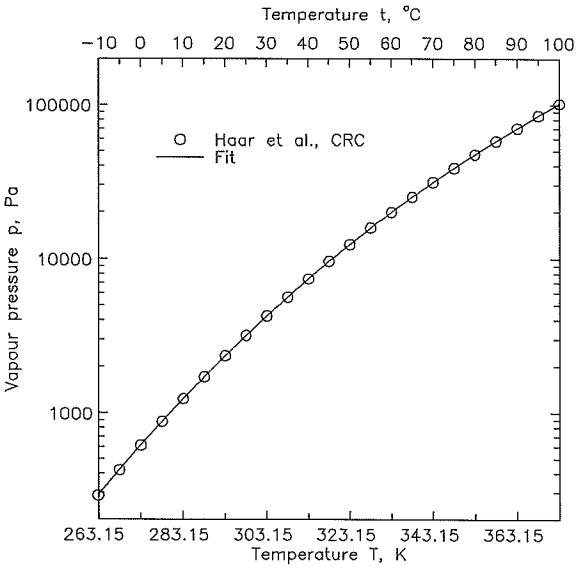

Figure 2.4. **Vapour pressure of free water as a function of temperature.** (Data from Handbook of Chemistry and Physics (CRC) [3], p. D-192 for the range 263.15K to 272.15K and from Haar *et al.* [4], pp. 5-6 for 273.16K to 373.15K).

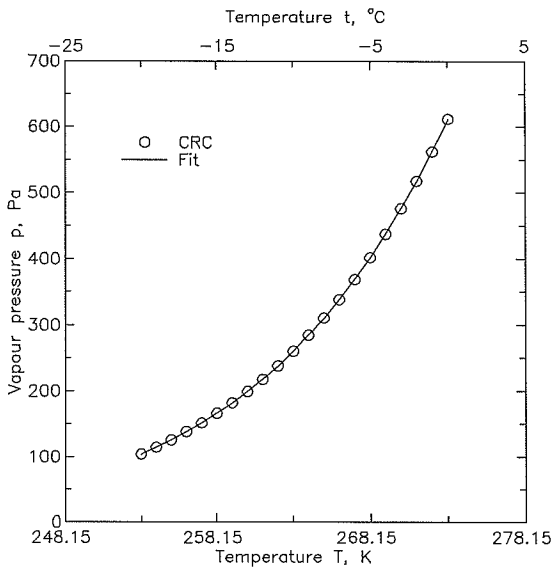

Figure 2.5. **Vapour pressure of ice as a function of temperature.** (Data from Handbook of Chemistry and Physics (CRC) [3], p. D-192).

$$H_2O(l) \rightarrow H_2O(g) \tag{2.11}$$

at constant temperature and pressure. Using the Clausius-Clapeyron equation at equilibrium gives

$$\mathrm{d}\ln p_s = \frac{\Delta_r H_T^\theta}{RT^2}\mathrm{d}T \tag{2.12}$$

Assuming that the specific heat capacity is independent of temperature

$$\mathrm{d}\ln p_s \approx \frac{\Delta_r H_{298}^\theta + \Delta_r c_p (T - 298.15\ \mathrm{K})}{RT^2}\mathrm{d}T \tag{2.13}$$

Integration of Eq. (2.13) from p_0 and $T_0 = 298.15$ K to p_s and T gives

$$\int_{p_0}^{p_s} \mathrm{d}\ln p_s = \int_{T_0}^{T} \frac{\Delta_r H_{298}^\theta + \Delta_r c_p (T - T_0)}{RT^2}\mathrm{d}T$$

$$p_s = p_0 \exp\left(\frac{\Delta_r H_{298}^\theta - \Delta_r c_p T_0}{RT_0}\left(1 - \frac{T_0}{T}\right) - \frac{\Delta_r c_p}{R}\ln\left(\frac{T_0}{T}\right)\right)$$

$$= p_0 \exp\left(c_1\left(1 - \frac{T_0}{T}\right) + c_2 \ln\left(\frac{T_0}{T}\right)\right) \tag{2.14}$$

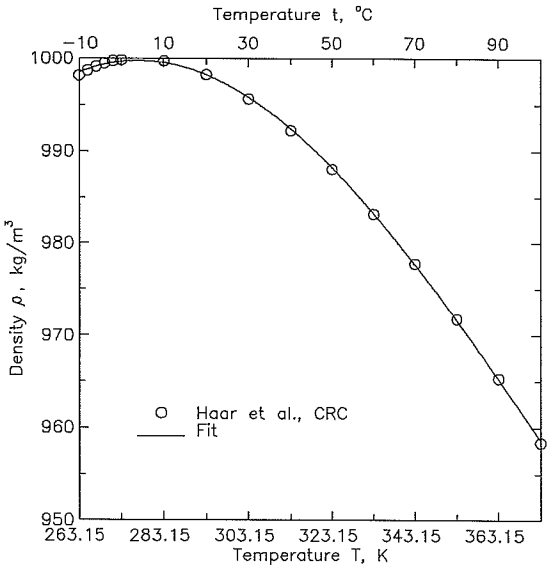

Figure 2.6 **Density of water as a function of temperature.** (Data from Handbook of Chemistry and Physics (CRC) [3] ,p. F-5 - F-6 for the range 263.15 K to 273.15 K and Haar *et al.* [4], pp. 5-6, for the range 273.16 K to 373.15 K) .

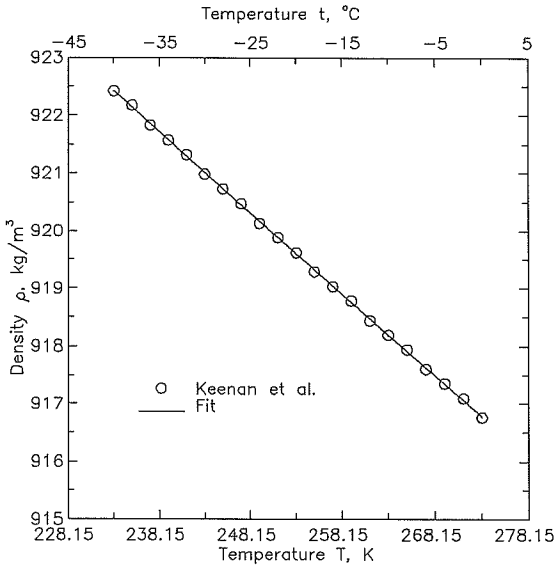

Figure 2.7. **Density of ice as a function of temperature.** (Data from Keenan *et al.* [5], p. 112).

The coefficients c_1 and c_2 were found by regression of data taken from Handbook of Chemistry and Physics [3] (subcooled liquid 263.16 K to 272.15 K) and Haar *et al.* [4] (273.16 K to 373.15 K) with p_0 = 3169.1 Pa. The result of the regression was c_1 = 22.129280 and c_2 = 4.3813201 which gives $\Delta_r H^{\theta}_{298}$ = 43993 J/mole and $\Delta_r c_p$ = -36.43 J/mole K. The model Eq. (2.14) is compared to data in Fig. 2.4.

The partial pressure of saturated water vapour over ice is found by observing the equilibrium

$$H_2O(s) \rightarrow H_2O(g) \tag{2.15}$$

at constant temperature and pressure. Using the Eq. (2.13) at equilibrium again gives an equation similar to Eq. (2.14) but now we also have to estimate p_0. The coefficients c_1 and c_2 was found by regression on data taken from Handbook of Chemistry and Physics [3] (253.16 K to 272.15 K). The result of the regression was c_1 = 19.773797, c_2 = -0.91133868 and p_0 = 4042.0 Pa which gives $\Delta_r H^{\theta}_{298}$ = 51275 J/mole and $\Delta_r c_p$ = 7.577 J/mole K. In Fig. 2.5 the model Eq. (2.14) is compared to data.

2.6 Density

Under the assumption of ideality the density of saturated water vapour as a function of temperature is given by the ideal gas equation as

$$\rho_1 = \frac{p_s M_{H_2O}}{RT} \tag{2.16}$$

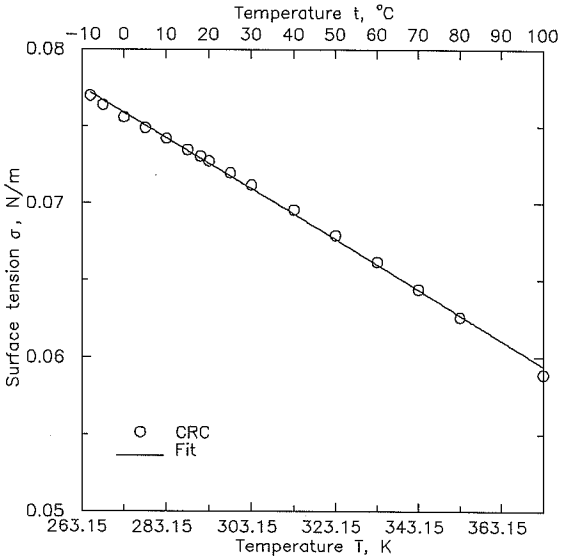

Figure 2.8. **Surface tension of water as a function of temperature.** (Data from Handbook of Chemistry and Physics (CRC) [3], p. F-33).

In Fig. 2.6 the density of water is shown as a function of temperature. It is seen that the empirical model

$$\rho_2 = c_0 + c_1 T + c_2 T^2 + c_3 T^3 \tag{2.17}$$

with c_0 = 77.4741 kg/m^3, c_1 = 8.20778 kg/m^3 K, c_2 = -0.02321 kg/m^3 K^2 and c_3 = 2.02118 · 10^{-5} kg/m^3 K^3 gives an appropriate description.

The density of ice is presented in Fig. 2.7. The density of ice is well described by the empirical relation

$$\rho_3 = c_0 + c_1 T \tag{2.18}$$

with c_0 = 955.327 kg/m^3 and c_1 = -0.141134 kg/m^3 K.

2.7 Surface tension

Surface tension σ (N/m) at the interface between water and air as a function of temperature can be calculated from the formula

$$\sigma(T) = B\left(\frac{T_c - T}{T_c}\right)^{\mu}\left(1 + b\frac{T_c - T}{T_c}\right) \tag{2.19}$$

according to Haar *et al.* [4], p. 307, with T_c = 647.15 K (critical temperature of water), B = 0.2358 N/m, b = -0.625 and μ = 1.256.

The formula covers the temperature range from the triple point to the critical temperature. It is not necessary to cover this entire range when dealing with building physics. In the temperature range 263.15 K (subcooled liquid) to 373.15 K (boiling point) one can use the linear expression

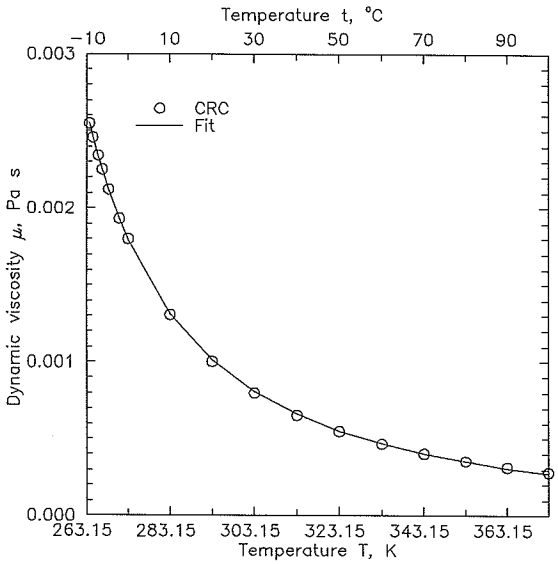

Figure 2.9. **Dynamic viscosity of water as a function of temperature.** (Data from Handbook of Chemistry and Physics (CRC) [3], pp. F-36).

$$\sigma = 0.07176 \text{ N/m} - 1.647 \cdot 10^{-4} \text{ N/m K}(T - 298.15 \text{ K}) \tag{2.20}$$

This equation is compared to data taken from Handbook of Chemistry and Physics [3], p. F-33, in Fig. 2.8. It is seen that the agreement is tolerable.

2.8 Viscosity

The dynamic viscosity μ (Pa s) of water in the liquid phase as a function of temperature can be calculated from the expression

$$\mu(T) = \frac{1}{c_0 + c_1 T + c_2 T^2} \tag{2.21}$$

in the temperature range 263.15 K (subcooled liquid) to 373.15 K (boiling point), with c_0 = 4354.82 $Pa^{-1}s^{-1}$, c_1 = -46.9678 $Pa^{-1}s^{-1}K^{-1}$ and c_2 = 0.121902 $Pa^{-1}s^{-1}K^{-2}$.

The coefficients have been estimated by non-linear regression on data taken from Handbook of Chemistry and Physics [3], pp. F-36. In Fig. 2.9 the fit is compared to the Handbook of Chemistry and Physics data.

The kinematic viscosity ν (m^2/s) is calculated from the dynamic viscosity as

$$\nu = \frac{\mu}{\rho} \tag{2.22}$$

2.9 Vapour conductivity in air

According to Vos *et al.* [6], p. 15 the conductivity of water vapour in air is

Table 2.2. **Constants for use in Eq. (2.25).** (The values of Schirmer were found in Krischer *et al.* [8], p. 175).

D_0 10^{-6} m²/s	n -	Reference
21.1	2.334	Bird *et al.* [7], p. 505
23	2.3	Krischer *et al.* [8], p. 175
22	1.81	Schirmer
21.7	1.88	de Vries [9], p. 1347
21.9	2.0	Lykow [10], p. 240

$$\delta_a = 0.185 \cdot 10^{-9} \text{ kg/s m Pa} \tag{2.23}$$

There is neither an indication of measurements nor reference to any source.

2.10 Vapour diffusivity in air

According to Bird *et al.* [7], p. 505 the temperature and pressure dependence of mass diffusivity at low pressures for the binary system H_2O with a non-polar gas can be calculated from the equation

$$D = 1.697 \cdot 10^{-6} \text{ m}^2/\text{s} \; \frac{(p_{c1}p_{c4}\,\text{Pa}^{-2})^{1/3}(T_{c1}T_{c4}\,\text{K}^{-2})^{5/12}\left(\frac{1\text{ g/mole}}{M_1}+\frac{1\text{ g/mole}}{M_4}\right)^{1/2}}{p_b\,\text{Pa}^{-1}}\left(\frac{T}{\sqrt{T_{c1}T_{c4}}}\right)^{2.334} \tag{2.24}$$

with the critical pressures p_{c1} = 22.06 MPa and p_{c4} = 3.688 MPa, critical temperatures T_{c1} = 647.1 K, T_{c4} = 132 K and molecular weights M_1 = 18.02 g/mole and M_4 = 28.97 g/mole, of water and air respectively.

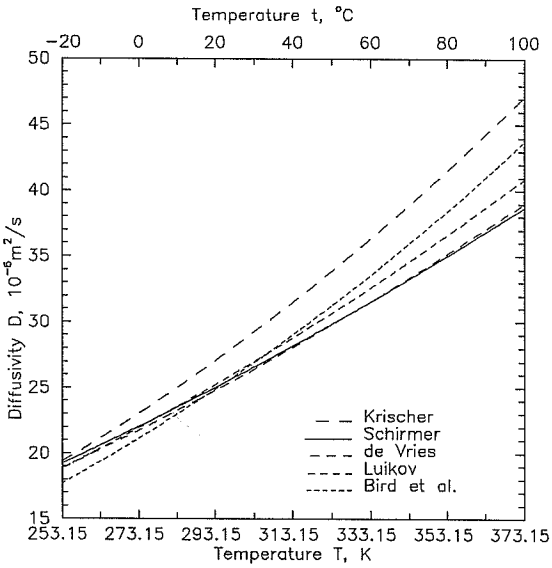

Figure 2.10. **Water vapour diffusivity as a function of temperature. The diffusivity was calculated with Eq. (2.25) and the constants from Table 2.2.**

Equation (2.24) can be rearranged to the form

$$D = D_0 \frac{p^\theta}{p_b} \left(\frac{T}{T_0} \right)^n \tag{2.25}$$

with p^θ = 101325 Pa and T_0 = 273.15 K. The values of the constants D_0 and n calculated from Eq. (2.24) are compared with constants found in various references in Table 2.2.

Equation (2.25) is plotted in Fig. 2.10 using the constants given in Table 2.2 over the temperature range 253.15 K to 373.15 K. The values of the constants D_0 and n are probably not valid in the entire range. According to Krischer *et al.* [8] the values given by Schirmer are only valid in the range from 293.15 K to 363.15 K. Nevertheless all the tabulated values of D_0 and n yields almost the same results over the whole range except from the values from Krischer *et al.* For use in building physics any of the listed values must be considered satisfying.

2.11 Thermal conductivity

Thermal conductivity of water vapour as a function of temperature can be described by the empirical relation

$$\lambda_1 = c_0 + c_1 T \tag{2.26}$$

with c_0 = -7.23323 · 10^{-3} J/s m K and c_1 = 8.53306 · 10^{-5} J/s m K^2. The data was taken from Haar *et al.* [4], Keenan *et al.* [5] and Hütte [11]. Figure 2.11 shows a comparison of data and Eq. (2.26). The number of data found was very limited.

Thermal conductivity of water in the liquid phase can be described with the empirical expression

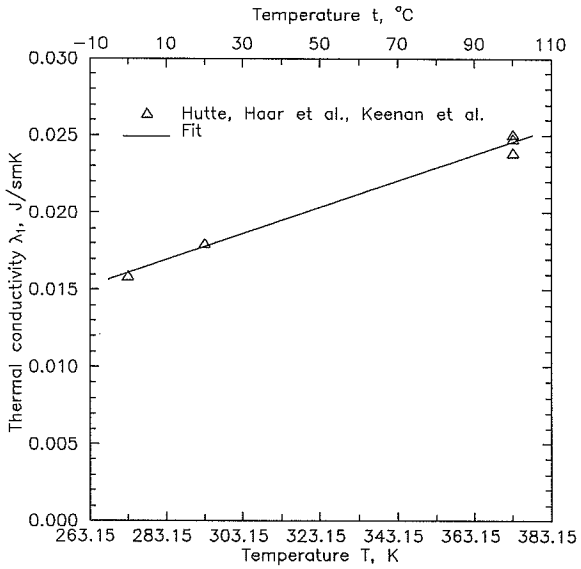

Figure 2.11. **Thermal conductivity of water vapour as a function of temperature.** (Data from Haar *et al.* [4], p. 260, Keenan *et al.* [5], p. 115 and Hütte [11], p. 1071).

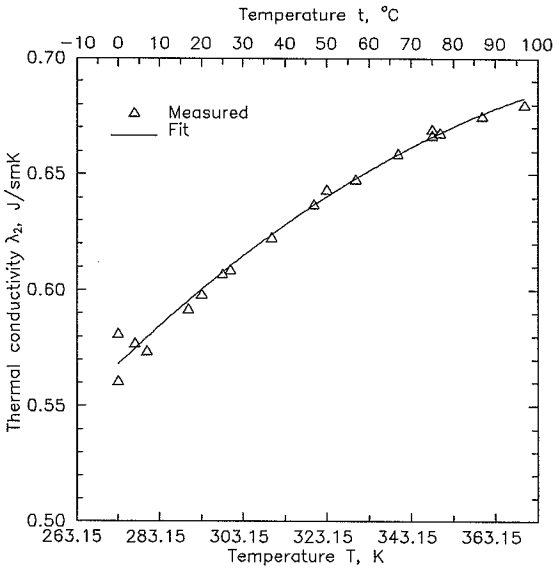

Figure 2.12. **Thermal conductivity of liquid water as a function of temperature.** (Data from Handbook of Chemistry and Physics [3], p. E-10, Haar *et al.* [4], p. 260 and Condon *et al.* [12], p. 5-67).

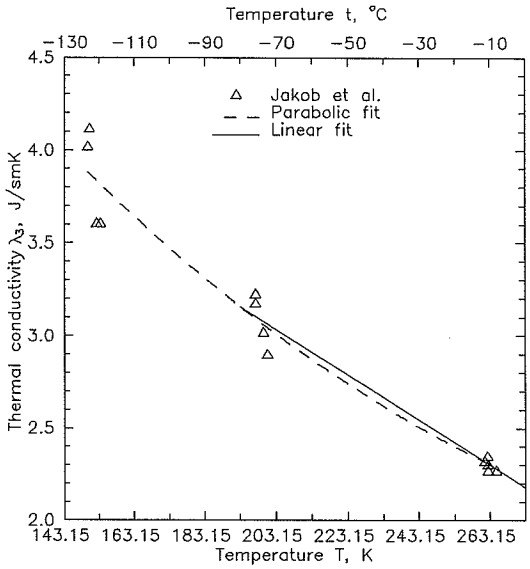

Figure 2.13. **Thermal conductivity of ice as a function of temperature.** (Data from Jakob *et al.* [13]).

$$\lambda_2 = c_0 + c_1 T + c_2 T^2 \tag{2.27}$$

with c_0 = -0.319048 J/s m K, $c_1 = 4.77095 \cdot 10^{-3}$ J/s m K^2 and $c_2 = -5.57656 \cdot 10^{-6}$ J/s m K^3. This expression is compared to data from Haar *et al.* [4] and Condon *et al.* [12] in Fig. 2.12.

The thermal conductivity of ice as a function of temperature was found in Jakob *et al.* [13]. As is seen in Fig. 2.13 one can use the empirical relation

$$\lambda_3 = c_0 + c_1 T \tag{2.28}$$

with c_0 = 5.50921 J/s m K and c_1 = -0.0121979 J/s m K^2.

3 Thermodynamic properties of porous materials and moist air

This chapter describes basic thermodynamic properties of moist porous materials and moist air in relation to coupled heat and moisture transfer.

3.1 Moisture concentration

This section presents a number of basic definitions of moisture concentration in air and in porous materials.

3.1.1 Moisture concentration in air

This section gives formulas, which are frequently used for the description of moisture concentration in humid air. In the following it is assumed that humid air is an ideal mixture of dry air and water vapour. The moisture concentration in humid air is dependent on the temperature T and the partial water vapour pressure p_1. In building physics the moisture concentration is often described by volumetric moisture content as

$$c = \frac{m_1}{V} = \frac{m_1}{n_1 R T} p_1 = \frac{M_1}{RT} p_1 \tag{3.1}$$

The use of c as symbol for volumetric moisture content should not be confused with molar concentration, which in the area of physical chemistry also is denoted by c.

The moisture content of the air, which is commonly used in the field of heating and ventilation, is found from the partial vapour pressure and the barometric pressure as

$$\mathrm{x} = \frac{m_1}{m_4} = \frac{M_1}{M_4} \frac{p_1}{p_b - p_1} \tag{3.2}$$

Relative humidity of moist air is defined as

$$\varphi = \frac{p_1}{p_s} \tag{3.3}$$

The relative humidity can also be calculated from the actual volumetric moisture concentration c and the volumetric moisture concentration at saturation c_s as

$$\varphi = \frac{c}{c_s} \tag{3.4}$$

The density of humid air is found from the partial water vapour pressure p_1 and the barometric pressure p_b as

$$\rho_{14} = \frac{m_1 + m_4}{V} = \frac{p_1 M_1}{RT} + \frac{p_4 M_4}{RT} = \frac{p_b M_4}{RT} - \frac{p_1 (M_4 - M_1)}{RT} \tag{3.5}$$

It is seen that the density of humid air is lower than that of dry air (M_1 = 18.02 g/mole and M_4 = 28.97 g/mole).

3.1.2 Moisture concentration in porous materials

The moisture concentration in porous materials is most commonly described through the concentration variables u, ψ and w, which denote kg water per kg dry material, m^3 water per m^3 material and kg water per m^3 material respectively.

The definition and principal method of measurement of the moisture content u in a test specimen is

$$u = \frac{m_{123}}{m_0} \approx \frac{m_{wet} - m_{105}}{m_{105}} \tag{3.6}$$

where m_{123} (kg) is the mass of water in specimen, m_0 (kg) is the mass of the specimen in dry condition, m_{wet} (kg) is the mass of wet specimen and m_{105} (kg) is the mass of the specimen dried in an oven at 105°C.

The distinction between mass of dry specimen m_0 and the mass of specimen dried in an oven at 105 °C m_{105} is simply due to reasons of measurement technique. m_{105} is the practical way of obtaining m_0. The reason why specimens must be dried at 105 °C (wood at 103 °C) is that physically or chemically adsorbed water is more difficult to evaporate than free water, which evaporates at 100 °C at a barometric pressure of 101325 Pa.

The relationship between u, ψ and w is given by the identity

$$\rho_0 u = \rho_2 \psi = w \tag{3.7}$$

where ρ_0 (kg/m^3) is the apparent dry density and ρ_2 (kg/m^3) is the density of water.

Which one of the variables u, ψ and w to use is merely a matter of taste. None of them offers any special advantages maybe with u being the exception because is easily measured in the laboratory with simple equipment and is independent of swelling/shrinkage due to change in moisture content.

The use of the concept degree of saturation is useful when one wishes to compare moisture related properties of specimens of identical type of material but with different porosities. Degrees of saturation is traditionally denoted by S. One has to differentiate between saturation obtained at vacuum or by capillary suction. The degree of saturation is correspondingly denoted S_{vac} and S_{cap} respectively and are defined as

$$S_{vac} = \frac{m_{wet} - m_{105}}{m_{vac} - m_{105}} \tag{3.8}$$

$$S_{cap} = \frac{m_{wet} - m_{105}}{m_{cap} - m_{105}} \tag{3.9}$$

where m_{vac} (kg) is the mass of the wet specimen saturated at vacuum and m_{cap} (kg) is the mass of the wet specimen saturated by capillary suction.

The degree of saturation is easily computed from u, ψ or w from the equalities

$$S_{cap} = \frac{u}{u_{cap}} = \frac{\psi}{\psi_{cap}} = \frac{w}{w_{cap}} \tag{3.10}$$

$$S_{vac} = \frac{u}{u_{vac}} = \frac{\psi}{\psi_{vac}} = \frac{w}{w_{vac}} \tag{3.11}$$

where u_{cap}, ψ_{cap} or w_{cap} is maximum moisture content obtained by capillary suction and u_{vac}, ψ_{vac} or w_{vac} is maximum moisture content obtained by saturation under vacuum.

3.2 Specific heat capacity

The enthalpy H (J) of a moist porous material is the simple sum of it's constituents dry material, water vapour, liquid water, ice and air

$$H = \sum_{i=0}^{4} H_i \tag{3.12}$$

The heat capacity C_p (J/K) at constant pressure is then

$$C_p = \left(\frac{\partial H}{\partial T}\right)_p = \sum_{i=0}^{4}\left(\frac{\partial H_i}{\partial T}\right)_p = \sum_{i=0}^{4} m_i c_{pi} = m_0 \sum_{i=0}^{4} u_i c_{pi} \tag{3.13}$$

with u_i (kg/kg) and c_{pi} (J/kg K) as the mass content and the specific heat capacity of constituent i respectively. The terms $u_1 c_{p1}$ and $u_4 c_{p4}$ are small compared with the other terms in Eq. (3.13).

Under the additional assumption that all liquid turns into ice below a certain freezing point temperature T_f the specific heat capacity of the moist porous material is given by

$$c_p = \begin{cases} c_{p0} + u c_{p2} & T > T_f \\ c_{p0} + u c_{p3} & T < T_f \end{cases} \tag{3.14}$$

Normally T_f is different from the triple point due to freezing point depression in small capillaries. T_f must be seen as a function of the pore size distribution. For practical purposes T_f is selected as a constant which expresses an effective freezing point depression. Figure 3.1 shows the jump in specific heat capacity when ice changes into water.

A second approach is the inclusion of the phase change enthalpy from the transition of water into ice and vice versa into the specific heat capacity. This method is described by Bonacina *et al.* [14]. The specific heat capacity of the moist porous material is given by

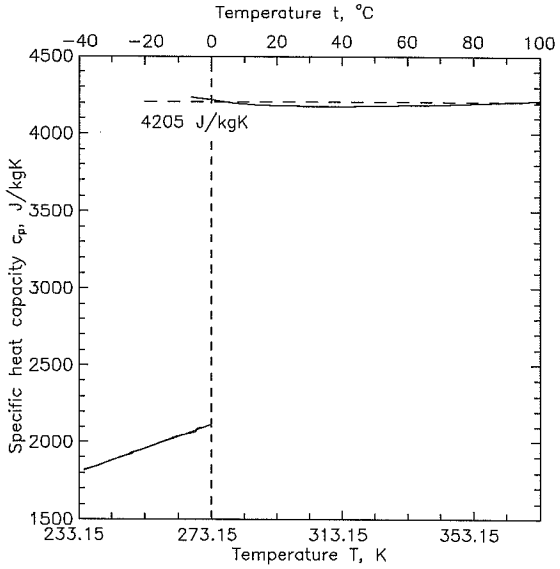

Figure 3.1. **Specific heat capacity of water and ice.** (Data from Fig. 2.2 and Fig. 2.3).

$$c_p = \begin{cases} c_{p0} + u c_{p3} & T < T_f - \Delta T \\ c_{p0} + u c_p^* & T_f - \Delta T \le T \le T_f + \Delta T \\ c_{p0} + u c_{p2} & T > T_f + \Delta T \end{cases} \tag{3.15}$$

where the following condition must be satisfied

$$\int_{T_f-\Delta T}^{T_f+\Delta T} (c_{p0} + u c_p^*) \mathrm{d}T = \Delta_l H^{\theta}_{T,s\to l} + \int_{T_f-\Delta T}^{T_f} (c_{p0} + u c_{p3}) \mathrm{d}T + \int_{T_f}^{T_f+\Delta T} (c_{p0} + u c_{p2}) \mathrm{d}T \tag{3.16}$$

3.3 Vapour pressure

This section describes the vapour pressure of a porous material originating from liquid adsorbed on the inner and outer surface and from capillary condensate. Also given is a short treatise on thermodynamics of adsorption. Some useful formulas for the mathematical description is reviewed.

3.3.1 Sorption isotherm

When a porous solid is in thermodynamic equilibrium with water vapour, a certain amount of water vapour is physically or chemically bound on the outer and especially on the inner surface. The amount of water bound by the material is dependent of the type of porous solid, the partial water vapour pressure and the temperature. At low vapour pressures the water vapour is adsorbed or chemically bound on the surfaces. As the vapour pressure increases and the adsorbate forms curved menisci and capillary condensation caused by surface tension takes place.

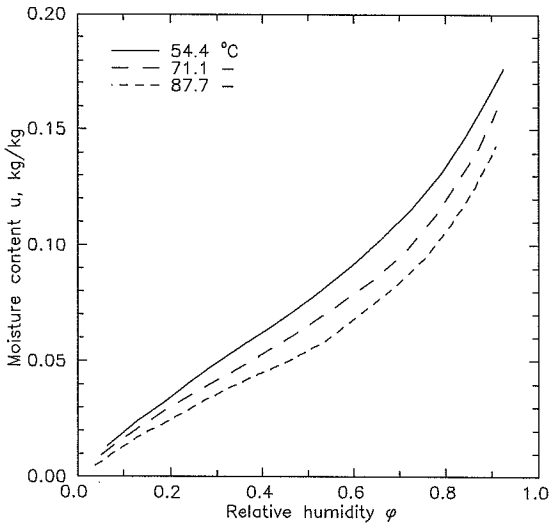

Figure 3.2. **Sorption isotherms for Sitka spruce, oscillating adsorption and desorption.** (From Stamm *et al.* [15]).

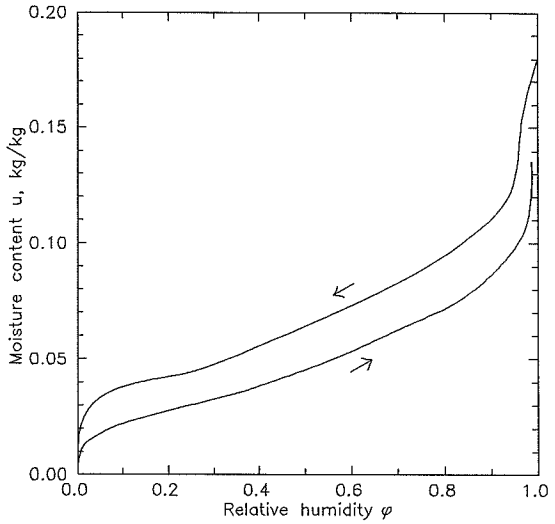

Figure 3.3. **Sorption isotherm for steam cured hardened cement paste.** T = 293.15 K, *w/c* = 0.35. (Calculated from isostere equations from Radjy *et al.* [17]).

The sorption isotherm gives the amount of adsorbate at a given constant temperature as a function of the partial water vapour pressure or more frequently as a function of the relative humidity. Figure 3.2 shows sorption isotherms for Sitka spruce taken from Stamm *et al.* [15].

In the early 1970s Radjy and Sellevold conducted a series of measurements of sorption of hardened ordinary Portland cement pastes reported in Radjy [16] and Radjy *et al.* [17]. They measured the partial water vapour pressure at isosteric conditions (constant moisture content $u = u_0$) as a function of temperature in the temperature range -10 °C to 100 °C. The isosteric vapour pressures were measured in a heating and a cooling cycle corresponding to desorption and adsorption respectively.

The isosteric vapour pressures were fitted to the model

$$\ln p_1 = A + B\frac{1000}{T} + C\ln T \tag{3.17}$$

from which the thermodynamic parameters of adsorption are easily computed. Figure 3.3 shows a sorption isotherm for steam cured hardened cement paste calculated from the above expression with values of A, B, and C taken from Radjy *et al.* [17].

The sorption isotherm in Fig. 3.3 shows markedly hysteresis. Hysteresis is due to the existence of "ink bottle" pores or different contact angle during adsorption and desorption. Hysteresis is not accounted for in this work. Pedersen [18] and Sandberg [19] has examined the effect of taken the hysteresis into account in the simulation of heat and moisture transfer in building constructions. They both concluded that the effect was limited. Pedersen found that taking the average of adsorption and desorption isotherm is giving a good description under periodic stationary conditions.

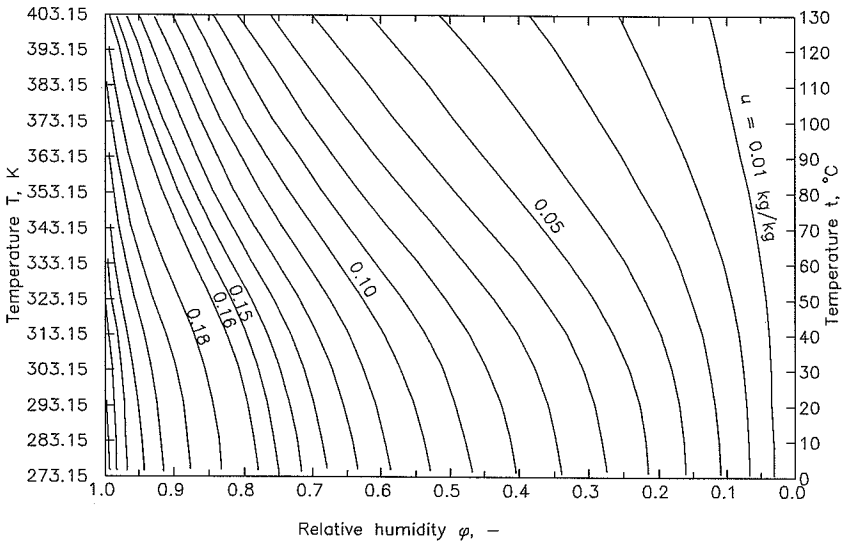

Figure 3.4. **Sorption isosteres for Sitka spruce.** (From Kollmann [20]).

Another way of presenting the thermodynamic equilibrium between a porous solid and water vapour is in the form of the isostere diagram. Figure 3.4 shows sorption isosteres for Sitka spruce taken from Kollmann [20] (note that values of relative humidity above 100 °C were extrapolated).

3.3.2 Gibbs free energy of adsorption

The knowledge of Gibbs free energy being a state function allows us to express the differential Gibbs free energy of adsorption $\Delta_r G_{T,\,a\to l}$ as

$$\Delta_r G_{T,a\to l} = \Delta_r G_{T,a\to g} - \Delta_r G_{T,l\to g} \tag{3.18}$$

This is of course also valid in the standard state so that

$$\Delta_r G^{\theta}_{T,a\to l} = \Delta_r G^{\theta}_{T,a\to g} - \Delta_r G^{\theta}_{T,l\to g} \tag{3.19}$$

Looking at the equilibrium

$$H_2O(a) \rightarrow H_2O(l) \tag{3.20}$$

and the use of Eq. (3.18) gives

$$\Delta_r G^{\theta}_{T,a\to l} = -RT\ln\frac{p_1}{p^{\theta}} - \left(-RT\ln\frac{p_s}{p^{\theta}}\right) = -RT\ln\frac{p_1}{p_s} = -RT\ln\varphi \tag{3.21}$$

From this equation it is seen that the differential Gibbs free energy of adsorption is easily computed as function of moisture content and temperature from sorption isotherms. Figure 3.5 shows the standard differential Gibbs free energy of adsorption for Sitka spruce calculated by Stamm *et al.* [15].

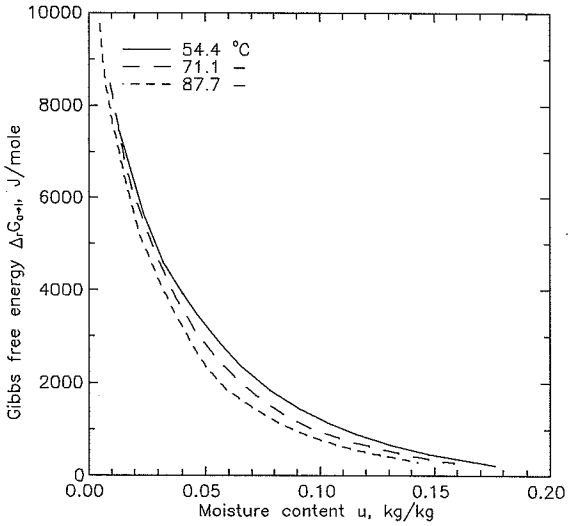

Figure 3.5. **Standard differential Gibbs free energy of adsorption for Sitka spruce.** (From Stamm *et al.* [15]).

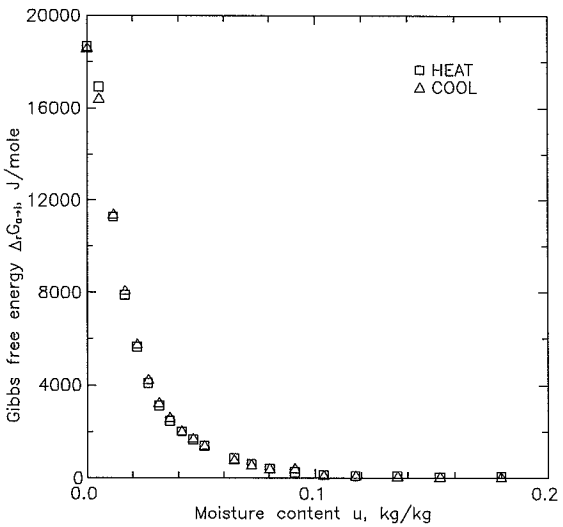

Figure 3.6. **Standard differential Gibbs free energy of adsorption for steam cured hardened cement paste.** T = 298.15 K, *w/c* = 0.35. (From Radjy *et al.* [17]).

Standard Gibbs free energy of the adsorbate is calculated from the differential Gibbs free energy and the standard free energy of the liquid as

$$G^{\theta}_{T,a} = G^{\theta}_{T,l} - \Delta_r G^{\theta}_{T,a\to l} \tag{3.22}$$

It is seen from Fig. 3.5 and Eq. (3.22) that the Gibbs free energy of the adsorbate is lower than that of free water. Also seen is that the Gibbs free energy of the adsorbate equals that of free water when the moisture content increases. As predicted by Eq. (3.21) this happens, when the relative humidity becomes close to 1, that is, when capillary condensation is dominating.

Figure 3.6 shows standard differential Gibbs free energy of adsorption for steam cured hardened cement paste with water/cement ratio 0.35 calculated from the sorption isotherms elaborated from the sorption isosteres measured by Radjy *et al.* [17].

3.3.3 Enthalpy of adsorption

The standard enthalpy of adsorption $\Delta_r H^{\theta}_{T,a\to g}$ is found by looking at the equilibrium

$$H_2O(a) \to H_2O(g) \tag{3.23}$$

Using the Clausius-Clapeyron equation gives

$$\frac{d\ln p_1}{dT} = \frac{\Delta_r H^{\theta}_{T,a\to g}}{RT^2} \tag{3.24}$$

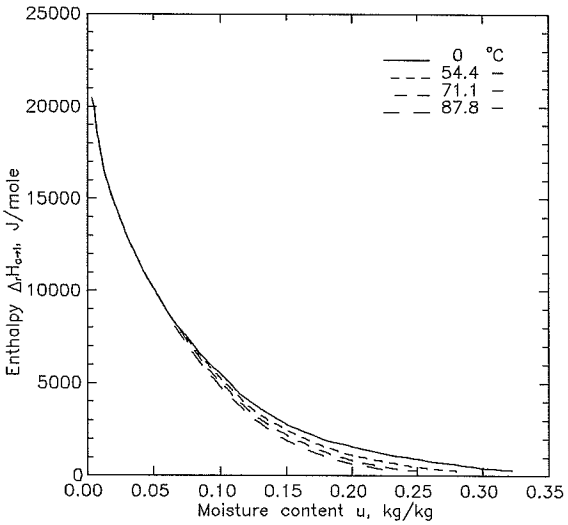

Figure 3.7. **Standard differential enthalpy of adsorption for Sitka spruce.** (From Stamm *et al.* [15]).

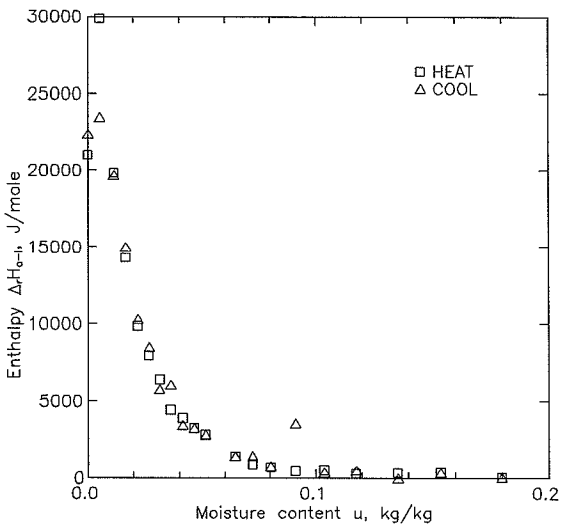

Figure 3.8. **Standard differential enthalpy of adsorption for steam cured hardened cement paste.** T = 298.15 K, *w/c* = 0.35. (From Radjy *et al.* [17]).

Dividing the enthalpy of adsorption into the differential enthalpy of adsorption $\Delta_r H^{\theta}_{T,a\to l}$ and the enthalpy of vaporization $\Delta_r H^{\theta}_{T,l\to g}$ turns Eq. (3.24) into

$$\frac{\mathrm{d}\ln p_1}{\mathrm{d}T} = \frac{\Delta_r H^{\theta}_{T,a\to l}}{RT^2} + \frac{\Delta_r H^{\theta}_{T,l\to g}}{RT^2} \tag{3.25}.$$

The second term of the right hand side of Eq. (3.25) is found from Eq. (2.12), which gives

$$\frac{\mathrm{d}\ln p_1}{\mathrm{d}T} = \frac{\Delta_r H^{\theta}_{T,a\to l}}{RT^2} + \frac{d\ln p_s}{\mathrm{d}T} \quad \Leftrightarrow \quad \frac{\mathrm{d}\ln p_1/p_s}{\mathrm{d}T} = \frac{\Delta_r H^{\theta}_{T,a\to l}}{RT^2} \quad \Leftrightarrow \quad \frac{\mathrm{d}\ln \varphi}{\mathrm{d}T} = \frac{\Delta_r H^{\theta}_{T,a\to l}}{RT^2} \tag{3.26}$$

with $\Delta_r H^{\theta}_{T,a\to l}$ being the standard differential enthalpy of adsorption which is found by looking at the equilibrium Eq. (3.20).

Standard enthalpy of the adsorbate is calculated from the standard differential enthalpy of adsorption and the standard enthalpy of the liquid as

$$H^{\theta}_{T,a} = H^{\theta}_{T,l} - \Delta_r H^{\theta}_{T,a\to l} \tag{3.27}$$

Figure 3.7 shows the standard differential enthalpy of adsorption for Sitka spruce calculated by Stamm *et al.* [15]. Standard differential enthalpy of adsorption for steam cured hardened cement paste calculated from the sorption isosteres measured by Radjy *et al.* [17] is shown in Fig. 3.8. In both cases the differential enthalpy of the adsorbate asymptotically equals that of free water, as the moisture content increases. The enthalpy of water adsorbed on steam cured hardened cement is seen to be equal to that of Sitka spruce, which indicates that the strength of the bond between the adsorbate and the adsorbent in both cases is almost equal.

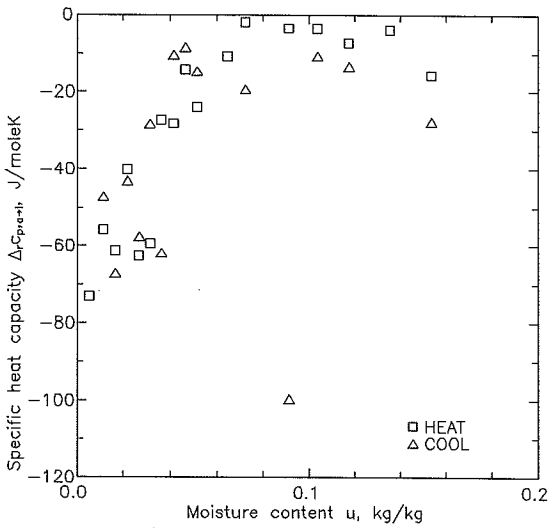

Figure 3.9. **Differential specific heat capacity of adsorption for steam cured hardened cement paste.** T = 298.15 K, *w/c* = 0.35. (From Radjy *et al.* [17]).

The standard enthalpy of adsorbed water is lower than that of free water, which means that the adsorbate is physically bound to the adsorbent and as a consequence is more difficult to evaporate than the free water. This is confirmed by matching Eq. (3.27) to Fig. 3.7 and Fig. 3.8.

3.3.4 Specific heat capacity of adsorption

Measurements of the specific heat capacity of adsorption are very seldom seen. Direct experimental measurement with a calorimeter is very difficult to realise, especially when the amount of adsorbate is low, and its heat capacity is only a fraction of that of the system adsorbent-adsorbate. Another method is numerical differentiation of the isosteric enthalpy of the adsorbate with respect to temperature. When the isosteric enthalpy is computed with the Clausius-Clapeyron equation the calculation of the differential specific heat of adsorption involves evaluation of second derivative of ln p_1 with respect to temperature. Numerical differentiation is error magnifying and the use of this procedure might lead to erroneous results.

Differential specific heat capacity of adsorption for steam cured hardened cement paste taken from Radjy *et al.* [17] is shown in Fig. 3.9. The specific heat was calculated from Eq. (3.17) and Eq. (3.25) as

$$\Delta_r c_{p,T,a\to l} = RC - \Delta_r c_{p,T,l\to g} \tag{3.28}$$

Qualitatively spoken the differential specific heat capacity becomes close to zero as the moisture content increases. At the zero moisture content the order of magnitude is -70 J/mole K.

Standard specific heat capacity of the adsorbate is calculated from the differential specific heat capacity and the specific heat of the liquid as

$$c_{p,T,a} = c_{p,T,l} - \Delta_r c_{p,T,a\to l} \tag{3.29}$$

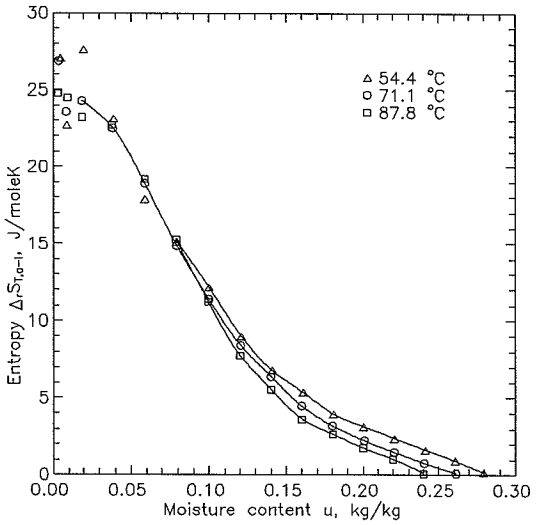

Figure 3.10. **Standard differential entropy of adsorption for Sitka spruce.** (From Stamm *et al.* [15]).

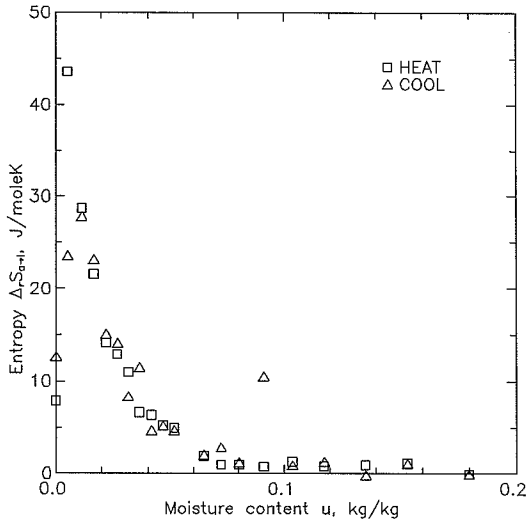

Figure 3.11. **Standard differential entropy of adsorption for steam cured hardened cement paste.** T = 298.15 K, *w/c* = 0.35. (From Radjy *et al.* [17]).

This gives the specific heat capacity of the adsorbate as $c_{p,T,a}$ = 145 J/mole K which is almost twice that of liquid water. An intuitively more correct value must be near that of ice that is $c_{p,T,a}$ = 38 J/mole K. It seems that the parameter C in Eq. (3.17) is more a fit parameter than an expression of the specific heat capacity of adsorption.

3.3.5 Entropy of adsorption

The differential entropy of adsorption is calculated from the definition of Gibbs free energy

$$G = H - TS \tag{3.30}$$

as

$$\Delta_r S_{T,a\to l} = \frac{\Delta_r H_{T,a\to l} - \Delta_r G_{T,a\to l}}{T} \tag{3.31}$$

This expression is also valid in the standard state so that

$$\Delta_r S^{\theta}_{T,a\to l} = \frac{\Delta_r H^{\theta}_{T,a\to l} - \Delta_r G^{\theta}_{T,a\to l}}{T} \tag{3.32}$$

Standard entropy of the adsorbate is calculated from the differential standard entropy and the standard entropy of the liquid as

$$S^{\theta}_{T,a} = S^{\theta}_{T,l} - \Delta_r S^{\theta}_{T,a\to l} \tag{3.33}$$

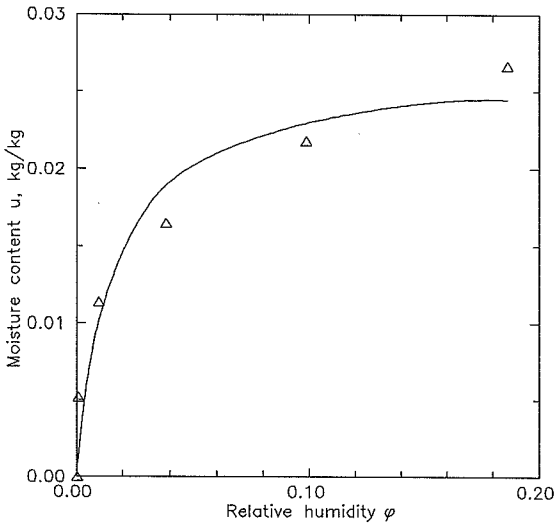

Figure 3.12. **Adsorption isotherm for steam cured hardened cement paste. Solid line is the Langmuir equation with** b = 0.0279 Pa^{-1} **and** u_m = 0.0265 kg/kg. T = 293.15 K, w/c = 0.35. (Data for adsorption isotherm (triangles) from Radjy *et al.* [17], see also Fig. 3.3).

Figure 3.10 shows the standard differential entropy of adsorption for Sitka spruce calculated by Stamm *et al.* [15]. Figure 3.11 shows the standard differential entropy for steam cured hardened cement paste calculated from vapour pressure isosteres measured by Radjy *et al.* [17]. From Eq. (3.33) and figure 3.10 and Fig. 3.11 it is seen that the standard entropy of adsorbed water is lower than standard entropy of free water. This means that the adsorbed water is in a more ordered state than the free water.

3.3.6 Models describing the sorption isotherm

Monomolecular adsorption of water vapour in a porous solid is well described by the Langmuir equation

$$u = \frac{u_m b p_1}{1 + b p_1} \tag{3.34}$$

where u (kg/kg) is the amount of adsorbate, u_m (kg/kg) is the mass of adsorbate necessary to cover the surface with a layer of one molecule thick adsorbate, b (Pa^{-1}) is a constant associated with the free energy of adsorption and p_1 (Pa) is the partial water vapour pressure. In Fig. 3.12 the Langmuir equation has been used for the description of adsorption data for steam cured hardened cement paste. It is seen that coincidence between the measured amount of

adsorbate and the amount predicted by the Langmuir equation is not totally satisfying. This means that b is not a constant, which tells us that the free energy of adsorption varies with the amount of adsorbate as it is already seen in Fig. 3.6.

See for instance Flood [21] for a derivation and more fulfilling description of the Langmuir equation.

BET Brunauer *et al.* [22] expanded Langmuir's model to the description of adsorption in more than one layer. The most well-known of the four adsorption equations in the original BET paper [22] is the two-parameter equation

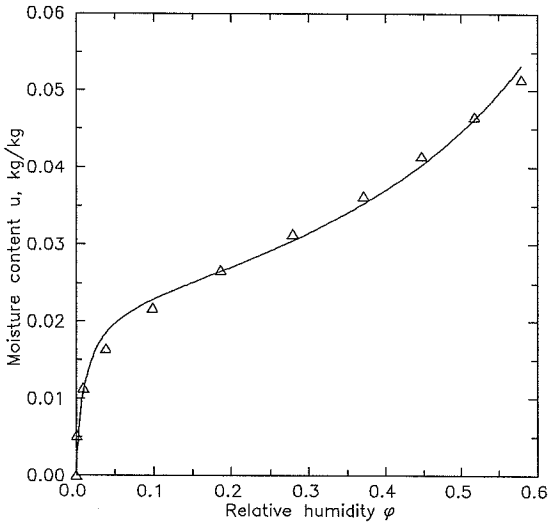

Figure 3.13. **Adsorption isotherm for steam cured hardened cement paste. Solid line is a fit obtained with the two-parameter BET equation with** $c = 94.2$ **and** $u_m = 0.0226$ kg/kg. $T = 293.15$ K, $w/c = 0.35$. (Data for adsorption isotherm (triangles) from Radjy *et al.* [17], see also Fig. 3.3).

$$u = \frac{c u_m \varphi}{(1-\varphi)(1+(c-1)\varphi)} \tag{3.35}$$

where c is a constant associated with the change in standard Gibbs free energy, when the vapour is adsorbed, and u_m (kg adsorbate/ kg solid) is the mass adsorbed in the first monolayer.

In their original paper [22] Brunauer *et al.* explained c as being a function of the enthalpy of adsorption of the first layer $\Delta_r H^\theta_{T,1}$ and the enthalpy of condensation $\Delta_r H^\theta_{T,g\to l}$

$$c = \exp\left(\frac{\Delta_r H^\theta_{T,1} - \Delta_r H^\theta_{T,g\to l}}{RT}\right) \tag{3.36}$$

In [21] Brunauer *et al.* gives the BET constant c a new meaning. Brunauer *et al.* quotes Goates *et al.* [Goates, J. R., and Hatch, C. V., *Soil Sci.*, Vol. 75, p. 275, 1953]. Goates and Hatch found from thermodynamic reasoning that the constant c more correctly is given by

$$c = \exp\left(-\frac{\Delta_r G^\theta_1 - \Delta_r G^\theta_{g\to l}}{RT}\right) \tag{3.37}$$

where $\Delta_r G^\theta_{T,1}$ is standard Gibbs free energy of adsorption on the bare surface and $\Delta_r G^\theta_{T,g\to l}$ is standard Gibbs free energy of condensation. In Fig. 3.13 the two-parameter BET equation has been fitted to adsorption data for steam cured hardened cement paste measured by Radjy *et al.* [17].

Nielsen [23] has modified the two parameter BET equation (3.35), so that it also can describe capillary condensation.

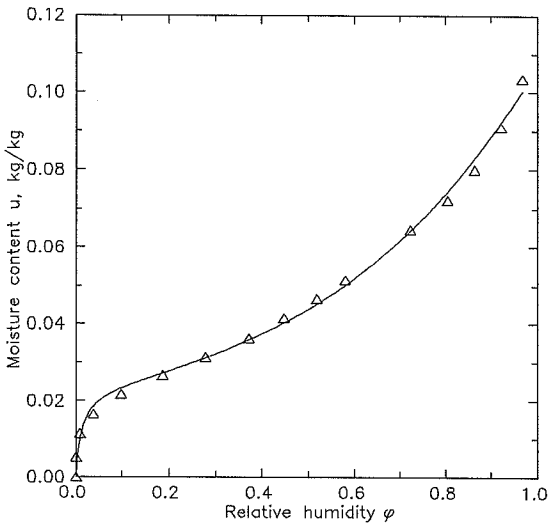

Figure 3.14. **Adsorption isotherm for steam cured hardened cement paste. Solid line is a fit with the modified BET equation (3.38) with** $c = 80.30$, $u_m = 0.0234$ kg/kg, $P = 1.027$ **and** $M = 2.552$. $T = 293.15$ K, $w/c = 0.35$. (Data for adsorption isotherm (triangles) from Radjy *et al.* [17], see also Fig. 3.3).

$$u = \frac{c u_m \varphi h(\varphi)}{1 + (c-1)\varphi} \tag{3.38}$$

with

$$h(\varphi) = 1 + \varphi + \sum_{k=1}^{M} \varphi^{P(k+1)} = 1 + \varphi + \varphi^{2P} \frac{1 - \varphi^{PM}}{1 - \varphi^{P}} \tag{3.39}$$

where c is a constant associated with the change in standard Gibbs free energy, when the vapour is adsorbed, and u_m (kg adsorbate/ kg solid) is the mass adsorbed in the first monolayer and P, M are dimensionless fit parameters greater than or equal to 1. In Fig. 3.14 Eq. (3.38) is fitted to the adsorption data for steam cured hardened cement paste from Radjy *et al.* [17].

3.3.7 A model for the sorption isotherm as a function of u and T

The modified Clausius-Clapeyron Equation (3.26) is useful for the description of the relative humidity as a function of temperature and moisture content. Under isosteric conditions ($u = u_0$) we may write the modified Clausius-Clapeyron Equation as

$$\frac{\mathrm{d} \ln \varphi(u_0)}{\mathrm{d}T} = \frac{\Delta_l H^{\theta}_{T,a \to l}(u_0)}{RT^2} \tag{3.40}$$

If it is assumed as a first approximation that the standard differential specific heat capacity is independent of temperature we may write Eq. (3.40) as

Table 3.1. **Constants used in the model Eq. (3.44), Eq. (3.47) and Eq. (3.48) for the relative humidity as a function of moisture content and temperature.** (Sorption data for steam cured hardened cement paste with $w/c = 0.35$ from Radjy *et al.* [17]. Sorption data for Sitka spruce from Kollmann [20]).

Material	$\Delta_r H^{\theta}_{298,a\to l}(0)$ J/mole	α_H -	$\Delta_r c_{p,a\to l}(0)$ J/mole K	α_c -	u_{vac} kg/kg
Steam cured hardened cement paste	24403	6.2345	-207.9	5.5477	0.1797
Sitka Spruce	4679	1.3515	344.1	4.1051	0.30

$$\frac{\mathrm{d}\ln\varphi(u_0)}{\mathrm{d}T} = \frac{\Delta_r H^{\theta}_{298,a\to l}(u_0) + \int_{298.15\,\mathrm{K}}^{T} \Delta_r c_{p,T,a\to l}(u_0)\mathrm{d}T}{RT^2}$$

$$\Leftrightarrow$$

$$\frac{\mathrm{d}\ln\varphi(u_0)}{\mathrm{d}T} = \frac{\Delta_r H^{\theta}_{298,a\to l}(u_0) + \Delta_r c_{p,a\to l}(u_0)\,(T - 298.15\,\mathrm{K})}{RT^2} \tag{3.41}$$

Knowing the relative humidity φ_0 at temperature T_0 and moisture content u_0 we may integrate Eq. (3.41) (still under the restriction of isosteric conditions) as

$$\int_{\varphi_0}^{\varphi} \mathrm{d}\ln\varphi(u_0) = \int_{T_0}^{T} \frac{\Delta_r H^{\theta}_{298,a\to l}(u_0) + \Delta_r c_{p,a\to l}(u_0)\,(T - 298.15\,\mathrm{K})}{RT^2}\mathrm{d}T$$

$$\Leftrightarrow$$

$$\ln\frac{\varphi(u_0)}{\varphi_0(u_0)} = \left[-\frac{\Delta_r H^{\theta}_{298,a\to l}(u_0) - \Delta_r c_{p,a\to l}(u_0)298.15\,\mathrm{K}}{R}\frac{1}{T} + \frac{\Delta_r c_{p,a\to l}(u_0)}{R}\ln T\right]_{T_0}^{T}$$

$$\Leftrightarrow$$

$$\varphi(u_0) = \varphi_0(u_0)\exp\left(\frac{\Delta_r H^{\theta}_{298,a\to l}(u_0)}{R}\left(\frac{1}{T_0} - \frac{1}{T}\right) + \frac{\Delta_r c_{p,a\to l}(u_0)}{R}\left(\frac{298.15\,\mathrm{K}}{T} - \frac{298.15\,\mathrm{K}}{T_0} + \ln\frac{T}{T_0}\right)\right) \tag{3.42}$$

If we conveniently select the reference temperature as $T_0 = 298.15$ K we finally get

$$\varphi(u_0, T) = \varphi_0(u_0, T_0)\exp\left(\frac{\Delta_r H^{\theta}_{298,a\to l}(u_0)}{R}\left(\frac{1}{T_0} - \frac{1}{T}\right) + \frac{\Delta_r c_{p,a\to l}(u_0)}{R}\left(\frac{T_0}{T} - 1 + \ln\frac{T}{T_0}\right)\right) \tag{3.43}$$

It is easily seen that Eq. (3.43) is similar to Eq. (3.17) which explains why Eq. (3.17) showed to be such a good model for fitting the isosteric vapour pressures measured by Radjy *et al.* [17].

It is now seen that the relative humidity as a function of temperature and moisture content can be found as

$$\varphi(u,T) = \varphi_0(u,T_0)\exp\left(\frac{\Delta_r H^{\theta}_{298,a\to l}(u)}{R}\left(\frac{1}{T_0}-\frac{1}{T}\right)+\frac{\Delta_r c_{p,a\to l}(u)}{R}\left(\frac{T_0}{T}-1+\ln\frac{T}{T_0}\right)\right) \tag{3.44}$$

where $T_0 = 298.15$ K and $\varphi_0(u,T_0)$ is the sorption isotherm at $T = 298.15$ K.

Inspection of Eq. (3.44) reveals that in order to avoid calculated values of relative humidity greater than 1 at vacuum saturation where $\varphi(u,T) = \varphi_0(u,T) \equiv 1$ the following restrictions must be fulfilled

$$\Delta_r H^{\theta}_{298,a\to l}(u_{vac}) \equiv 0 \tag{3.45}$$

$$\Delta_r c_{p,a\to l}(u_{vac}) \equiv 0 \tag{3.46}$$

These restrictions and a look at curves representing the standard differential enthalpy of adsorption as a function of moisture content (Fig. 3.7 and Fig. 3.8) together with the differential specific heat capacity of adsorption as a function of moisture content presented in Fig. 3.9 make the following empirical expressions look reasonable

$$\Delta_r H^{\theta}_{298,a\to l}(u) = \Delta_r H^{\theta}_{298,a\to l}(0)\left(1-\frac{u}{u_{vac}}\right)^{\alpha_H} \tag{3.47}$$

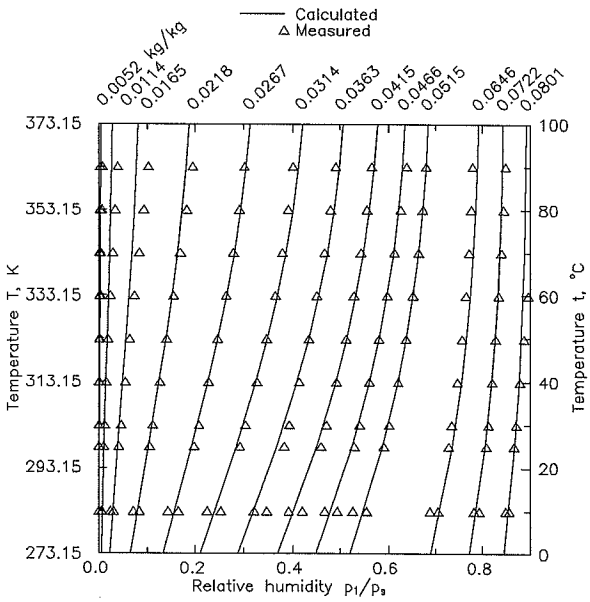

Figure 3.15. **Relative humidity as a function of moisture content and temperature. Steam cured hardened cement paste. *w/c* = 0.35. Solid lines: Calculated with Eq. (3.44), Eq. (3.47), Eq (3.48) and data from Table 3.1.** (Triangles: Data from Radjy *et al.* [17]).

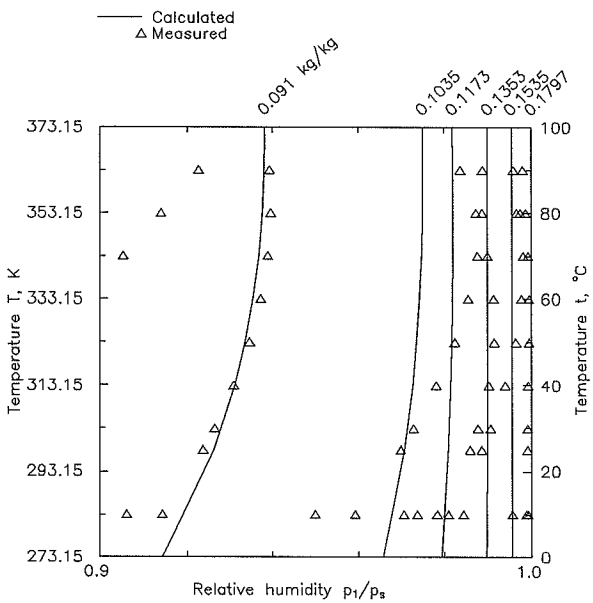

Figure 3.16. **Relative humidity as a function of moisture content and temperature. Steam cured hardened cement paste *w/c* = 0.35. Calculated with Eq. (3.44), Eq. (3.47), Eq (3.48) and data from Table 3.1.** (Triangles: Data from Radjy *et al.* [17]).

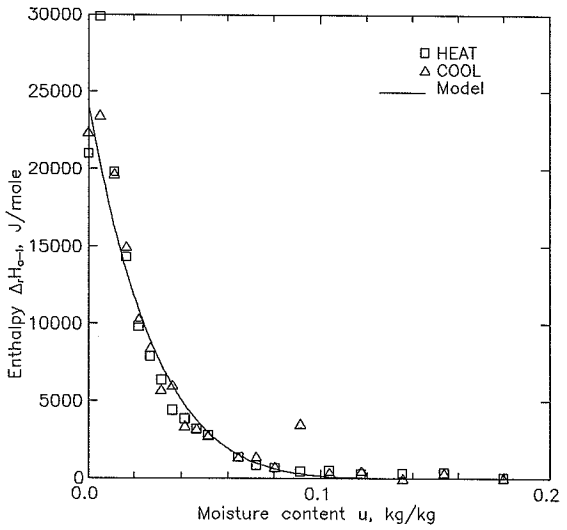

Figure 3.17. **Standard differential enthalpy of adsorption as a function of moisture content. Steam cured hardened cement paste.** $T = 298.15$ K, $w/c = 0.35$. **Solid line: Calculated with Eq. (3.47) and data from Table 3.1.** (Markers: Data from Radjy *et al.* [17]).

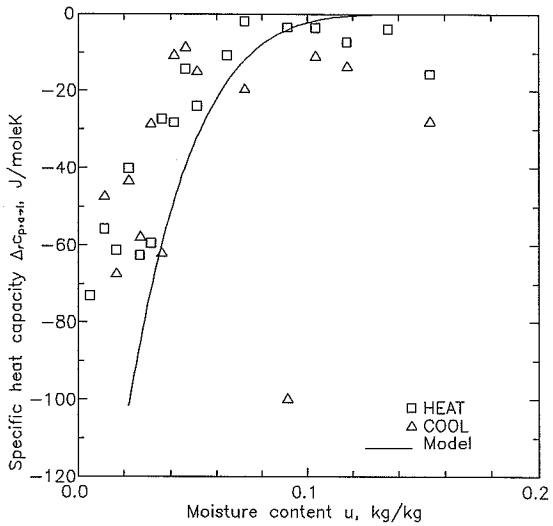

Figure 3.18. **Standard differential heat capacity of adsorption as a function of moisture content. Steam cured hardened cement paste.** $T = 298.15$ K, $w/c = 0.35$. **Solid line: Calculated with Eq. (3.47) and data from Table 3.1.** (Markers: Data from Radjy *et al.* [17]).

$$\Delta_r c_{p,a\to l}(u) = \Delta_r c_{p,a\to l}(0)\left(1-\frac{u}{u_{\text{vac}}}\right)^{\alpha_c} \tag{3.48}$$

The sorption data for steam cured hardened cement paste measured by Radjy *et al.* [17] (see Fig. 3.3) was fitted to the model Eq. (3.44) together with the empirical expressions Eq. (3.47) and Eq. (3.48). In advance a cubic spline was fitted to the sorption isotherm $\varphi_0(u,T_0)$ at $T_0 = 298.15$ K.

Figure 3.15 and Fig. 3.16 shows the sorption isosteres calculated with Eq. (3.44), (3.47) and (3.48) and the constants found from the non-linear regression analysis (see Table 3.1). The calculated sorption isosteres for relative humidities below 0.9 (Fig. 3.15) are quite close to the measured ones (calculated with Eq. (3.17)). At relative humidities above 0.94 (Fig. 3.16) there is a discrepancy between measured and calculated sorption isosteres. This s mainly due to measurement errors.

The standard differential enthalpy of adsorption as a function of moisture content calculated with Eq. (3.47) and the constants given in Table 3.1 is presented in Fig. 3.17. It is seen that the coincidence between measured and calculated values is good except at a very low moisture content where the calculated differential enthalpy of adsorption is underestimated.

The standard differential specific heat capacity of adsorption calculated with Eq. (3.48) and the constants given in Table 3.1 is shown in Fig. 3.18. The shape of the functional is correct but the values at a low moisture content are numerically seen overestimated.

The model Eq. (3.44) has also been used to fit the sorption data for Sitka Spruce presented by Kollmann [20] (see Fig. 3.4). Again a cubic spline was used for the description of the sorption isotherm at $T_0 = 298.15$ K, as well as the Equations (3.47) and (3.48) were used for the description of the standard differential enthalpy and specific heat capacity respectively. The regression constants are found in Table 3.1.

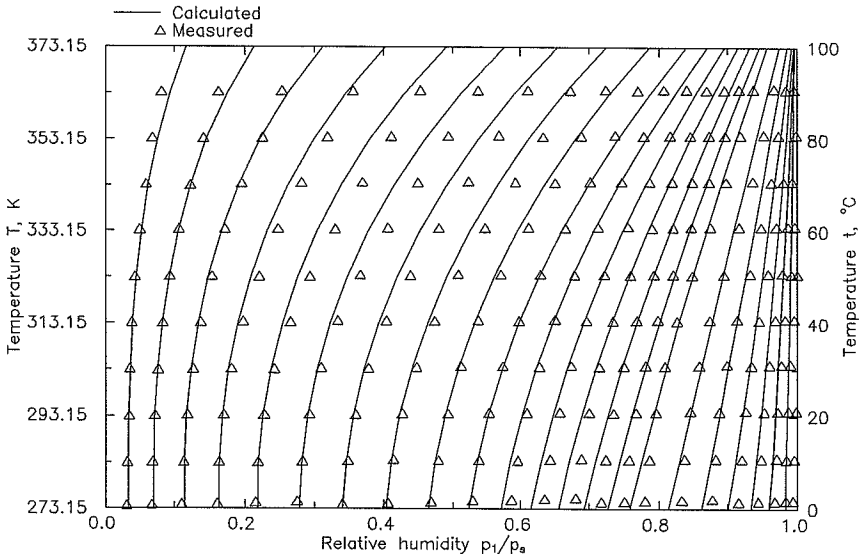

Figure 3.19. **Relative humidity as a function of moisture content and temperature. Sitka spruce. Solid lines: Calculated with Eq. (3.44), Eq. (3.47), Eq (3.48) and data from Table 3.1. Moisture content: see Fig. 3.4.** (Triangles: Data from Kollmann [20]).

The measured and calculated sorption isosteres are compared in Fig. 3.19. The correspondence is acceptable for most purposes but it is noticed that the model is not capable of describing the double convex shape of the isosteres at moisture contents above 0.10 kg/kg. Modelling this double convexity would have required that the standard differential specific heat capacity was a function of temperature.

The standard differential enthalpy of adsorption as a function of moisture content for Sitka Spruce calculated with Eq. (3.47) and the constants given in Table 3.1 is compared to the enthalpy of adsorption measured by Stamm *et al.* [17] in Fig. 3.20. It is seen that the calculated enthalpy of adsorption at low moisture content is underestimated compared to the values found by Stamm *et al.*

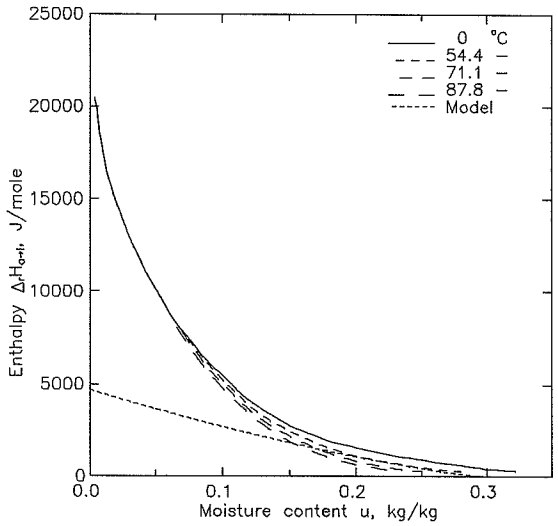

Figure 3.20. **Standard differential enthalpy of adsorption as a function of moisture content. Sitka spruce. Model: $T = 298.15$ K, calculated with Eq. (3.47) and data from Table 3.1; based on sorption data from Kollmann [20].** (Other temperatures: Measured by Stamm *et al.* [15]).

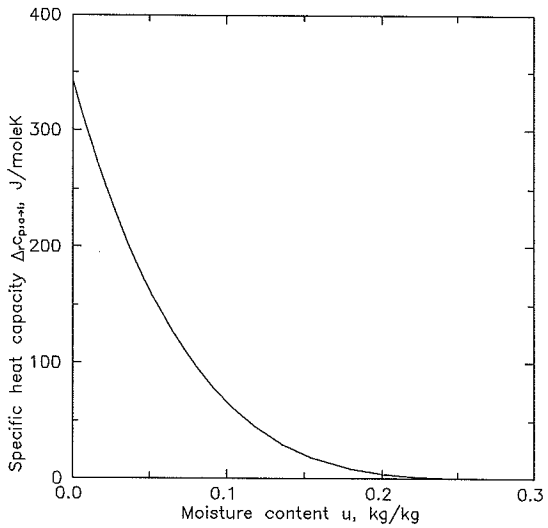

Figure 3.21. **Standard differential heat capacity of adsorption as a function of moisture content. Sitka spruce. $T = 298.15$ K. Calculated with Eq. (3.48) and data from Table 3.1. Based on sorption data from Kollmann [20].**

As was the case with the steam cured hardened cement paste, the standard differential heat capacity calculated for Sitka Spruce with Eq (3.48) and constants from Table 3.1 seems to be overestimated (see Fig. 3.21). The absolute maximum possible differential heat capacity of adsorption of the first monolayer should be less than that of water in the liquid phase (75.3 J/mole K).

According to Fig. 3.21 and Table 3.1 this is not so, which means that the heat capacity of the adsorbed monolayer according to Eq. (3.29) is negative. This is of course impossible. Although the shapes of the functionals in Fig. 3.20 and Fig. 3.21 might be correct, their absolute values are to be regarded as fit parameters at least for the present sorption data for Sitka Spruce. It is nevertheless possible to use Eq. (3.44) successfully for the description of relative humidity as a function of moisture content and temperature.

3.4 Suction pressure

When capillary condensation is dominating that is when the relative water vapour pressure φ approaches 1 the sorption isotherm is no longer a convenient description of the equilibrium between water and the porous solid. Instead one can use the hydraulic pressure p_2 (Pa), which is a sum of three separate potentials

$$p_2 = p_g + p_m + p_p \tag{3.49}$$

where p_g (Pa) is the pressure due to gravity, p_m (Pa) is the pressure due to matrix potential originating from curved menisci and osmotic forces and p_p (Pa) is pressure due to external forces. In this work only the pressure originating from curved menisci is considered and the equilibrium between water and the porous solid is then given by the suction curve.

The suction pressure p_{suc} (Pa) is the negation of the hydraulic pressure p_2

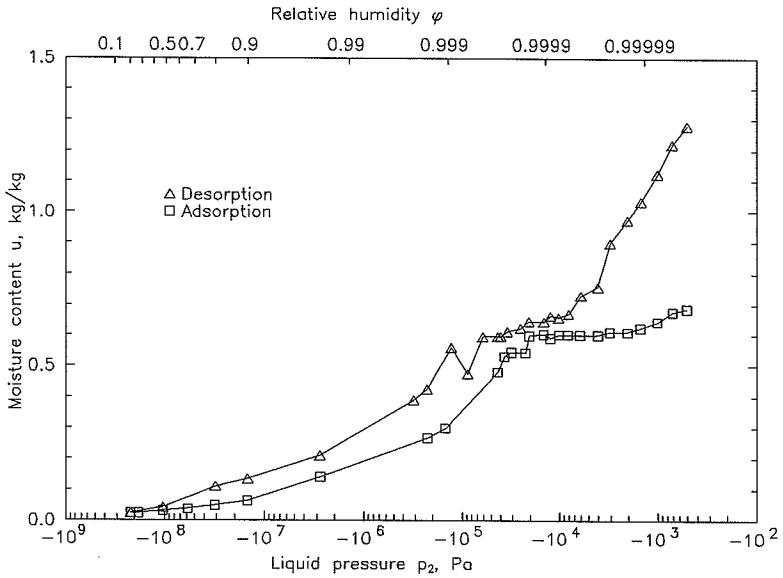

Figure 3.22. **Suction pressure of cellular concrete.** $\rho_0 = 500$ kg/m^3. (From Bomberg [24]).

$$p_{suc} = -p_2 \tag{3.50}$$

For reasons of simplicity this work only makes use of the hydraulic pressure, but the term suction is sometimes used as synonym.

The equilibrium moisture content of a porous solid at a given hydraulic pressure can be found from the suction curve (the term suction isotherm would be more correct). Experimental methods for the measurement of suction curves is described in section 7.6. Figure 3.22 shows the adsorption and desorption suction curve for cellular concrete measured by Bomberg [24].

Suction curves can also be calculated from measurements of pore size distributions by use of the Laplace equation

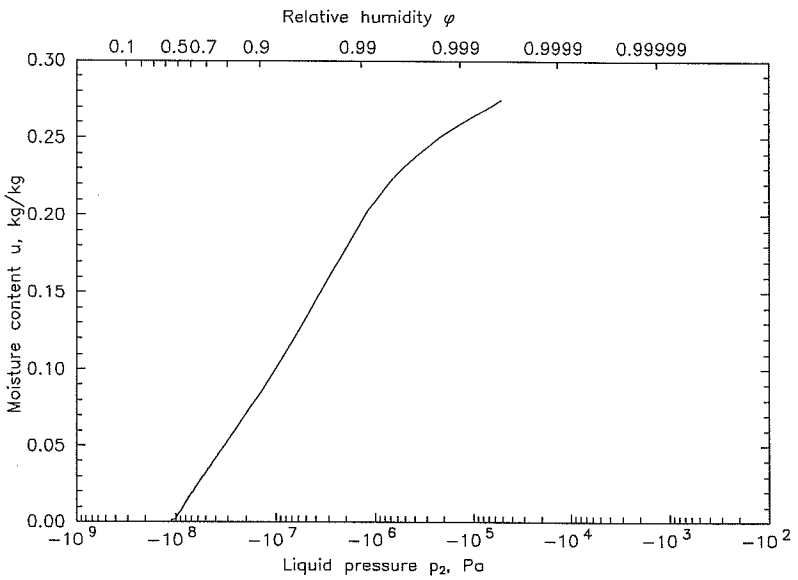

Figure 3.23. **Suction pressure of steam cured hardened cement paste.** $w/c = 0.5$. **Calculated from pore size distribution.** (Pore size distribution data from Sørensen [25]).

$$p_2 = -\frac{2\sigma\cos\theta}{r} \tag{3.51}$$

Figure 3.23 shows a suction curve for steam cured hardened cement paste with water/cement ratio 0.5 calculated from its pore size distribution. The pore size distribution was measured by Sørensen [25] by means of mercury intrusion porosimetry and water vapour adsorption. In the calculation of the hydraulic pressure it was assumed that the contact angle between water in the liquid phase and the solid matrix was 0°.

3.4.1 Relation between vapour and suction pressure

The relation between vapour and suction pressure of water absorbed by a porous material is found by combining the Kelvin equation

$$\ln\varphi = -\frac{M_1 2\sigma\cos\theta}{\rho_2 RTr} \tag{3.52}$$

and the Laplace equation (3.51) to

$$\ln\varphi = \frac{M_1}{\rho_2 RT} p_2 \tag{3.53}$$

In the following the implications of Eq. (3.53) will be examined by analysis of the isosteric temperature dependence of the relative humidity. From Eq. (3.53) we have

$$\begin{aligned}\left(\frac{\partial\ln\varphi}{\partial T}\right)_u &= \frac{M_1}{R}\frac{\partial}{\partial T}\left(\frac{p_2}{\rho_2 T}\right)_u \\ &= \frac{M_1}{R}\frac{\left(\frac{\partial p_2}{\partial T}\right)_u \rho_2 T - p_2\frac{\partial}{\partial T}(\rho_2 T)}{(\rho_2 T)^2} \\ &= \frac{M_1}{R}\left(\frac{\left(\frac{\partial p_2}{\partial T}\right)_u}{\rho_2 T} - \frac{p_2\left(\rho_2 + T\frac{\partial\rho_2}{\partial T}\right)}{(\rho_2 T)^2}\right)\end{aligned} \tag{3.54}$$

The temperature dependence of the suction pressure is given by the Laplace equation as

$$\left(\frac{\partial p_2}{\partial T}\right)_u = -\frac{2\cos\theta}{r}\frac{\partial\sigma}{\partial T} = \frac{p_2}{\sigma}\frac{\partial\sigma}{\partial T} \tag{3.55}$$

which inserted in Eq. (3.54) gives

$$\left(\frac{\partial\ln\varphi}{\partial T}\right)_u = \frac{M_1}{R}\left(\frac{p_2\frac{\partial\sigma}{\partial T}}{\sigma\rho_2 T} - \frac{p_2\left(\rho_2 + T\frac{\partial\rho_2}{\partial T}\right)}{(\rho_2 T)^2}\right)$$

$$= \frac{M_1 p_2}{\rho_2 RT}\left(\frac{1}{\sigma}\frac{\partial\sigma}{\partial T} - \frac{\rho_2 + T\frac{\partial\rho_2}{\partial T}}{\rho_2 T}\right) \tag{3.56}$$

Using Eq. (3.53) again we get

$$\left(\frac{\partial \ln\varphi}{\partial T}\right)_u = \ln\varphi\left(\frac{1}{\sigma}\frac{\partial\sigma}{\partial T} - \frac{\rho_2 + T\frac{\partial\rho_2}{\partial T}}{\rho_2 T}\right) \tag{3.57}$$

From Eq. (3.26) we have

$$\Delta_t H^{\theta}_{T,a\to l} = RT^2\left(\frac{\partial \ln\varphi}{\partial T}\right)_u \tag{3.58}$$

Substituting into Eq. (3.57) we obtain

$$\Delta_t H^{\theta}_{T,a\to l} = RT\ln\varphi\left(\frac{T}{\sigma}\frac{\partial\sigma}{\partial T} - 1 - \frac{T}{\rho_2}\frac{\partial\rho_2}{\partial T}\right)$$

$$= -RT\ln\varphi + TRT\ln\varphi\left(\frac{1}{\sigma}\frac{\partial\sigma}{\partial T} - \frac{1}{\rho_2}\frac{\partial\rho_2}{\partial T}\right) \tag{3.59}$$

From Eq. (3.21), Eq. (3.32) and Eq. (3.59) follows

$$\Delta_t G^{\theta}_{T,a\to l} = -RT\ln\varphi \tag{3.60}$$

$$\Delta_t S^{\theta}_{T,a\to l} = RT\ln\varphi\left(\frac{1}{\sigma}\frac{\partial\sigma}{\partial T} - \frac{1}{\rho_2}\frac{\partial\rho_2}{\partial T}\right) \tag{3.61}$$

The isosteric temperature dependence of the relative humidity can now be calculated by integration of Eq. (3.57) from a known point (φ_0, T_0) on the sorption isotherm to (φ, T)

$$\int_{\varphi_0}^{\varphi}\frac{1}{\ln\varphi}\mathrm{d}\ln\varphi = \int_{T_0}^{T}\left(\frac{1}{\sigma}\frac{\partial\sigma}{\partial T} - \frac{1}{T} - \frac{1}{\rho_2}\frac{\partial\rho_2}{\partial T}\right)\mathrm{d}T \Leftrightarrow$$

$$[\ln(\ln\varphi)]_{\varphi_0}^{\varphi} = [\ln\sigma(T) - \ln T - \ln\rho_2(T)]_{T_0}^{T} \Leftrightarrow$$

$$\ln\frac{\ln\varphi}{\ln\varphi_0} = \ln\frac{\sigma(T)}{\sigma(T_0)}\frac{T_0}{T}\frac{\rho_2(T_0)}{\rho_2(T)} \Leftrightarrow$$

$$\varphi = \varphi_0^{\alpha(T)}, \quad \alpha(T) = \frac{\sigma(T)}{\sigma(T_0)}\frac{T_0}{T}\frac{\rho_2(T_0)}{\rho_2(T)} \tag{3.62}$$

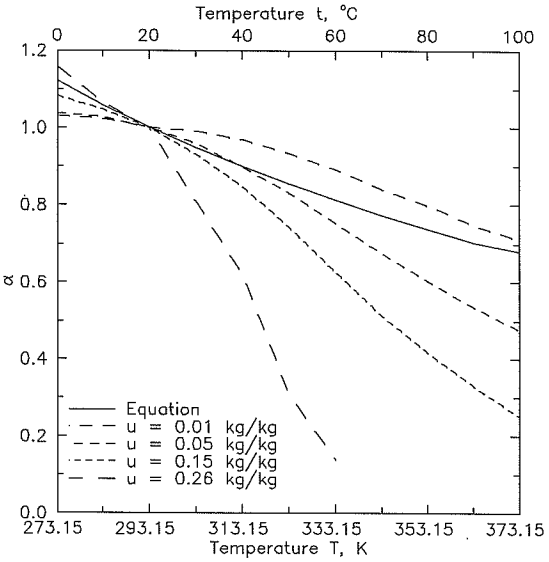

Figure 3.24. **Comparison of α computed with Eq. (3.62) (solid line) and computed from isosteres (dashed lines).** (Data for isosteres from Kollmann [20], see also Fig. 3.4).

Equation (3.62) states that it is possible to calculate the sorption isotherms at other temperatures from the knowledge of one sorption isotherm and the knowledge of the temperature dependence of surface tension and density of water. Fauconnier [26] found an identical result. Unfortunately life is not that easy!

In Fig. 3.24 α from Eq. (3.62) is compared to α calculated from the sorption isosteres for Sitka spruce given by Kollmann (see. Fig. 3.4). α from Eq. (3.62) was calculated with Eq. (2.17) and Eq. (2.20). α calculated from the sorption isosteres clearly depends strongly on the moisture content. This is not foreseen by Eq. (3.62), whose applicability therefore is very limited.

The question is now, where the preceding analysis failed? It seems most probable that the answer is found in Eq. (3.55), where the contact angle was assumed to be independent of temperature. The contact angle is given by the surface tensions of the three phases involved, liquid (*l*), solid (*s*) and moist air (*a*) as

$$\cos\theta = \frac{\sigma_{sa} - \sigma_{ls}}{\sigma_{la}} \tag{3.63}$$

where σ_{la} (N/m) is the surface tension between the adsorbed liquid and the moist air, σ_{ls} (N/m) is the surface tension between the adsorbed liquid and the solid and σ_{sa} (N/m) is the surface tension between the moist air and the solid. All three surface tensions are dependent on temperature, but it is unlikely, that their temperature dependence are proportional. If this is the case, the contact angle depends on temperature, and the assumption used in the derivation of Eq. (3.55) does not hold.

4 Moisture transfer

This chapter gives the basic equations for the description of vapour and liquid moisture transfer in porous materials. Moisture transfer due to convection and gravity is neglected.

4.1 Transfer of vapour

Water vapour transfer in air is described by Fick's 1st law

$$\vec{j}_1 = -\delta_a \frac{\partial p_1}{\partial x} \tag{4.1}$$

where j_1 (kg/m^2 s) is the water vapour flux, δ_a (kg/m s Pa) is the water vapour conductivity in air, p_1 (Pa) is the partial water vapour pressure, and x (m) is the space coordinate. Fick did not use partial pressure as the driving potential. Fick did not study gaseous diffusion but examined the diffusion of a solute in a solvent (sodium chloride in destilled water, Fick [27]). As a consequence he used concentration as the driving potential. In [10], p. 244 Lykow favoured the use of partial water vapour pressure, which is used as driving potential in this work.

The water vapour conductivity if often replaced in Eq. (4.1) by the water vapour diffusivity of air D (m^2/s) and the specific moisture capacity of air $(\partial x/\partial p_1)_T$. In this case we get

$$\vec{j}_1 = -D\rho_4 \left(\frac{\partial x}{\partial p_1}\right)_T \frac{\partial p_1}{\partial x} \tag{4.2}.$$

The weight fraction x of water vapour in air must not be confused with the space coordinate x in the water vapour gradient $\partial p_1/\partial x$. The specific moisture capacity of air at constant total (barometric) pressure can under the assumption of an ideal water vapour-air mixture be evaluated as

$$\begin{aligned}
\left(\frac{\partial x}{\partial p_1}\right)_{p_b} &= \left(\frac{\partial}{\partial p_1}\frac{m_1}{m_4}\right)_{p_b} \\
&= \left(\frac{\partial}{\partial p_1}\frac{M_1}{M_4}\frac{p_1}{p_b - p_1}\right)_{p_b} \\
&= \frac{M_1}{M_4}\frac{p_b}{(p_b - p_1)^2} \\
&= \frac{M_1 p_b}{RT(p_b - p_1)\rho_4}
\end{aligned} \tag{4.3}$$

Combining Eq. (4.2) and Eq. (4.3) gives the following expression for the description of water vapour transfer in air

$$\vec{j}_1 = -D\frac{M_1}{RT}\frac{p_b}{p_b - p_1}\frac{\partial p_1}{\partial x} \tag{4.4}$$

The factor $p_b/(p_b\text{-}p_1)$ in the above equation is equal to the Stefan diffusion correction factor but was here derived in another way.

When we instead of dealing with vapour transfer in air are dealing with vapour transfer in porous materials, it is necessary to modify Eq. (4.4) to

$$\vec{j}_1 = -\zeta(u)D\frac{M_1}{RT}\frac{p_b}{p_b - p_1}\frac{\partial p_1}{\partial x} \tag{4.5}$$

where $\zeta(u)$ is a factor which accounts for the decrease in vapour diffusivity caused by the solid matrix, the interconnection of pores and the filling of pores with adsorbate and capillary condensate.

Two often quoted alternative formulations of Eq. (4.5) are

$$\vec{j}_1 = -\delta_p\frac{\partial p_1}{\partial x} \tag{4.6}$$

and

$$\vec{j}_1 = -\delta_\varphi\frac{\partial \varphi}{\partial x} \tag{4.7}$$

where δ_p (kg/m s Pa) and δ_φ (kg/m s) are the water vapour conductivity of the porous material.

The moisture content u is often used a driving potential for the description of moisture transfer in porous materials. In the case of vapour transfer we then have to change the vapour gradient into a moisture and a temperature gradient as

$$\begin{aligned}\frac{\partial p_1}{\partial x} &= \left(\frac{\partial p_1}{\partial u}\right)_T\frac{\partial u}{\partial x} + \left(\frac{\partial p_1}{\partial T}\right)_u\frac{\partial T}{\partial x} \\ &= p_s\left(\frac{\partial \varphi}{\partial u}\right)_T\frac{\partial u}{\partial x} + \left(\frac{\partial p_1}{\partial T}\right)_u\frac{\partial T}{\partial x}\end{aligned} \tag{4.8}$$

Using the Clausius-Clapeyron equation

$$\frac{\mathrm{d}\ln p_1}{\mathrm{d}T} = \frac{\Delta_l H_{T,a\to g}}{RT^2} \tag{4.9}$$

on the equilibrium (3.23) between the adsorbed water $H_2O(a)$ (and capillary condensated water) and the water vapour $H_2O(g)$ gives the water vapour pressure p_1 dependence on temperature at constant moisture content as

$$\left(\frac{\partial p_1}{\partial T}\right)_u = \frac{\Delta_r H_{T,a\to g}}{RT^2} p_1 = \frac{\Delta_r H_{T,a\to g}}{RT^2} \varphi p_s \tag{4.10}$$

Equation (4.8) now turns into

$$\frac{\partial p_1}{\partial x} = p_s \left(\frac{\partial \varphi}{\partial u}\right)_T \frac{\partial u}{\partial x} + \frac{\Delta_r H^{\theta}_{T,a\to g}}{RT^2} \varphi p_s \frac{\partial T}{\partial x} \tag{4.11}$$

The vapour flux as a function of moisture content and temperature is found by combining Eq. (4.5) and Eq. (4.11) to

$$\vec{j}_1 = -\zeta(u) D \frac{M_1}{RT} \frac{p_b}{p_b - p_1} p_s \left(\left(\frac{\partial \varphi}{\partial u}\right)_T \frac{\partial u}{\partial x} + \frac{\Delta_r H^{\theta}_{T,a\to g}}{RT^2} \varphi \frac{\partial T}{\partial x} \right) \tag{4.12}$$

or using Luikov's nomenclature

$$\vec{j}_1 = -a_{m1} \rho_0 \left(\frac{\partial u}{\partial x} + \delta_1 \frac{\partial T}{\partial x} \right) \tag{4.13}$$

with the water vapour diffusivity a_{m1} (m^2/s) and the water vapour thermogradient coefficient δ_1 (K^{-1}) given by

$$a_{m1} = \frac{\zeta(u) D M_1}{\rho_0 RT} \frac{p_b}{p_b - p_1} p_s \left(\frac{\partial \varphi}{\partial u}\right)_T \tag{4.14}$$

$$\delta_1 = \frac{\Delta_r H^{\theta}_{T,a\to g}}{RT^2 \left(\frac{\partial \varphi}{\partial u}\right)_T} \varphi \tag{4.15}.$$

4.2 Transfer of liquid

The transfer of a liquid in a porous material is described by the Darcy's first law

$$\vec{j}_2 = -K \frac{\partial p_2}{\partial x} \tag{4.16}$$

where j_2 (kg/m^2 s) is the flux of water in the liquid phase, K (kg/m s Pa) is the capillary conductivity, p_2 (Pa) is the hydraulic water pressure originating from curved menisci, and x (m) is the space coordinate. In the following the influence of moisture content and temperature on the capillary conductivity K and driving potential p_2 in the Darcy equation will be discussed.

A porous material can be idealized as a bank of cylindrical capillary tubes with different lengths and radii. The moisture flow through any of the capillary tubes can be described by the Poiseuille equation

$$\dot{m} = -\frac{\pi r^4}{8\nu}\frac{\partial p_2}{\partial x} \tag{4.17}$$

where $\dot{m}$ (kg/s) is the mass flow through capillary, r (m) is the radius of the capillary and ν (m^2/s) is the kinematic viscosity.

Equation (4.17) gives the moisture flux through one capillary tube as

$$\vec{j}_2 = \frac{\dot{m}}{A} = \frac{\dot{m}}{\pi r^2} = -\frac{r^2}{8\nu}\frac{\partial p_2}{\partial x} \tag{4.18}$$

Comparing this equation with the Darcy equation (4.14) gives a qualitative expression for the temperature and moisture dependence of the capillary conductivity

$$K = \frac{f(r)}{8\nu} = \frac{p(u)}{\nu(T)} \tag{4.19}$$

The function $p(u)$ contains information about the pore structure, i. e. both the pore size distribution as well as the tortuosity factors of the pores. In this way the moisture and the temperature dependence of the capillary conductivity has been separated. $p(u)$ can be seen as a function which describes the morphology of the porous material.

The transfer of water in the liquid phase as a function of moisture content and temperature is found from Eq. (4.16) as

$$\vec{j}_2 = -K\left(\left(\frac{\partial p_2}{\partial u}\right)_T \frac{\partial u}{\partial x} + \left(\frac{\partial p_2}{\partial T}\right)_u \frac{\partial T}{\partial x}\right) \tag{4.20}$$

or using Luikov's nomenclature

$$\vec{j}_2 = -a_{m2}\rho_0\left(\frac{\partial u}{\partial x} + \delta_2\frac{\partial T}{\partial x}\right) \tag{4.21}$$

with the diffusivity of water in the liquid phase a_{m2} (m^2/s) and the thermogradient coefficient of liquid water δ_2 (K^{-1}) given by

$$a_{m2} = \frac{K}{\rho_0}\left(\frac{\partial p_2}{\partial u}\right)_T \tag{4.22}$$

$$\delta_2 = \frac{\left(\frac{\partial p_2}{\partial T}\right)_u}{\left(\frac{\partial p_2}{\partial u}\right)_T} \tag{4.23}$$

5 Heat transfer

This chapter describes the three fundamental modes of heat transfer, namely conduction, convection, and radiation. This chapter is included for reference purposes and it is not intended to be a fulfilling description of all the various aspects regarding heat transfer. The interested reader is instead referred to the large number of excellent monographs in this area, see for instance Pitts *et al.* [28], Bird *et al.* [7], Gröber *et al.* [29], Eckert *et al.* [30], Carslaw *et al.* [31], Luikov [32],[35] and Luikov *et al.* [33].

5.1 Conduction

The conduction of heat through a porous solid is governed by Fourier's law

$$\vec{q} = -\lambda \frac{\partial T}{\partial x} \tag{5.1}$$

where q (J/s m^2 = W/m^2) is the heat flux, λ (J/s m K = W/m K) is the thermal conductivity, T (K or °C) and x (m) is the space coordinate.

The thermal conductivity λ is for heating and ventilation purposes normally a conglomerate parameter encomprising pure conduction, radiation, latent heat transfer and sometimes also heat transfer due to free convection of air in the pore space (for instance with very low density fibrous insulation materials). The thermal conductivity is generally a function of temperature and moisture content. For building physical purposes the temperature dependence is in most cases neglected. The free convection part of measured thermal conductivity, if present, is accepted as an indistinguishable part.

Because of its relatively high thermal conductivity water has a considerable influence on the thermal conductivity of wet porous materials.

In the simulation of coupled heat and moisture transfer the latent heat transfer due to evaporation and condensation of water is in the majority of cases accounted for explicitly and should therefore not be accounted for in the thermal conductivity. This has to be realised, when one has to use thermal conductivities taken from literature.

The influence of radiation heat transfer on the thermal conductivity is only important when dealing with very high temperatures, where the thermal resistance of materials with zero porosity is greater than that of porous materials. This is of no relevance to the problems dealt with in this work, and the thermal radiation heat transfer inside the porous material is accepted to be a limited part of the thermal conductivity.

5.2 Convection

Newton's law of cooling describes the convection heat transfer from a solid to a surrounding fluid

$$\vec{q} = h(T_s - T_\infty) \tag{5.2}$$

where q (J/s m^2 = W/m^2) is the heat flux, h (J/s m^2 K = W/m^2 K) is the convective heat transfer coefficient, and T_s, T_∞ (K or °C) is the temperature of the surface and of the surrounding fluid respectively.

In this work heat transfer due to convection is not accounted for, because the focus has been on the simulation of the internal transfer in isotropic porous materials.

5.3 Radiation

Radiant heat transfer from one gray surface to a second enclosed by the first is calculated with the equation

$$Q_{1\to 2} = \frac{A_1 \sigma_s (T_1^4 - T_2^4)}{\frac{1}{\varepsilon_1} + \frac{A_1}{A_2}\left(\frac{1}{\varepsilon_2} - 1\right)} \tag{5.3}$$

where $Q_{1\to 2}$ (J/s = W) is the heat transfer from the gray surface with surface area A_1 (m^2) to the gray surface with surface area A_2 (m^2), $\sigma_s = 5.6697 \cdot 10^{-8}$ J/s m^2 K^4 is the Stefan-Boltzmann constant, and T_i (K), ε_i (-) is the absolute temperature and the emissivity of surface i respectively. Equation (5.3) was presented by Christiansen in [34] under the restriction that the surfaces do not see "themselves".

6 Coupled heat and moisture transfer

This chapter describes the elucidation of the set of partial differential equations, which are governing coupled heat and moisture transfer. The analysis is similar to those given by many other researchers. The resulting set of equations is similar to that given by Luikov in [35] and in [36] and Philip and de Vries in [37].

Our starting point is a piece of porous material containing air and water in the form of vapour, liquid and solid. The dry density of the porous material is denoted by ρ_0 (kg/m^3). The mass content of constituent i is denoted by u_i (kg constituent/kg dry material), i.e. u_1 is the water vapour content, u_2 is the content of water in the liquid phase, u_3 is the content of ice, and u_4 is the content of dry air.

The equation of continuity is

$$\rho_0 \frac{\partial u_i}{\partial \tau} = -\mathrm{div}\vec{j}_i + I_i \qquad ,i = 1,2,3,4 \tag{6.1}$$

where τ (s) is the time, j_i (kg/m^2 s) is the mass flux of constituent i involving both diffusive and convective transfer, and I_i (kg/m^3 s) is the mass source or sink of constituent i due to phase transition or chemical conversion.

The energy equation is

$$c_p \rho_0 \frac{\partial T}{\partial \tau} = -\mathrm{div}\vec{q} + \sum_{i=1}^{4} H_i I_i + \sum_{i=1}^{4} \vec{j}_i c_{pi} \cdot \nabla T \tag{6.2}$$

where T (K or °C) is the temperature, c_p (J/kg K) is the specific heat capacity of the moist porous material as defined in Eq. (3.13), q (J/s m^2 or W/m^2) is the heat flux due to conduction, H_i (J/kg) is the specific enthalpy of constituent i, and c_{pi} (J/kg K) is the specific heat capacity of constituent i.

We will now restrict ourselves to the region of positive Celsius temperatures. Later on this restriction will be removed. The restriction implies that ice does not exist, i.e.

$$u_3 = 0 \tag{6.3}$$

$$I_3 = 0 \tag{6.4}$$

In advance is was obvious that

$$\vec{j}_3 = \vec{0} \tag{6.5}$$

The mass content of water vapour u_1 and the mass content of dry air u_4 is negligible, which together with Eq. (6.3) yields

$$u \approx u_2 \tag{6.6}$$

If chemical conversion is omitted the only sources and sinks are phase transitions between liquid water and water vapour (evaporation/condensation), i.e.

$$I_1 = -I_2 \tag{6.7}$$

$$I_4 = 0 \tag{6.8}$$

The equation of continuity Eq. (6.1) can now be simplified with the results of the equations (6.3-6.8) to

$$\rho_0 \frac{\partial u}{\partial \tau} = -\mathrm{div}(\vec{j}_1 + \vec{j}_2) \tag{6.9}$$

The water vapour flux j_1 and the liquid flux j_2 are found from Eq. (4.13) and Eq. (4.21), which inserted in Eq. (6.9) gives

$$\rho_0 \frac{\partial u}{\partial \tau} = -\mathrm{div}(-a_{m1}\rho_0(\nabla u + \delta_1 \nabla T) - a_{m2}\rho_0(\nabla u + \delta_2 \nabla T)) \Leftrightarrow$$

$$\frac{\partial u}{\partial \tau} = \mathrm{div}(a_m(\nabla u + \delta \nabla T)) \tag{6.10}$$

with

$$a_m = a_{m1} + a_{m2} \tag{6.11}$$

$$\delta = \frac{a_{m1}\delta_1 + a_{m2}\delta_2}{a_{m1} + a_{m2}} \tag{6.12}$$

In the absence of a gradient of total pressure causing convective heat transfer and under the assumption that the diffusive moisture transfer is so slow that it does not cause convective heat transfer, it is acceptable to omit the third term of the right hand side of Eq. (6.2).

In [35] Luikov has shown that the sources and sinks in the second term of the right hand side of Eq. (6.2) under the restrictions given in Eq. (6.4) and in Eq. (6.8) can be written as

$$I_2 = -I_1 = \varepsilon \rho_0 \frac{\partial u}{\partial \tau} \tag{6.13}$$

with

$$\varepsilon = \frac{a_{m1}}{a_{m1} + a_{m2}} \tag{6.14}$$

The energy equation with the above mentioned simplifications and the use of Eq. (6.14) and Eq. (5.1) is now

$$c_p \rho_0 \frac{\partial T}{\partial \tau} = -\mathrm{div}(-\lambda \nabla T) + \varepsilon \Delta_1 H^{\theta}_{T,a \to g} \rho_0 \frac{\partial u}{\partial \tau} \tag{6.15}$$

The resulting set of partial differential equations Eq. (6.10) and Eq. (6.15) which describes coupled heat and moisture transfer in porous materials is in the 1-dimensional case

$$\frac{\partial u}{\partial \tau} = \frac{\partial}{\partial x}\left(a_{\mathrm{m}} \frac{\partial u}{\partial x}\right) + \frac{\partial}{\partial x}\left(a_{\mathrm{m}} \delta \frac{\partial T}{\partial x}\right) \tag{6.16}$$

$$\frac{\partial T}{\partial \tau} = \frac{\partial}{\partial x}\left(\frac{\lambda}{\rho_0 c_p} \frac{\partial T}{\partial x}\right) + \frac{\varepsilon \Delta_{\mathrm{r}} H^{\theta}_{T,a \to g}}{c_p} \frac{\partial u}{\partial \tau} \tag{6.17}$$

It is only possible to solve this set of equations analytically in a limited number of cases. Generally one has to use numerical methods, i.e. finite element methods or finite difference methods. In this work a finite difference method given by Pedersen *et al.* in [38] is used.

The restriction of Eq. (6.3) and (6.4) can now be relieved, i.e. the presence of ice will be allowed.

This can be realised by using the concept outlined in section 3.2 where the phase change enthalpy is included in the specific heat capacity. The procedure is given by Eq. (3.15) and Eq. (3.16) which also keeps track of the amount of water present in the form of liquid and ice respectively when the temperature is in the range T_{f}-ΔT - T_{f}+ΔT. From Eq. (3.16) the amount of ice in this temperature range is found as

$$u_3 = \frac{u\left[\int_{T_{\mathrm{f}}-\Delta T}^{T_{\mathrm{f}}+\Delta T} c_p^{*} \mathrm{d}T - \int_{T_{\mathrm{f}}}^{T_{\mathrm{f}}+\Delta T} c_{p2} \mathrm{d}T\right] - \Delta_{\mathrm{r}} H^{\theta}_{T,s \to l}}{\int_{T_{\mathrm{f}}-\Delta T}^{T_{\mathrm{f}}} c_{p3} \mathrm{d}T - \int_{T_{\mathrm{f}}}^{T_{\mathrm{f}}+\Delta T} c_{p2} \mathrm{d}T} \tag{6.18}$$

6.1 Other models for heat and moisture transfer

A number of other researchers have published models for heat and moisture transfer in porous media, see for instance Krischer [8], Harmathy [39], Kiessl [40], Andersson [41] or Siang [42]. None of them seems to offer any major advantages over the one presented in the preceding section.

Pedersen [18] on the contrary presented a very elegant approach to overcome the problem with coupled heat and moisture transfer in porous bodies composed of several different building materials. Pedersen did not use of a set of coupled equation like the ones presented as Eq. (6.16) and (6.17) but instead used the expression for the fluxes of water vapour, liquid and heat Eq. (4.6), (4.16) and (5.1) respectively together with the sorption isotherms and the suction curves. The fluxes were summed up directly in finite control volumes ready for computer implementation. In this way the computational method was directly based on continuous transfer potentials and the problems arising from discontinuity in the transfer potentials at the boundaries between adjacent layers of different materials was overcome.

7 Measurement of material properties

This chapter describes a number of methods for the estimation of the material properties, which it is necessary to know in order to be able to use models for coupled heat and moisture transfer. Examples of the variation of the material properties with temperature and moisture content are presented.

Luikov [35],[10] presented a number of methods of Soviet origin. These methods are not presented in this work. In addition to the methods presented in this chapter there also exists a number of so-called inverse methods. These methods are presented in chapter 8.

7.1 Thermal conductivity

This section gives a short introduction to measurement of thermal conductivity. Various national and international standards for the measurement of thermal conductivity of materials in dry condition exist. These methods are steady-state methods based on the use of a guarded hot plate apparatus or a heat flow meter such as described in ISO/DIS 8302 [43] and ISO/DIS 8301 [44] respectively.

Furthermore, a proposal for the measurement of thermal conductivity as a function of moisture content has been forwarded as ISO/DIS 10051 [45]. The proposal is based on the use of the above mentioned guarded hot plate apparatus or heat flow meter.

In addition to the steady-state methods a number of non-stationary methods have been published. An example of such a method is presented below.

7.1.1 Non-stationary methods

Thermal probes are a frequently used non-stationary method for the determination of thermal conductivity. An example of the design of such a thermal probe is given in Perrin *et al.* [46] and Foures *et al.* [47], [48].

The thermal probe was composed of a cylindrical heating element of 1 mm diameter onto which a 0.5 mm thermocouple was attached (see. Fig. 7.1). The heating element was made with a 85 Ω/m electrical wire. The principle of operation is that a current is supplied to the electrical wire and the thermal conductivity is estimated from the transient temperature evolution.

Perrin *et al.* [46] used the thermal probe for the determination of thermal conductivity of mortar (Fig. 7.2) and brick (Fig. 7.3) as a function of moisture content and temperature. Furthermore, Perrin and co-workers used calibrated thermal probes for measurement of moisture content profiles in mortar and brick specimens under transient moisture conditions.

7.1.2 Stationary methods

In stationary methods the thermal conductivity is calculated from the Fourier equation (5.1) and knowledge of the thickness of the slab, the surface temperatures and the heat flux as

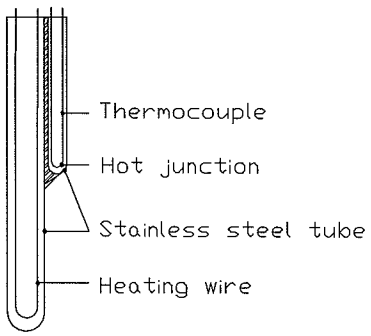

Figure 7.1. **Thermal probe.** (From Perrin *et al.* [46]).

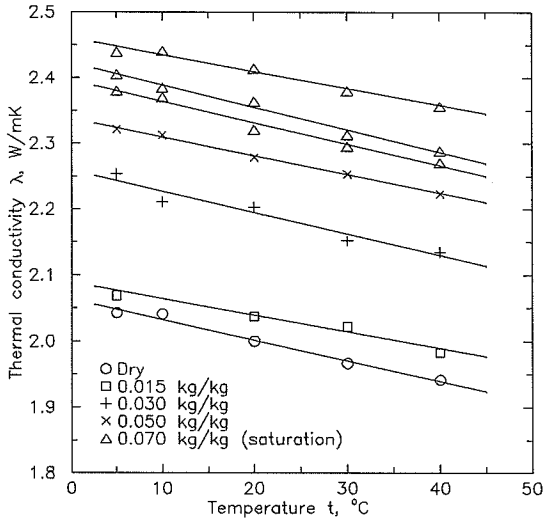

Figure 7.2. **Thermal conductivity of mortar as a function of temperature and moisture content.** (From Perrin *et al.* [46]).

$$\lambda = -\frac{\vec{q}}{\frac{\partial T}{\partial x}} = -\frac{\vec{q}}{\frac{T_1 - T_2}{L}} \tag{7.1}$$

The heat flux is measured with heat flow meters or in guarded hot plate measurements. These methods are thoroughly described in the comprehensive heat transfer literature.

7.2 Specific heat capacity

The specific heat capacity of a wet porous material is by definition found from the specific heat capacities and the mass content of the involved constituents. This was shown in section 3.2. The heat capacity of the constituents are found from calorimetric measurements.

7.3 Vapour conductivity

In this section the cup method for measurement of water vapour conductivity of porous materials is introduced. Four methods for the evaluation of the water vapour conductivity from cup method measurements are presented.

7.3.1 Cup method

The cup method is the most frequently used method for the determination of water vapour conductivity. It has its name from the experimental set-up, where the test specimen under observation is placed as lid in a cup-like container. Figure 7.4 shows the cup type used at the Building Materials Laboratory, the Technical University of Denmark.

The principle in the cup method is to have known steady relative humidities (vapour pressures) and then determine the water vapour flux through the test specimen. The temperature must

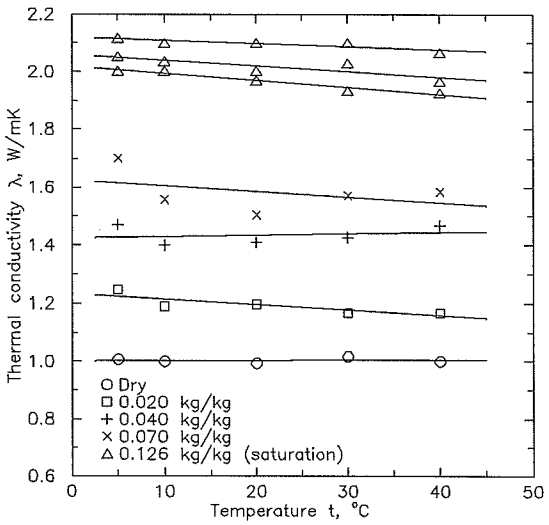

Figure 7.3. **Thermal conductivity of brick as a function of temperature and moisture content..** . (From Perrin *et al.* [46]).

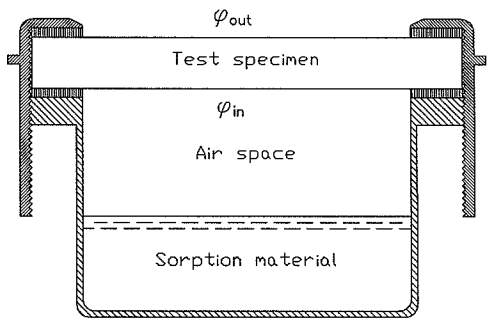

Figure 7.4. **The cup method for measurement of water vapour conductivity of porous materials. Cup type used at Building Materials Laboratory.** (After West *et al.* [50]).

be constant. The water vapour flux is calculated from measurements of the mass of the cup as a function of time $m(\tau)$ (kg) and the effective transmission area A (m^2) as

$$j_1 = \frac{1}{A}\frac{d}{d\tau}m(\tau) \tag{7.2}$$

In its most simple form the water vapour conductivity is calculated from Fick's first law Eq. (4.6) as

$$\delta_p = \frac{-\vec{j}_1}{\frac{\partial p_1}{\partial x}} \approx \frac{-j_1}{\frac{(\varphi_i - \varphi_o)p_s(T)}{L}} \tag{7.3}$$

where φ_i is the relative humidity at the inner surface of the specimen, φ_o is the relative humidity of the outer surface of the specimen, $p_s(T)$ (Pa) is the saturation water vapour pressure, T (K) is the temperature, at which the experiment is performed and L (m) is the thickness of the test specimen.

Equation (7.3) is valid only, when the water vapour conductivity is constant i.e. does not depend on vapour pressure. In this case the vapour pressure profile is linear as shown in Fig. 7.5a.

Despite of this fact Eq. (7.3) is often used for an approximate determination of the water vapour conductivity as a function of the water vapour pressure (or the relative humidity). In this case the water vapour pressure is then varied in steps. The water vapour conductivity is calculated from Eq. (7.3) and taken as valid at the mean water vapour pressure of the inside and outside water vapour pressures.

When the water vapour conductivity depends on the water vapour pressure, the vapour pressure profile is non-linear as shown schematically in Fig. 7.5b.

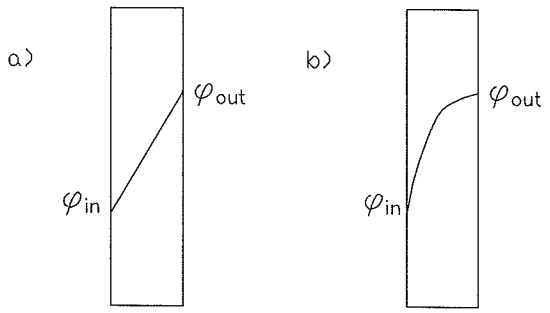

Figure 7.5. **Relative humidity profile in test specimen in the cup method. Schematically. (a) water vapour conductivity independent of relative humidity. (b) water vapour conductivity dependent of relative humidity.**

The variation of water vapour conductivity of outer sapwood of spruce measured with the cup method by Bertelsen [51] is shown in Fig. 7.6. It is seen that the vapour conductivity is exponentially growing with relative humidity.

Tveit [52] measured the water vapour conductivity of several building materials with the cup method as a function of temperature and relative humidity. The measurements were made partly in adsorption and partly in desorption. An example of the vapour conductivity of pine is shown in Fig. 7.7.

7.3.2 Bazant and Najjar's method

Bazant *et al.* [53] presented a very elegant method for the determination of water vapour conductivity from cup measurements. In this method the water vapour pressure is kept constant at one of the surfaces and varied at the other. If for instance the water vapour pressure is kept constant inside the cup, then the water vapour flux through the specimen can be regarded as a function of the outside water vapour pressure

$$j_1 = j_1(p_{out}) \tag{7.4}$$

Integration of Fick's first law Eq. (4.6) now yields

$$\int_{p_1}^{p_{out}} \delta_p(p)\mathrm{d}p = -\int_0^L j_1(p_{out})\mathrm{d}x = Lj_1(p_{out}) \tag{7.5}$$

The water vapour conductivity is now found by differentiation of both sides of Eq. (7.5) with respect to p_{out}

$$\delta_p(p_{out}) = -L\frac{\mathrm{d}j_1(p_{out})}{\mathrm{d}p_{out}} \tag{7.6}$$

7.3.3 Inverted wet-cup

Schou [54] and Thorsen [55] extended the cup method to cover the superhygroscopic range. The so-called "inverted-cup" method makes use of an experimental arrangement equivalent

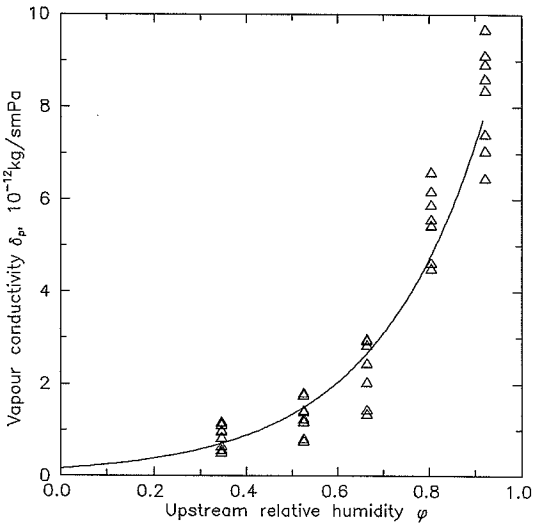

Figure 7.6. **Vapour conductivity of outer sapwood of spruce as a function of upstream relative humidity.** $\rho_0 = 420$ kg/m^3, $T =$ 296.45 K. (From Bertelsen [51]).

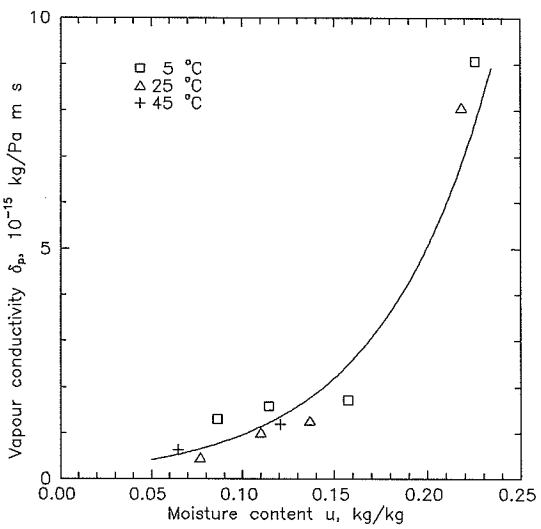

Figure 7.7. **Vapour conductivity of pine as function of moisture content and temperature.** $\rho_0 = 530$ kg/m^3. (From Tveit [52]).

to the ordinary cup method but with the cup turned upside down compared to the design outlined in Fig. 7.4. Furthermore, Thorsen [55] presented an air-escaped inverted cup. The intention with air-escaping the cup was to avoid subpressure in the cup when measuring on low permeability materials.

Schou and Thorsen assumed it possible to evaluate the liquid as well as the as the water vapour conductivity from the inverted cup experiment. It was assumed that in a specimen of thickness L the liquid transport takes place in a certain fraction $L - x$ of the thickness in the flow direction taken from the inside of the cup towards the outside. Finally, the transport in the rest x of the thickness is assumed to take place as vapour transport.

The distance x from the outside surface of the test specimen to capillary suction front inside the specimen was calculated by Thorsen and Schou under the following assumptions

- The relative humidity at the water front is 0.98
- Constant relative humidity and temperature at the outside surface
- Known stationary flow through the specimen

from the expression

$$x = \frac{m_{vac} - m_{wet}}{m_{vac} - (\tilde{u} + 1)m_{105}} L \tag{7.7}$$

where m_{vac} (kg) is the mass of the vacuum saturated test specimen, m_{wet} (kg) is the mass of the wet test specimen when the moisture flux is stationary, m_{105} (kg) is the mass of the specimen in oven dry condition and $\tilde{u}$ (kg/kg) is the mean moisture content of the vapour diffusion part of the specimen. $\tilde{u}$ is evaluated from the sorption isotherm of the material under investigation and the mean relative humidity in the vapour diffusion part of the specimen ((0.98 + φ_{out})/2).

The liquid conductivity is then evaluated from the Darcy Equation (4.16) and Eq. (3.53) as

$$K = -\frac{\vec{j}_2}{\frac{\partial p_2}{\partial x}} \approx -\frac{j_2}{\frac{p_2(L-x)-p_2(L)}{L-x}} \approx -\frac{j_2}{\frac{\rho_2 RT \ln(0.98)}{M_1}} \tag{7.8}$$

The water vapour conductivity is evaluated from Eq. (7.3) as

$$\delta_p = -\frac{j_1}{\frac{(\varphi_{out}-0.98)p_s(T)}{x}} \tag{7.9}$$

7.3.4 Evaluation with a least squares method

If the cup measurements are not made in the manner described by Bazant and Najjar (see section 7.3.2) the evaluation of the water vapour conductivity as a function of the relative water vapour pressure presents a difficulty. This section suggests a least squares method to overcome this difficulty.

Our starting point is the situation outlined in Fig. 7.5b, i.e. the relative humidity profile is non-linear. It is assumed that it is possible to describe the water vapour conductivity with an empirical expression of the form

$$\delta_\varphi = \delta_\varphi(\varphi) = \delta_\varphi(\varphi, \underline{c}) \quad , \quad \underline{c} = [c_1, c_2, \ldots, c_n]^T \tag{7.10}$$

where $\underline{c}$ is an unknown vector. Furthermore, it is assumed that it is possible to perform an analytical integration of this expression. The task now is to determine $\underline{c}$, whereafter it is possible to tabulate the empirical expression giving the water vapour conductivity as a function of the relative humidity.

The steady state condition in Fig. 7.5b is mathematically described by Fick's second law as

$$\frac{\partial}{\partial x}\left(\delta_\varphi(\varphi, \underline{c})\frac{\partial \varphi}{\partial x}\right) = 0 \tag{7.11}$$

Two times integration yields

$$\Delta_\varphi(\varphi, \underline{c}) = k_1 x + k_2 \quad , \quad \Delta_\varphi(\varphi, \underline{c}) = \int \delta_\varphi(\varphi, \underline{c}) d\varphi \tag{7.12}$$

where k_1 and k_2 are constants introduced from the integration. The boundary conditions are found from the Fig. 7.5b (the x-axis is positive in the direction of flow) as

$$\begin{aligned} \varphi &= \varphi_{out} \quad \text{for} \quad x = 0 \\ \varphi &= \varphi_{in} \quad \text{for} \quad x = L \end{aligned} \tag{7.13}$$

which gives

$$k_1 = \frac{1}{L}(\Delta_\varphi(\varphi_{in}, \underline{c}) - \Delta_\varphi(\varphi_{out}, \underline{c}))$$
$$k_2 = \Delta_\varphi(\varphi_{out}, \underline{c}) \tag{7.14}$$

Equation (7.12) now turns into

$$\Delta_\varphi(\varphi, \underline{c}) = (\Delta_\varphi(\varphi_{in}, \underline{c}) - \Delta_\varphi(\varphi_{out}, \underline{c}))\frac{x}{L} + \Delta_\varphi(\varphi_{out}, \underline{c}) \tag{7.15}$$

which gives the following expression for the water vapour flux

$$\begin{aligned}
\vec{j}_1 &= -\delta_\varphi(\varphi, \underline{c})\frac{\partial \varphi}{\partial x} \\
&= -\frac{\delta_\varphi(\varphi, \underline{c})}{\frac{\partial x}{\partial \varphi}} \\
&= -\frac{\delta_\varphi(\varphi, \underline{c})}{\frac{L}{\Delta_\varphi(\varphi_{in}, \underline{c}) - \Delta_\varphi(\varphi_{out}, \underline{c})}\frac{d}{d\varphi}\Delta_\varphi(\varphi, \underline{c})} \\
&= -\frac{\Delta_\varphi(\varphi_{in}, \underline{c}) - \Delta_\varphi(\varphi_{out}, \underline{c})}{L}
\end{aligned} \tag{7.16}$$

This expression is then fitted to a series of measurements of water vapour flux, inside and outside relative humidities with a least squares method which as output has an estimate on the vector $\underline{c}$.

A demonstration of the use of this method is given in the following part of this section. Table 7.1 shows a series of cup-measurements on a test specimen with thickness $L = 0.022$ m of an unspecified material. The measurements were presented as one of 4 test cases by Wadsö [56]. Admittedly the measurements are well-suited for treatment with Bazant and Najjar's method. Nevertheless they are used to illustrate the method presented in this section

It is assumed that it is possible to describe the water vapour conductivity with the empirical expression

$$\delta_\varphi(\varphi, \underline{c}) = c_1 \exp(c_2 \varphi) \tag{7.17}$$

which yields

$$\Delta_\varphi(\varphi, \underline{c}) = \frac{c_1}{c_2}\exp(c_2 \varphi) \tag{7.18}$$

From Eq. (7.16) we get

Table 7.1. **Water vapour flux through porous material during cup method measurement as a function of inside and outside relative humidity.** (From Wadsö [56]).

φ_{in}	φ_{out}	j_1 10^{-9} kg/m^2 s
0.40	0.50	13.2
0.40	0.55	20.0
0.40	0.60	26.8
0.40	0.65	34.5
0.40	0.70	43.2
0.40	0.75	54.4
0.40	0.80	63.6
0.40	0.85	77.3
0.40	0.90	90.9
0.40	0.95	113.6

$$j_1 = -\frac{c_1}{c_2 L}(\exp(c_2\varphi_{in}) - \exp(c_2\varphi_{out})) \tag{7.19}$$

A non-linear regression analysis with Eq. (7.19) as model, φ_{in} and φ_{out} as the dependent variables and j_1 as the independent variable gave $c_1 = 0.89367 \cdot 10^{-9}$ kg/m s and $c_2 = 2.2698$. Figure 7.8 shows the calculated versus measured vapour fluxes.

The relative humidity profiles in the test specimen during the cup-measurement is found by combination of Eq. (7.19) and Eq. (7.15) to

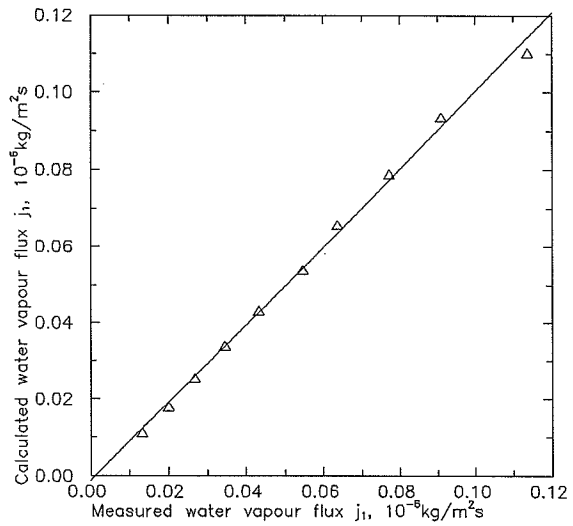

Figure 7.8. **Calculated versus measured water vapour flux. Calculated with Eq. (7.18) and $c_1 = 0.89367 \cdot 10^{-9}$ kg/m s and $c_2 = 2.2698$ found by non-linear regression of data from Table 7.1.**

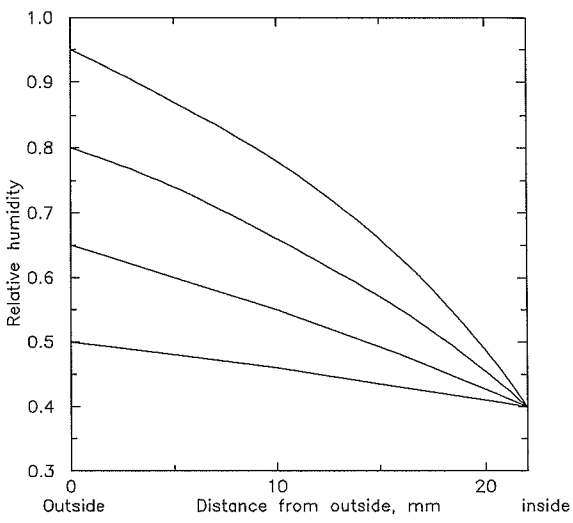

Figure 7.9. **Relative humidity profile during cup experiment. Calculated with Eq. (7.20) for the measurements given in Table 7.1.**

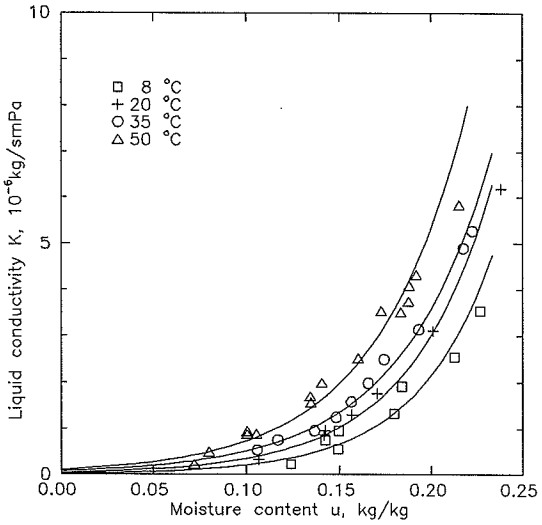

Figure 7.10. **Liquid conductivity of quartz sand as a function of temperature and moisture content.** (From Bories *et al.* [59], Crausse *et al.* [60]).

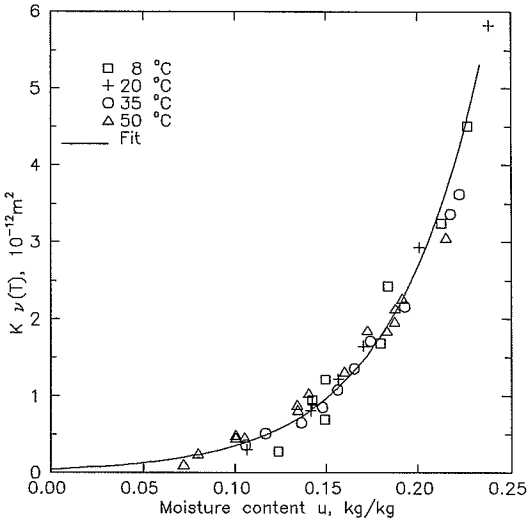

Figure 7.11. **Product of liquid conductivity and kinematic viscosity as a function of moisture content.** (After Bories *et al.* [59], Crausse *et al.* [60]).

$$\varphi = \frac{1}{c_2} \ln\left([\exp(c_2\varphi_{in}) - \exp(c_2\varphi_{out})] \frac{x}{L} + \exp(c_2\varphi_{out}) \right) \tag{7.20}$$

The relative humidity profiles calculated with the expression Eq. (7.20) for the measurements presented in Table 7.1 are shown in Fig. 7.9.

7.4 Liquid conductivity

In this section two methods for the measurement of liquid conductivity of porous material are presented.

7.4.1 Darcy experiment

In the classical experiment by Darcy the flow of water through a saturated sand bed was examined. It was found that the flow rate was proportional to the pressure gradient. The proportionality factor K (kg/m s Pa) which is denoted the capillary conductivity is found from the Darcy's first law Eq. (4.16) as

$$K = -\frac{\vec{j}_2}{\frac{\partial p_2}{\partial x}} \tag{7.21}$$

7.4.2 Bories *et al.*'s method

Bories and co-workers from the Study Group on Porous Media at the Institut de Mécanique des Fluides, C.N.R.S. in Toulouse developed an approach for the simulation of coupled heat

and moisture transfer in porous media based on the use of the set of equations (6.16) and (6.17), see Bories *et al.* [57], [59], Bombaud *et al.* [58], and Crausse *et al.* [60], [61], [62]. As a part of this approach, methods for the measurement of the necessary material properties were developed.

The experimental set-up is shown in Fig. 7.12. The test specimen has the shape of a column encapsulated in a steel tube. The steel tube is connected to a water reservoir through a reversible constant flow pump. During the experiment the moisture content distribution $u(x)$ is monitored with the gamma ray equipment. Simultaneously the hydraulic pressure distribution $p_2(x)$is measured with the pressure transducers. The moisture flux j_2 (kg/m^2 s) is found by integration of the moisture profiles.

With the described experimental set-up and procedure it is possible to simultaneously determine the hydraulic pressure $p_2(u,T)$ as a function of moisture content and temperature. The liquid conductivity $K(u,T)$ as a function of moisture conductivity is found from Darcy's first law Eq. (7.21).

The liquid conductivity of quartz sand was measured as a function of moisture content and temperature. The measurements were reported in [59], [60], [61], see Fig. 7.10. The experiments were carried out at a number of different but constant temperatures. The experiments were one-dimensional isothermal drying experiments.

According to Eq. (4.19) it is theoretically possible to separate the temperature dependence and the moisture content dependence of the liquid conductivity. This is illustrated in Fig. 7.11 where the product of liquid conductivity and kinematic viscosity is shown as a function of moisture content. It it seen that the four liquid conductivities measured at four different temperatures (Fig. 7.10) collapses to one master profile. This master profile is seen to be well described by the empirical relation

$$K\nu(T) = 46.2029 \cdot 10^{-15}\ \mathrm{m}^2 \exp(20.3163u) \tag{7.22}$$

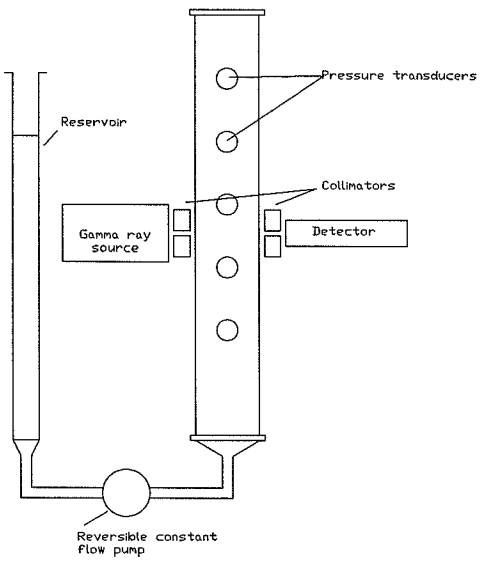

Figure 7.12. **Experimental set-up for measurement of moisture content andsuction pressure during isothermal drying or water up-take. The moisture content is measured by gamma ray spectroscopy. The suction pressure is measured by means of pressure transducers. The water flux is found from integration of the moisture profiles.** (From Bombaud *et al.* [58], Crausse *et al.* [60]).

7.5 Sorption isotherms

Sorption isotherms are measured by observing the equilibrium between water physically or chemically bound on the outer and the inner surface of a test specimen of a porous material and the water vapour in the surrounding air. In a sorption experiment the mass of water bound by the test specimen, the water vapour pressure and the temperature is measured.

As the name reflects, the sorption isotherm is measured at constant temperature. At constant temperature water vapour pressure and relative humidity are synonymous. It is possible to establish the sorption isotherm in adsorption as well as in desorption (see Fig. 3.3). In principle, adsorption isotherms are measured by bringing the porous material from an absolute dry condition into moisture equilibrium at a given water vapour pressure. In principle, desorption isotherms are measured by desiccating the porous material from an absolute wet condition to equilibrium at a given water vapour pressure. By measuring the amount of adsorbate in the test specimen at a number of different water vapour pressures it is possible to construct the sorption isotherm.

The absolute dry condition is obtained by oven-drying the test specimen under investigation or by desiccating it in a desiccator, for instance with silica gel or $Mg(ClO_4)_2$. The absolute wet condition is obtained by vacuum or pressure saturation. It has to be noted that the methods described here might destroy the structure of some materials and therefore should be used with care. Alternatively, less rigoristic definitions have to be applied. In this case, care should be taken that the experimental conditions are such that they can be categorized as true adsorption or true desorption.

The experimental apparatus for the measurement of sorption isotherms are a laboratory with a well-known and constant temperature, a drying oven, a laboratory scale, a vacuum pump and a number of desiccators with different salt solutions or pure water yielding a definite relative water vapour pressure. Small samples of the material under investigation are placed in the desiccators. In order to reduce the experimental time and avoid adsorption of other atmospheric gases, the desiccators should be evacuated to the saturation water vapour pressure of the salt solution at the actual experimental temperature.

The mass of the samples is measured at regular intervals until constant mass is obtained. The moisture content is now computed from this steady state mass and the mass of the dry specimen.

The desiccators and the salt solutions might conveniently be replaced by high precision climate chambers, where it is possible to control as well the relative humidity as the temperature.

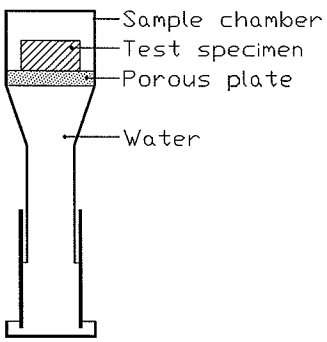

Figure 7.13. **Suction plate apparatus.** (From Lund-Hansen [64]).

In stead of sorption isotherms one can measure the sorption isosteres and calculate the sorption isotherms from the latter. In the isostere experiment the moisture content of a test specimen is kept constant and the vapour pressure is measured as a function of temperature. An equipment for measurement of sorption isosteres is described by Radjy *et al.* [17].

Examples of sorption isotherms are found in section 3.3, where also the thermodynamics of adsorption is presented.

7.6 Suction curves

Suction curves are measured with suction plate apparatus, pressure plates membrane, centrifuge, rate of penetration of wetting liquids and displacement. These methods are reviewed by Fagerlund [63]. An example of a suction plate apparatus taken from Lund-Hansen [64] is shown in Fig. 7.13.

Furthermore, it is possible calculate a part of a suction curve from the sorption isotherm, mercury intrusion porosimetry and microcalorimeter measurements. Generally it is possible to calculate suction curves from pore size distributions and the Laplace Equation (3.51).

An example of a suction curve for cellular concrete is shown in Fig. 3.22.

7.7 Vapour diffusivity

The water vapour diffusivity of a porous material can be calculated from Eq. (4.14) if the factor $\zeta(u)$ and the sorption isotherm $u(\varphi,T)$ are known. This method was used by Crausse *et al.* [61], [62] to calculate the water vapour diffusivity of glass wool, see Fig 7.14. In stead of the sorption isotherm Crausse *et al.* used the suction curve $p_2(u,T)$ of glass wool and the Kelvin equation (3.52). The factor $\zeta(u)$ was assumed to be a linear function of the moisture content

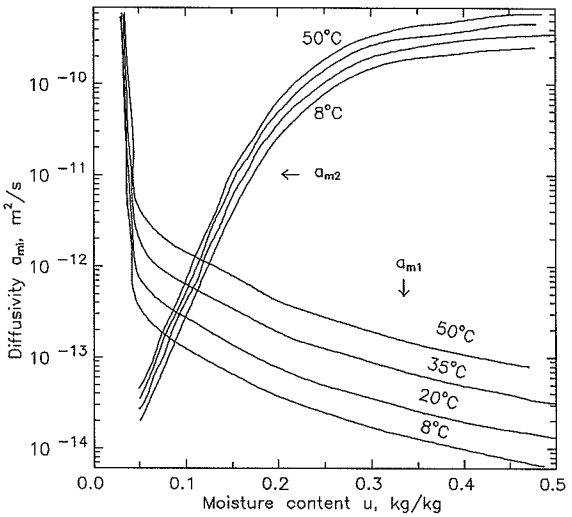

Figure 7.14. **Water vapour and liquid diffusivity of glass wool as a function of temperature and moisture content. Perpendicular to the fibres.** ρ_0 = 77 kg/m^3. (From Crausse *et al.* [61], [62]).

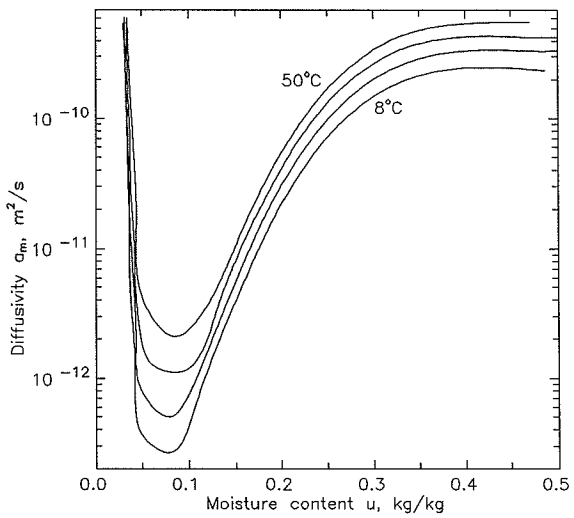

Figure 7.15. **Moisture diffusivity of glass wool as a function of temperature and moisture content. Perpendicular to the fibres.** ρ_0 = 77 kg/m^3. (Data from Crausse *et al.* [61], [62]).

given by $\zeta(0) = 1$ and $\zeta(u_{vac}) = 0$.

Furthermore, it is possible to calculate the water vapour diffusivity of a porous material from the water vapour conductivity δ_p measure with the cup-method, the saturation water vapour pressure p_s, the dry density ρ_0 and the sorption isotherm $u(\varphi,T)$, as

$$a_{m1} = \frac{\delta_p p_s}{\rho_0 \left(\frac{\partial u}{\partial \varphi}\right)_T} \tag{7.23}$$

Equation (7.23) can be found by combination of Eq. (4.5), (4.6) and (4.14).

7.8 Liquid diffusivity

This section describes methods for the measurement of liquid diffusivity.

7.8.1 Boltzmann transformation

Isothermal flow of moisture in the form of liquid is described by Fick's second law

$$\frac{\partial u}{\partial \tau} = \frac{\partial}{\partial x}\left(a_{m2}(u)\frac{\partial u}{\partial x}\right) \tag{7.24}$$

Introducing the Boltzmann transformation

$$\lambda = x\tau^{-1/2} \quad \Leftrightarrow \quad x = \lambda\sqrt{\tau} \quad \Leftrightarrow \quad \tau = (x/\lambda)^2 \tag{7.25}$$

into Eq. (7.24) gives

$$\frac{\partial u}{\partial (x/\lambda)^2} = \frac{\partial}{\partial (\lambda\sqrt{\tau})}\left(a_{m2}(u)\frac{\partial u}{\partial (\lambda\sqrt{\tau})}\right) \quad \Leftrightarrow$$

$$\frac{1}{x^2}\frac{\partial u}{\partial \lambda^{-2}} = \frac{1}{\sqrt{\tau}\partial\lambda}\left(\frac{a_{m2}(u)}{\sqrt{\tau}}\frac{\partial u}{\partial \lambda}\right) \quad \Leftrightarrow$$

$$\frac{1}{(\lambda\sqrt{\tau})^2}\frac{1}{-2\lambda^{-3}}\frac{\partial u}{\partial \lambda} = \frac{1}{\tau}\frac{\partial}{\partial \lambda}\left(a_{m2}(u)\frac{\partial u}{\partial \lambda}\right) \quad \Leftrightarrow$$

$$\frac{\lambda}{-2}\frac{\partial u}{\partial \lambda} = \frac{\partial}{\partial \lambda}\left(a_{m2}(u)\frac{\partial u}{\partial \lambda}\right) \tag{7.26}$$

It is seen that we now have an equation in two variables and thereby the ordinary differential equation

$$-\frac{\lambda}{2}\frac{du}{d\lambda} = \frac{d}{d\lambda}\left(a_{m2}(u)\frac{du}{d\lambda}\right) \tag{7.27}$$

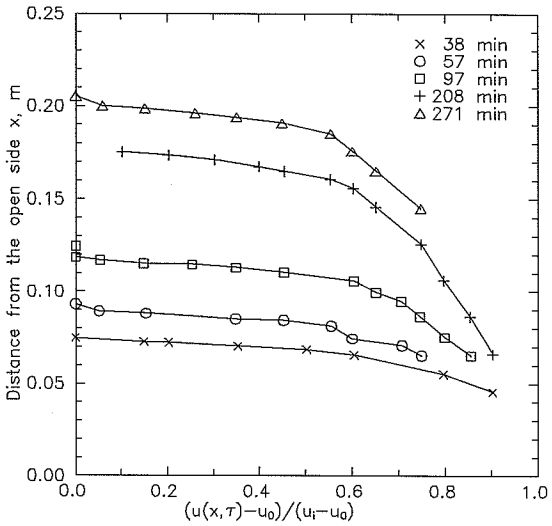

Figure 7.16. **Moisture profiles measured during water absorption into a mortar bar (1:3:12 OPC/lime/sand).** (Data from Hall [65], p. 53).

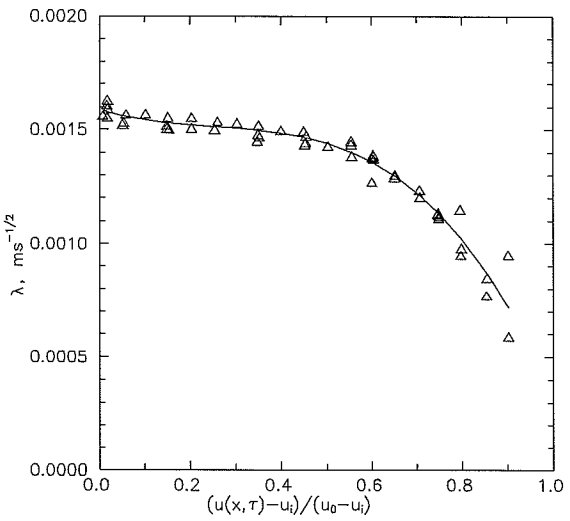

Figure 7.17. **Boltzmann transformed moisture profiles calculated from data in Fig 7.16.**

where it is possible to separate the variables and perform integration as

$$-\frac{1}{2}\int \lambda(u)\mathrm{d}u = \int \mathrm{d}\left(a_{m2}(u)\frac{\mathrm{d}u}{\mathrm{d}\lambda}\right) + I_0 \tag{7.28}$$

I_0 is a constant introduced by the integration.

The initial and boundary conditions applied with a semi-infinite body under isothermal water uptake or drying are

$$\begin{aligned} u(x,\tau) &= u_i \quad \text{for} \quad x \geq 0 \quad \text{and} \quad \tau = 0 \\ u(x,\tau) &= u_0 \quad \text{for} \quad x = 0 \quad \text{and} \quad \tau > 0 \\ u(x,\tau) &= u_i \quad \text{for} \quad x \to +\infty \quad \text{and} \quad \tau > 0 \end{aligned} \tag{7.29}$$

The corresponding Boltzmann transformed initial and boundary conditions are

$$\begin{aligned} u(\lambda) &= u_i \quad \text{for} \quad \lambda \to +\infty \\ u(\lambda) &= u_0 \quad \text{for} \quad \lambda = 0 \\ u(\lambda) &= u_i \quad \text{for} \quad \lambda \to +\infty \end{aligned} \tag{7.30}$$

The use of these boundary and initial conditions with Eq. (7.28) gives

$$a_{m2}(u) = -\frac{1}{2}\frac{\mathrm{d}\lambda}{\mathrm{d}u}\int_{u_i}^{u} \lambda(u)\mathrm{d}u \tag{7.31}$$

In Fig. 7.16 moisture profiles measured by Hall [65] are shown. The corresponding Boltzmann transformed moisture profiles are shown in Fig. 7.17. It is seen that the profiles shown

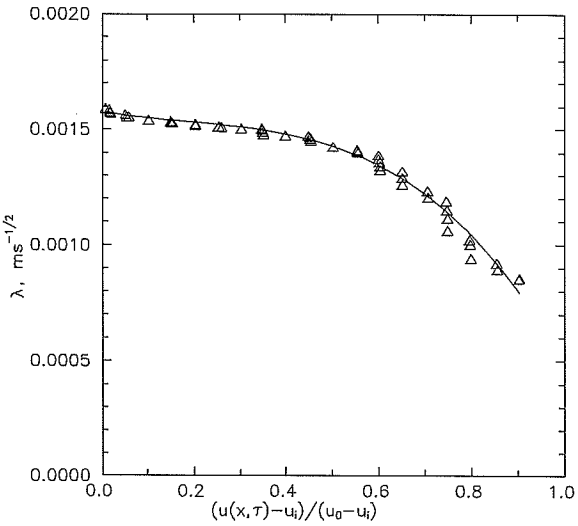

Figure 7.18. **Smoothed Boltzmann transformed moisture profiles calculated from Fig 7.17.**

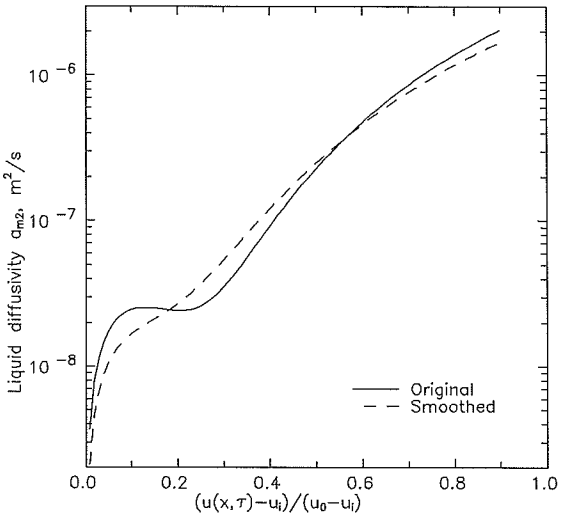

Figure 7.19. **Liquid diffusivity of mortar (1:3:12 OPC/lime/sand) as a function of moisture content.**

in Fig. 7.16 now have collapsed to one master profile. According to Kohonen [66] this process is equal to volume averaging of the liquid diffusivity, which is very important due to the pronounced spatial inhomogenity of building materials. A third order polynomial of the form

$$\lambda(u) = c_0 + c_1 u + c_2 u^2 + c_3 u^3 \tag{7.32}$$

has been fitted to the Boltzmann transformed moisture profile in Fig. 7.17 and the liquid diffusivity a_{m2} has been calculated from Eq. (7.31). The moisture content u was transformed into the dimensionless moisture content $(u(x,\tau)-u_i)/(u_0-u_i)$.

The calculated liquid diffusivity is very sensitive to deflections of the fitted polynomial originating from measurement errors and spatial inhomogenity not eliminated by the Boltzmann transformation. This sensitivity is due to the error magnification of the numerical differentiation, which must be performed in order to evaluate Eq. (7.31). It is therefore often necessary to perform data smoothing on the Boltzmann transformed data. Is not easy to give guide-lines for data smoothing. Smoothing of data is an art, not an exact science. In Fig. 7.18 the data from Fig. 7.17 is smoothed by use of a "windowed median" and a polynomial of third order is fitted the smoothed data (see Press *et al.* [67] for a description of the "windowed median" technique).

In Fig. 7.19 the liquid diffusivities as a function of moisture content calculated from the polynomials shown in Fig. 7.17 and Fig. 7.18. are compared. It is seen that the diffusivity calculated from the unsmoothed data exhibits a more pronounced minimum for a dimensionless moisture content equal to 0.2 than the liquid diffusivity calculated from the smoothed data. The reason is that the least squares method used to estimate the coefficients of the polynomial puts most stress on the "outliers". A maybe more feasible method is "robust" data fitting, "robust" in the sense that less stress is put on the "outliers" (see e.g. Madsen [68]).

7.8.2 Sorptivity measurements

In this section two methods for the calculation of liquid diffusivity from sorptivity measurements are presented. Sorptivity measurements are also known as capillary suction experiments.

Sorptivity measurements are very simple laboratory experiments to perform. All that is needed is a laboratory scale, a watch and a drying oven. The principle of the sorptivity measurement is that one end of a test specimen of the material under investigation is brought in contact with water and the weight change of the specimen is recorded.

Sorptivity measurements exhibit the well known characteristic weight increase proportional with the square root of time. An example of the sorptivity of cellular concrete is presented in Fig. 7.20. The sorptivity curve is calculated from moisture profiles measured by Nielsen [69], see Fig. 7.21.

For both of the two presented methods it is assumed that the sorption takes place as diffusion into a semi-infinite media. It is assumed that the diffusivity is constant whereby Eq. (7.24) is reduced to

$$\frac{\partial u}{\partial \tau} = a_{m2}\frac{\partial^2 u}{\partial x^2} \tag{7.33}$$

The boundary conditions and initial conditions are the ones given by Eq. (7.29) although it is seen from Fig. 7.21 that the boundary conditions in reality are not fully satisfied. Under these restrictions the error function solution

$$u(x,\tau) = u_0 - (u_0 - u_i)\mathrm{erf}\left(\frac{x}{2\sqrt{a_{m2}\tau}}\right) \tag{7.34}$$

can be applied where the error function is given as

$$\mathrm{erf}(x) = \frac{2}{\sqrt{\pi}}\int_0^x \exp(-\lambda^2)\mathrm{d}\lambda \tag{7.35}$$

According to Standard Mathematical Tables [70] the error function can also be series expanded to

$$\mathrm{erf}(x) = \frac{2}{\sqrt{\pi}}\sum_{n=0}^{\infty}\frac{(-1)^n}{n!(2n+1)}x^{2n+1} \tag{7.36}$$

In the analysis of sorption is often tacitly assumed that the water moves into the test specimen as a sharp front behind which specimen is saturated and ahead of which the specimen is completely dry. The error function solution is not well fitted for the description of such a front. The distance x from the wet surface to the place in a semi-infinite body where the moisture content is zero is found from Eq. (7.34) assuming that $u_i = 0$ as

$$u(x,\tau) = 0 \quad \Leftrightarrow \quad \mathrm{erf}\left(\frac{x}{2\sqrt{a_{m2}\tau}}\right) = 1 \tag{7.37}$$

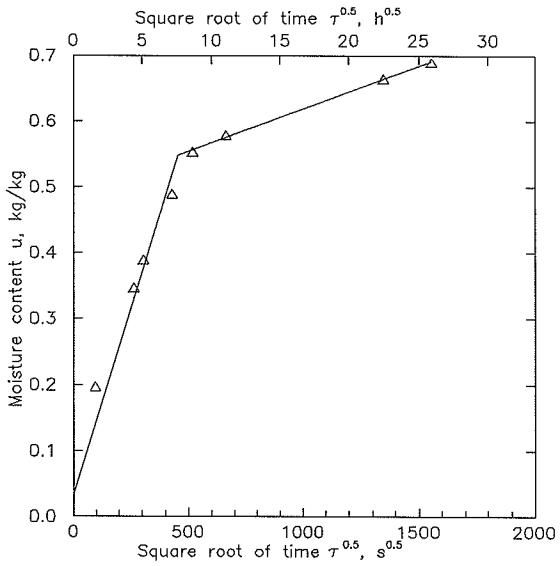

Figure 7.20. **Moisture content of cellular concrete as function of the square root of time. Calculated from the data presented in Fig 7.21.**

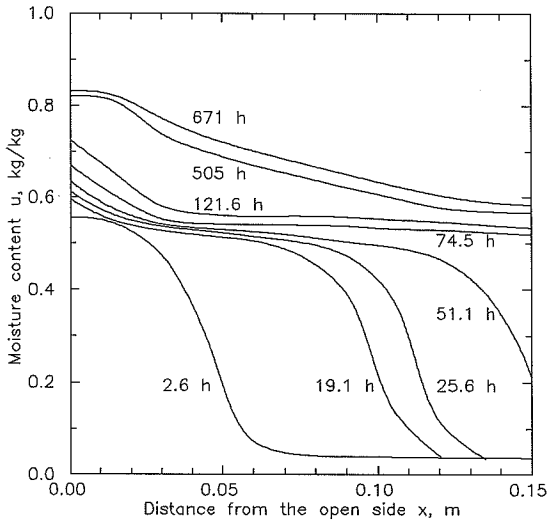

Figure 7.21. **Moisture content of cellular concrete as a function of time and distance during capillary suction.** ρ_0 = 573 kg/m^3. (From Nielsen [69]).

It is seen that the argument of the error function and thereby x must be equal to infinity in order to fulfil that the value of the error function is equal to 1. This is a natural limitation originating from partial differential equations similar to the Fick's second law type. This is frequently overcome by assuming that the position of the front and the respective error function solution argument are given by (*first* method)

$$x = 4\sqrt{a_{m2}\tau} \quad \Rightarrow \quad \frac{x}{2\sqrt{a_{m2}\tau}} = 2 \tag{7.38}$$

The error function taken to the argument of 2 is approximately

$$\text{erf}(2) = 0.99532 \tag{7.39}$$

which is seen to be an approximation to the right hand side of Eq. (7.37).

The mass of water m_2 (kg) taken up by the specimen during the sorptivity measurement is proportional to the square root of time, τ (s),

$$m_2 = SA\rho_2\sqrt{\tau} \tag{7.40}$$

where S (m s$^{-1/2}$) is defined as the sorptivity, A (m^2) is area of the specimen subjected to water, ρ_2 (kg/m^3) is the density of water. If the water moves frontwise into the specimen the mass of water in the specimen is given by

$$m_2 = xAp\rho_2 \tag{7.41}$$

where p (-) is the open porosity. If all the porosity is assumed to be open combination of Eq. (7.40) and (7.41) gives

$$x = \frac{S}{p}\sqrt{\tau} = \frac{S}{1-\frac{\rho_0}{\rho_s}}\sqrt{\tau} \tag{7.42}$$

where ρ_s (kg/m^3) is the solid density.

The approximate description of the front position Eq. (7.38) and Eq. (7.42) yields the *first* expression for the liquid diffusivity

$$a_{m2} = \frac{1}{16}\left(\frac{S}{1-\rho_0/\rho_s}\right)^2 \tag{7.43}$$

The *second* expression for the liquid diffusivity, calculated from sorptivity measurements, is found by regarding Fick's first law for the water flux throughout the specimen

$$\vec{j}_2 = -a_{m2}\rho_0\frac{\partial u}{\partial x} \tag{7.44}$$

The validity of Eq. (7.33) and (7.34) is still taken as granted. The moisture content gradient is found by differentiation by Leibniz' rule of Eq. (7.34) as

$$\frac{\partial u}{\partial x} = \frac{u_i - u_0}{\sqrt{\pi a_{m2}\tau}}\exp\left(-\frac{x^2}{4a_{m2}\tau}\right) \tag{7.45}$$

The moisture content gradient at the surface where water enters the specimen is then

$$\left.\frac{\partial u}{\partial x}\right|_{x=0} = \frac{u_i - u_0}{\sqrt{\pi a_{m2}\tau}} \tag{7.46}$$

The mass of water taken up by the specimen per unit area at a given time is found by integration of the flux at the surface

$$\int_0^{\tau'} j_2|_{x=0}\,d\tau = -\int_0^{\tau'} a_{m2}\rho_0\frac{u_i - u_0}{\sqrt{\pi a_{m2}\tau}}\,d\tau \tag{7.47}$$

to

$$\frac{m_2}{A} = 2\sqrt{\frac{a_{m2}}{\pi}}\rho_0(u_0 - u_i)\sqrt{\tau'} \tag{7.48}$$

If the boundary condition at the wet surface is taken as $u_0 = u_{vac}$ and Eq.(7.48) is combined with Eq. (7.40) the liquid diffusivity is given by

$$a_{m2} = \frac{\pi}{4}\left(\frac{S\rho_2}{\rho_0(u_{vac} - u_i)}\right)^2 \tag{7.49}$$

7.9 Moisture diffusivity

In this section methods for the determination of moisture diffusivity are presented. In addition to these methods the moisture diffusivity is easily calculated from Eq. (6.11) as the sum of the water vapour diffusivity a_{m1} and the liquid diffusivity a_{m2}, see Fig. 7.15 where the moisture diffusivity is calculated from the liquid and water vapour diffusivities in Fig. 7.14.

7.9.1 Krischer's method

Krischer [8] has described a method for the measurement of moisture diffusivity from an isothermal one-dimensional drying experiment (in principle also from a capillary suction experiment). In the experiment the specimen is subjected to the boundary conditions

$$\begin{aligned} &\frac{\partial u}{\partial x} = 0 \qquad \text{for} \quad x = 0 \quad \text{and} \quad \tau > 0 \\ &u(x,\tau) = u_0 \quad \text{for} \quad x = L \quad \text{and} \quad \tau > 0 \end{aligned} \tag{7.50}$$

where L (m) is the thickness of the specimen in the flow direction.

The isothermal moisture flow is assumed to be governed by Fick's second law

$$\frac{\partial u}{\partial \tau} = \frac{\partial}{\partial x}\left(a_m \frac{\partial u}{\partial x}\right) \tag{7.51}$$

To use the method it is necessary to have a knowledge of the moisture content as a function of time and distance from the open end of the test specimen under investigation. The moisture profiles shown in Fig. 7.21 are an example of the type of measurements, which it is necessary make in order to use the method.

Equation (7.51) is integrated as

$$\begin{aligned} \int_0^{x'} \frac{\partial u}{\partial \tau} dx &= \int_0^{x'} \frac{\partial}{\partial x}\left(a_m \frac{\partial u}{\partial x}\right) dx \\ &= a_m \frac{\partial u}{\partial x}\bigg|_{x=x'} - a_m \frac{\partial u}{\partial x}\bigg|_{x=0} \end{aligned} \tag{7.52}$$

As the flux is zero for $x = 0$ the moisture diffusivity is found from Eq. (7.52) as

$$a_m = \frac{\int_0^{x'} \frac{\partial u}{\partial \tau} dx}{\frac{\partial u}{\partial x}\Big|_{x=x'}} \tag{7.53}$$

The numerator and the denominator can be found by numerical integration and numerical differentiation respectively of the moisture profiles. The moisture diffusivity can be taken as valid at the mean moisture content between the moisture contents at $x = x'$ given by the moisture profiles used in the calculation. By using several profiles and values of x' the moisture diffusivity is found as a function of moisture content.

7.9.2 Stationary moisture flux

The stationary moisture flux experiment is somewhat equivalent to the cup method experiment. A test specimen is subjected to stationary boundary conditions under which a one-dimensional flow takes place. The moisture flux through the specimen is monitored and when it is stationary the moisture concentration or the relative humidity profile is evaluated.

The moisture concentration profile is evaluated by slicing the test specimen and use of Eq. (3.6). Other methods are the use of γ-ray spectroscopy or calibrated electrical conductance/capacity methods. Finally, the moisture concentration profile can be evaluated from the relative humidity profile and the sorption isotherm of the material under investigation.

The relative humidity profile is measured with relative humidity sensors in the specimen at various depths, see Hedenblad [71].

With the knowledge of the moisture concentration profile and the moisture flux j_{12} (kg/m^2 s) we are in a situation equivalent to the one in Fig. 7.5b. The moisture diffusivity as a function of moisture content is evaluated from the flux expression

$$\vec{j}_{12} = \vec{j}_1 + \vec{j}_2 = -a_m \rho_0 \frac{\partial u}{\partial x} \tag{7.54}$$

as

$$a_m = -\frac{\vec{j}_{12}}{\rho_0 \frac{\partial u}{\partial x}} \tag{7.55}$$

Equation (4.13), Eq. (4.21) and Eq. (6.11) were used in the derivation of Eq. (7.55). Isothermal conditions are assumed. The partial derivative $\partial u/\partial x$ of the moisture content u with respect to the space coordinate x is evaluated numerically from the moisture content profile at a number of locations x_i. The moisture diffusivity is evaluated at the corresponding moisture contents u_i.

If only the relative humidity profile is known the water vapour pressure conductivity can be evaluated as a function of relative humidity as

$$\delta_\varphi = -\frac{\vec{j}_{12}}{\frac{\partial \varphi}{\partial x}} \tag{7.56}.$$

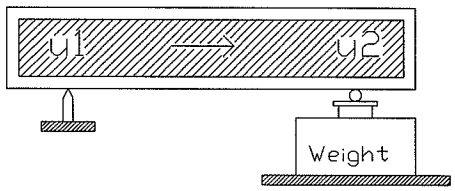

Figure 7.22. **Moment method. Experimental set-up.** (From Gaffner [73]).

Van der Kooi [72] and Krischer *et al.* [8] used the stationary moisture flux method for the determination of moisture diffusivity of cellular concrete as a function of moisture content. Hedenblad [71] used the stationary moisture flux method for the determination of water vapour conductivity of concrete.

7.9.3 Moment method

Gaffner [73] has described the so-called moment method for the measurement of moisture diffusivity. The experimental set-up is schematically shown in Fig. 7.22 . The principle in the moment method is that a sealed bar composed of two pieces of the porous material under investigation with different initial moisture contents u_1 and u_2 respectively is placed on a laboratory scale and a fulcrum. As the moisture content difference between the two half-parts of the bar equilibrates with time the reading on the balance changes. The weight change with time is dependent on the moisture diffusivity.

An analysis of this experiment can be found in Cunningham *et al.* [74]. The following elucidation follows that given by Cunningham *et al.*

Referring to Fig. 7.22 we have

$$F_1 + F_2 = F_T \tag{7.57}$$

where F_1 (N) is the vertical reaction from the fulcrum, F_2 (N) is the vertical reaction from the balance and F_T (N) is the gravitational force acting in the centre of gravity of the specimen. Therefore, by differentiation with respect to time we get

$$\frac{dF_1}{d\tau} = -\frac{dF_2}{d\tau} \tag{7.58}$$

since F_T is constant in a sealed specimen.

Taking moments about the fulcrum on the balance, we get

$$F_1 L_0 - F_T \gamma - A g \int_{-\alpha}^{\beta} \rho_0 u(x) x dx = 0 \tag{7.59}$$

where L_0 (m) is the horizontal distance between the fulcrums, γ (m) is the horizontal distance from the fulcrum of the balance to the centre of gravity, A (m^2) is the cross-sectional area of the test specimen, g (m/s^2) is the acceleration due to gravity, $-\alpha$ (m) is the horizontal distance from the balance fulcrum to the nearest end of the test specimen, β (m) is the horizontal distance from the balance fulcrum to the remote end of the test specimen, $u(x)$ (kg/kg) is the moisture content at the distance x from the balance fulcrum, ρ_0 (kg/m^3) is the dry density of the specimen.

Differentiation with respect to τ gives

$$L_0 \frac{dF_1}{d\tau} - A g \rho_0 \int_{-\alpha}^{\beta} \frac{du}{d\tau} x dx = 0 \tag{7.60}$$

or

$$-L_0\frac{dF_2}{d\tau}-Ag\rho_0\int_{-\alpha}^{\beta}\frac{du}{d\tau}x\,dx=0 \tag{7.61}$$

Combination of Fick's second law of diffusion Eq. (7.51) with Eq. (7.61) yields

$$-L_0\frac{dF_2}{d\tau}-Ag\rho_0\int_{-\alpha}^{\beta}x\frac{\partial}{\partial x}\left(a_m\frac{\partial u}{\partial x}\right)dx=0 \tag{7.62}$$

Integrating by parts

$$-L_0\frac{dF_2}{d\tau}-Ag\rho_0\left(\beta a_m\frac{\partial u}{\partial x}\bigg|_{\beta}+\alpha a_m\frac{\partial u}{\partial x}\bigg|_{-\alpha}-a_m(u(\beta)-u(-\alpha))\right)=0 \tag{7.63}$$

Assuming a_m to be constant over the range of interest, then

$$a_m=\frac{L_0\frac{dF_2}{d\tau}}{-Ag\rho_0\left(u(\beta)-u(-\alpha)-\beta\frac{\partial u}{\partial x}\big|_{\beta}-\alpha\frac{\partial u}{\partial x}\big|_{-\alpha}\right)} \tag{7.64}$$

If it is assumed that a uniform moisture content distribution of u_2 and u_1 exists in the right- and left-hand side of the test specimen respectively, then

$$F_2=u_2\rho_0LAg=u(-\alpha)\rho_0LAg \tag{7.65}$$

and

$$F_1=u_1\rho_0LAg=u(\beta)\rho_0LAg \tag{7.66}$$

where L (m) is the half of the length of the total sample.

Since the sample is sealed at each end and the initial moisture content is assumed uniform in each piece, then

$$\frac{\partial u}{\partial x}\bigg|_{\beta}=\frac{\partial u}{\partial x}\bigg|_{-\alpha}=0 \tag{7.67}$$

Hence, we have

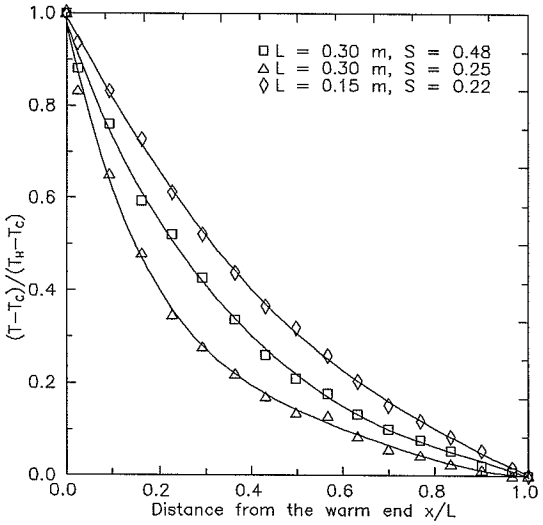

Figure 7.23. **Steady-state temperature profiles in Waukegan soil. L refers to the length of the test specimen. T_C and T_H refers to the temperature of the cold and the warm end of the specimen respectively. $T_C = 19.6$ °C, $T_H = 40.4$ °C for specimen with $S = 0.48$. $T_C = 20.1$ °C, $T_H = 40.0$ °C for specimen with $S = 0.25$. $T_C = 21.0$ °C, $T_H = 40.0$ °C for specimen with $S = 0.22$.** (From Shah *et al.* [75]).

$$a_m = \frac{L_0 \frac{dF_2}{d\tau}}{A g \rho_0 (u_2 - u_1)}$$

$$= \frac{L_0 L \frac{dm}{d\tau}}{A \rho_0 (u_2 - u_1)}$$

$$= \frac{L_0 L \frac{dm}{d\tau}}{m_2 - m_1} \tag{7.68}$$

where m_1 (kg) and m_2 (kg) are respectively the initial mass of moisture in part 1 and 2 of the specimen and m (kg) is the mass reading from the balance.

7.10 Thermogradient coefficient

In this section two methods for the determination of the thermogradient coefficient are presented.

7.10.1 Measurement of the thermogradient coefficient

A method for the measurement of the thermogradient coefficient is found directly from Eq. (6.16).

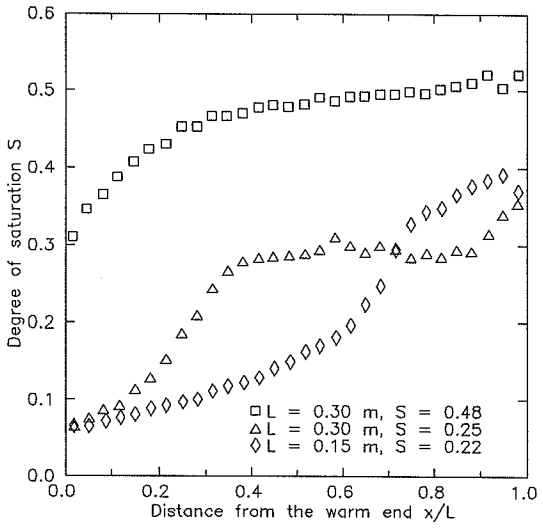

Figure 7.24. **Steady-state moisture profiles in Waukegan soil. L refers to length of the test specimen.** (From Shah *et al.* [75]).

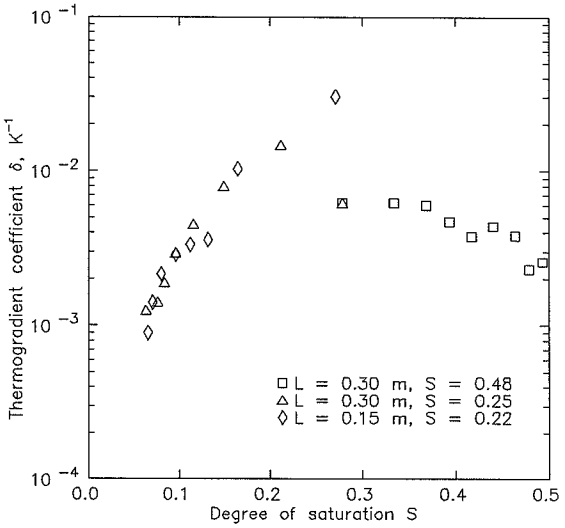

Figure 7.25. **Thermogradient coefficient of Waukegan soil.** (From Shah *et al.* [75]).

Consider a sealed moist test specimen of a porous material subjected to a 1-dimensional thermal gradient. After a certain period of experimental time has elapsed a steady-state condition is obtained, where neither the moisture content nor the temperature changes in any point of the test specimen. This means that the total moisture flux is zero and then it follows from Eq. (6.16) that

$$\delta = -\frac{\frac{\partial u}{\partial x}}{\frac{\partial T}{\partial x}} \tag{7.69}$$

Shah *et al.* [75] used this method for the measurement of the thermogradient coefficient of soils. In their experimental set-up Shah and co-workers used sealed cylindrical soil samples with a diameter of 3.5 cm and a length of 15 and 30 cm. Fig 7.23 shows the steady-state temperature profiles measured by Shah *et al.* at three different degrees of saturation in a sample of Waukegan soil. The steady-state temperature conditions were reached within 18 days. In Fig. 7.24 the corresponding steady-state moisture profiles are presented. The steady-state moisture conditions were reached within 58 days. The thermogradient coefficient calculated from Eq. 7.69 is shown in Fig. 7.25.

The Waukegan soil is classified as silt loam and is composed of 28.0% gravel and sand (> 0.074 mm), 61.0% silt (0.005 - 0.074 mm) and 11.0% clay (< 0.005 mm). The moisture content at saturation of Waukegan soil is 0.370 kg/kg.

7.10.2 Calculation of the thermogradient coefficient

Another method for the calculation of the thermogradient coefficient is found in Eq. (6.12). In order to use Eq. (6.12) it is necessary to know the vapour diffusivity given by Eq. (4.14), the vapour thermogradient coefficient given by Eq. (4.15), the liquid diffusivity given by Eq.

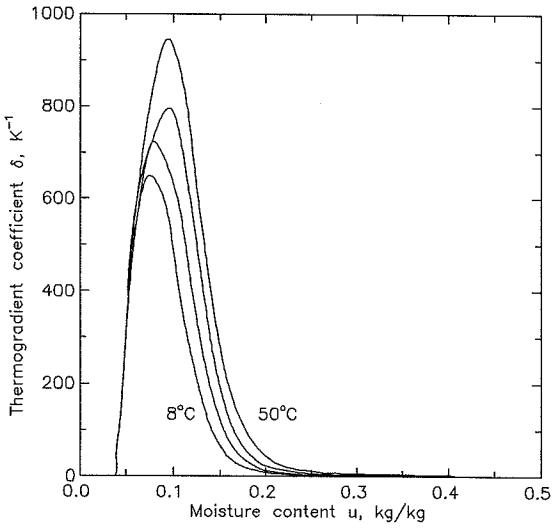

Figure 7.26. **Thermogradient coefficient of glass wool as a function of temperature and moisture content. Perpendicular to the fibres. Temperatures:** 8 ° C, 20 ° C, 35 ° C **and** 50 ° C. $\rho_0 = 77$ kg/m^3. (From Crausse *et al.* [61], [62]).

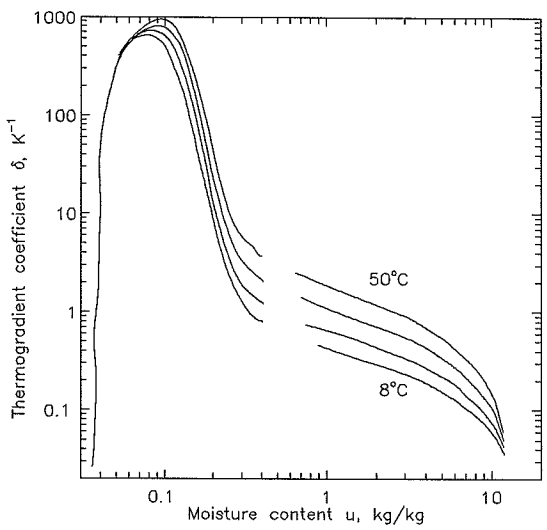

Figure 7.27. **Thermogradient coefficient of glass wool as a function of temperature and moisture content. Perpendicular to the fibres. Temperatures:** 8 ° C, 20 ° C, 35 ° C **and** 50 ° C. $\rho_0 = 77$ kg/m^3. (From Crausse *et al.* [61], [62]).

(4.22) and the liquid thermogradient coefficient given by Eq. (4.23). The moisture content and temperature dependence of the thermogradient coefficient is given by the latter four equations.

The temperature dependence of the vapour diffusivity a_{m1} as given by Eq. (4.14) can be calculated by use of the temperature dependence of the water vapour diffusivity in air given by Eq. (2.25), of the saturation water vapour pressure given by Eq. (2.14) and of the relative humidity as described in section is chapter 3.

The temperature dependence of the vapour thermogradient coefficient δ_1 given by Eq. (4.15) can be approximated with help from Eq. (2.1), (2.8), (2.9) and Table 2.1.

The temperature dependence of the liquid diffusivity a_{m2} as given by Eq. (4.22) can be approximated from the postulate given in Eq. (4.19) and the temperature dependence of the kinematic viscosity of water ν given by Eq. (2.21), (2.22) and (2.17).

The temperature dependence of the suction pressure p_2 can be approximated from Eq. (3.22) and the surface tension of water σ as a function of temperature given by Eq. (2.20).

Figure 7.26 and Fig. 7.27 shows the thermogradient coefficient of glass wool calculated by Crausse *et al.* [61], [62] by the method presented in the last part of this section. Crausse *et al.* used the suction pressure p_2 instead of the relative humidity φ.

7.11 Condensation factor

There is no direct method for the measurement of the condensation factor ε (-). The condensation factor is calculated from Eq. (6.14), the water vapour diffusivity a_{m1} and the liquid diffusivity a_{m2} as

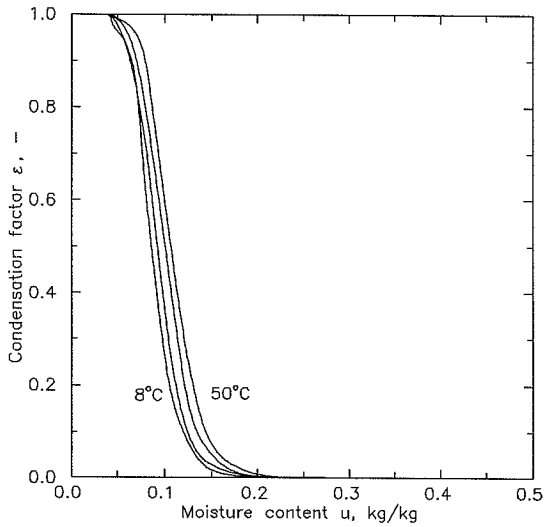

Figure 7.28. **Condensation factor of glass wool as a function of temperature and moisture content. Perpendicular to the fibres. Temperatures:** 8 ° C, 20 ° C, 35 ° C **and** 50 ° C. $\rho_0 = 77$ kg/m^3. (Data from Crausse *et al.* [61], [62]).

$$\varepsilon = \frac{a_{m1}}{a_{m1} + a_{m2}} \tag{6.14}$$

An example of the condensation factor of glass wool as a function of moisture content and temperature is presented in Fig 7.28. The data for water vapour diffusivity and liquid diffusivity were taken from Crausse *et al.* [61], [62], see also Fig 7.14 and Fig. 7.15.

8 Inverse methods

This section describes the use of inverse methods for the estimation of the transfer coefficients in models for coupled heat and moisture transfer in porous media. Inverse methods are often referred to as ill posed problems.

The growing popularity of inverse methods from the beginning of the 1970s must be attributed to the fact that computer power has become increasingly cheaper. In the 1960s numerical solution of simple linear partial differential equations was a time consuming and expensive task for the computers of that time. The exponential growth of computer power has made it possible two solve more complex types of equations and even do it over and over again, which it is sometimes necessary to do, when the subject dealt with is inverse methods.

8.1 General

Inverse methods in the field of heat and moisture transfer was first used for pure heat transfer problems. In the early 1970s Russian researchers paid a great deal of attention to this kind of methods. This section presents two papers on this subject.

Artyukhin [76] determined the thermal diffusivity $a(T)$ as a function of temperature under the assumption of the polynomial dependence

$$a(T) = \sum_{k=0}^{N} c_k T^k \tag{8.1}$$

from the conditions

$$\frac{\partial T}{\partial \tau} = a(T)\frac{\partial^2 T}{\partial x^2} \quad , \qquad 0 < x < b, \qquad 0 < \tau \le \tau_m \tag{8.2}$$

$$-\frac{\partial T(0,\tau)}{\partial X} = q_1(\tau) = -1 \tag{8.3}$$

$$-\frac{\partial T(b,\tau)}{\partial X} = q_2(\tau) = 0 \tag{8.4}$$

$$T(x,0) = \phi(x) = 0 \quad , \qquad 0 \le x \le b \tag{8.5}$$

$$T(x_p,\tau) = T_p'(\tau) \quad , \qquad p = 0,1,2,\ldots,M \quad , \qquad 0 \le x_p \le b \tag{8.6}$$

where $q_1(\tau)$ and $q_2(\tau)$ are the boundary condition, $\varphi(x)$ are the initial conditions and $T_p'(\tau)$ are measured temperatures in the points x_p , p = 1, 2,..., M, where thermocouples or another type of temperature sensors are located. The unknown polynomial coefficients c_i in Eq. (8.1) are found from the condition

$$\mathrm{I}(c_0, c_1, \ldots, c_N) = \sum_{p=1}^{M} \int_0^{\tau_m} (T_p'(\tau) - T_p(\tau))^2 \mathrm{d}\tau \rightarrow \min \tag{8.7}$$

where $T_p'(\tau)$ are the calculated temperatures at the points x_p.

The functional I was minimised using the method of steepest descent. The solution to the equations (8.2) - (8.5) was calculated numerically with an implicit finite difference method.

Artyukhin tested the method on a temperature distribution in an infinite plate of thickness $b = 1$ calculated with an a priori known thermal diffusivity $a(T) = 0.8 + 0.4\,T$ in a grid given by

$$\omega = \{x_i = hi, \quad i = 0,1,\ldots,50; \quad \tau_j = \Delta\tau j, \quad j = 0,1,\ldots,50\} \tag{8.8}$$

The polynomial coefficients (c_0,c_1) were regenerated from the initial guess $(c_0,c_1) = (0.5,0.2)$ in 55 iterations. The temperature at $x = b$ was used as input data for the regeneration.

Yankelev *et al.* [77] used a minimax method for the determination of the thermal conductivity and the volumetric heat capacity on the form

$$\lambda = c_0 + c_1 T \tag{8.9}$$

$$c_p \rho_0 = c_3 + c_4 T \tag{8.10}$$

The unknown coefficients c_0, c_1, c_2, c_3 were found from the condition

$$I(c_0, c_1, c_3, c_4) = \max| T_j'(\tau_j, x_j, c_0, c_1, c_2, c_3) - T_j(\tau_j, x_j)| \rightarrow \min \tag{8.11}$$

The temperatures T_j' are calculated from the equation

$$c_p \rho_0 \frac{\partial T}{\partial \tau} = \frac{\partial}{\partial x}\left(\lambda(T)\frac{\partial T}{\partial x}\right) \tag{8.12}$$

and the boundary conditions

$$\lambda(T)\frac{\partial T}{\partial x}\bigg|_{x=0} = q_1(\tau) \tag{8.13}$$

$$\frac{\partial T}{\partial x}\bigg|_{x=l} = 0 \tag{8.14}$$

The equations (8.12)-(8.14) were solved numerically with a finite difference method. As input for the optimisation, temperatures measured and calculated at the surfaces of a slab were used.

Table 8.1. **Thermal conductivity and volumetric heat capacity as a function of temperature for insulation materials. Note that the temperatures t must be inserted in** °C. (Measured by Yankelev *et al.* [77] with an inverse method).

Material	Thermal conductivity W/m K	Volumetric heat capacity kJ/m^3
Cellular polyurethane	0.036+0.00023·t	91.69+1.256·t
Phosphate styrene cellular plastic	0.0485+0.000238·t	155.16+1.256·t
Mineralised slabs	0.043+0.00024·t	160.77+1.465·t

Yankelev *et al.* determined the thermal conductivity and volumetric heat capacity of three insulation materials with the optimisation method. The results are shown in Table 8.1.

8.2 Ganoulis' method

In 1980, Ganoulis [78] proposed an inverse method for the estimation of transfer coefficients in the Luikov model (Eq. (6.16)-(6.17)) for coupled heat and mass transfer in porous media.

Ganoulis restricted the problem to the stationary moisture transfer equation

$$\frac{\partial}{\partial x}\left(a_{\mathrm{m}}(x)\frac{\partial u}{\partial x}\right)+f(x)=0 \tag{8.15}$$

which for

$$f(x)=-8(1+2x) \tag{8.16}$$

$$a_{\mathrm{m}}(x)=1+x \tag{8.17}$$

has the exact solution

$$u(x)=4x^2 \tag{8.18}$$

Ganoulis used this solution to check the rate of convergence and the validity of the applied optimisation method. Ganoulis used a gradient method to minimise the functional

$$\mathrm{I}(c_0)=\int_0^{\tau}\int_{\Re}(u'(x,\tau,c_0)-u(x,\tau))^2\mathrm{d}\Re\mathrm{d}\tau \tag{8.19}$$

with the following model for the moisture diffusivity

$$a_{\mathrm{m}}(x)=1+c_0x \tag{8.20}$$

and where $u'(x,\tau,c_0)$ are the moisture contents calculated by solving Eq. (8.15) with a finite element method and $u(x,\tau)$ are measured moisture contents (in this case the moisture contents given by Eq. (8.18)). The boundary conditions is given by Eq. (8.18).

8.3 Kohonen's method

Kohonen [66] used an inverse method for the calculation of the moisture diffusivity a_{m} in the isothermal equation

$$\frac{\partial u}{\partial \tau}=\frac{\partial}{\partial x}\left(a_{\mathrm{m}}\frac{\partial u}{\partial x}\right) \tag{8.21}$$

Kohonen recommended the use of Chebyshev polynomials to express the moisture diffusivity as

$$a_m(u) = \sum_{i=0}^{N} c_i T_i \tag{8.22}$$

where T_i is the Chebyshev polynomial of order i.

8.4 Salonvaara's method

Salonvaara [79] used a least squares method to minimise the functional

$$I(c_0, c_1, \ldots, c_m) = \sum_{i=2}^{k-1} (u_i'(x_i, \tau, c_0, \ldots, c_m) - u_i(x_i, \tau))^2 \tag{8.23}$$

and thereby determining the moisture diffusivity a_m and the thermal moisture diffusivity $a_{m,T}$, which is the product of the moisture diffusivity a_m and the thermogradient coefficient δ, from the equation of moisture continuity Eq. (6.16). Salonvaara solved Eq. (6.16) numerically with the Crank-Nicolson finite difference method.

Salonvaara used an exponential function of a polynomial for the mathematical description of a_m and $a_{m,T}$

$$a_m = \exp(c_0 + c_1 u + c_2 u^2 + \ldots + c_n u^n) \tag{8.24}$$

8.5 Method used in this work

In a paper [80] by the author the material properties in the Luikov model, given by Eq. (6.16) and (6.17), a, a_m, ε and δ was as an approximation regarded as functions, for example polynomials in u and T containing the unknown coefficients c_i, $i = 1, 2, \ldots, n$,

$$a(u,T) = c_1 + c_2 u + c_3 T + c_4 u^2 + c_5 uT + \ldots + c_q T^0 \tag{8.25}$$

$$a_m(u,T) = c_{q+1} + c_{q+2} u + c_{q+3} T + \ldots + c_r T^0 \tag{8.26}$$

$$\varepsilon(u,T) = c_{r+1} + c_{r+2} u + c_{r+3} T + \ldots + c_s T^0 \tag{8.27}$$

$$\delta(u,T) = c_{s+1} + c_{s+2} u + c_{s+3} T + \ldots + c_t T^0 \tag{8.28}$$

a (m^2/s) is the thermal diffusivity given by $a = \lambda/\rho_0 c_p$.

By collecting the c's in the vector

$$\underline{c} = [c_1 \quad c_2 \quad \ldots \quad c_q \quad \ldots \quad c_r \quad \ldots \quad c_s \quad \ldots \quad c_t]^T = [c_1 \quad c_2 \quad \ldots \quad c_m]^T \tag{8.29}$$

our task is now to estimate $\underline{c}$ by minimising the functional

$$I(\underline{c}) = \sum_{i=1}^{n_u} (w(u_i(\tau_i, x_i) - u_i'(\tau_i, x_i, \underline{c})))^2 + \sum_{j=1}^{n_T} (T_j(\tau_j, x_j) - T_j'(\tau_j, x_j, \underline{c}))^2 \tag{8.30}$$

where $T_j(\tau_j,x_j)$, $u_i(\tau_i,x_i)$ are temperatures and moisture contents measured at discrete points in the porous material.

$T_j'(\tau_j,x_j,\underline{c})$, $u_i'(\tau_i,x_i,\underline{c})$ are temperatures and moisture contents calculated for a given value of $\underline{c}$ by numerically solving the equations (6.16), (6.17). In this work Eq.(6.16) and (6.17) are solved with a so-called Alternating Potential Implicit finite difference method described by Pedersen *et al.* in [38]. As boundary conditions, moisture contents and temperatures measured as functions of time *inside* the porous material, are used. This eliminates the need for simulating convective boundary conditions which might cause inaccuracies.

w in Eq. (8.30) is a weight factor which compensates the difference in absolute value between moisture contents and temperatures. Normally a value of $w = 100$ has been applied in this work.

In the following the inverse method for the estimation of $\underline{c}$ is described. The method is an ordinary non-linear least-squares based curve-fitting method taken from Madsen [81] and adopted to to functions of several variables in Hansen [82].

The method is the following: Given a real function

$$y = f(\underline{x}, \underline{c}) \tag{8.31}$$

where

$$\underline{x} = [x_1 \quad x_2 \quad \dots \quad x_p]^T \tag{8.32}$$

$$\underline{c} = [c_1 \quad c_2 \quad \dots \quad c_m]^T \tag{8.33}$$

which is differentiable with respect to all the variables x_i, but not necessarily linear with respect to the constants c_i.

The problem is then: Given n observations $y_j(\underline{x_j})$, find the vector $\underline{c}$, that makes the functional f the best possible approximation to the n observations, such that

$$I(\underline{c}) = \sum_{j=1}^{n} (y_j - f(\underline{x_j}, \underline{c}))^2 \tag{8.34}$$

is minimised.

We are seeking a vector $\underline{c}^* = [c_1^* \; c_2^* \; \dots \; c_m^*]^T$ such that

$$I(\underline{c}^*) = \min_{\underline{c} \in R^m} I(\underline{c}) \tag{8.35}$$

Assume that there exists an initial guess $\underline{c}^0 = [c_1^0 \; c_2^0 \; \dots \; c_m^0]^T$ close to $\underline{c}^*$. If

$$\underline{c}^* = \underline{c}^0 + \underline{e}^* \tag{8.36}$$

then the elements of $\underline{e}^*$ are small and it is allowable to make use of the Taylor series expansion

$$f(\underline{x},\underline{c}^*) \approx f(\underline{x},\underline{c}^0) + e_1^* \frac{\partial f}{\partial c_1}(\underline{x},\underline{c}^0) + \ldots + e_m^* \frac{\partial f}{\partial c_m}(\underline{x},\underline{c}^0) \tag{8.37}$$

Combining Eq. (8.37) with Eq. (8.35) yields

$$\begin{aligned} \min_{\underline{c} \in R^m} I(\underline{c}) &= I(\underline{c}^*) \\ &= \sum_{j=1}^{n} (y_j - f(\underline{x},\underline{c}^*))^2 \\ &\approx \sum_{j=1}^{n} \left(y_j - f(\underline{x},\underline{c}^0) - e_1^* \frac{\partial f}{\partial c_1}(\underline{x},\underline{c}^0) - \ldots - e_m^* \frac{\partial f}{\partial c_m}(\underline{x},\underline{c}^0) \right)^2 \\ &= H(\underline{e}^*) \end{aligned} \tag{8.38}$$

where

$$\underline{e}^* = [e_1^* \quad \ldots \quad e_m^*]^T \tag{8.39}$$

It is seen that

$$H(\underline{e}^*) \approx \min_{\underline{e} \in R^m} H(\underline{e}) \tag{8.40}$$

We will now find an approximation to $\underline{e}^*$ by determining the vector $\underline{e} = [e_1 \ \ldots \ e_m]^T$ which minimizes the sum of squares

$$\sum_{j=1}^{n} (y_j^0 - e_1 f_1(\underline{x}_j) - \ldots - e_m f_m(\underline{x}_j))^2 \tag{8.41}$$

with

$$y_j^0 = y_j - f(\underline{x}_j,\underline{c}^0) \tag{8.42}$$

$$f_k(\underline{x}) = \frac{\partial f}{\partial c_k}(\underline{x}_j,\underline{c}^0) \tag{8.43}$$

This is an ordinary Linear Least Squares problem which makes $\underline{e}$ the solution to the equation

$$\underline{\underline{A}}\,\underline{e} = \underline{b} \tag{8.44}$$

where

$$a_{ik} = \sum_{j=1}^{n} f_k(\underline{x}_j) f_i(\underline{x}_j) \tag{8.45}$$

$$b_i = \sum_{j=1}^{n} y_j^0 f_i(\underline{x}_j) \tag{8.46}$$

A new estimate on $\underline{c}$ is now found as

$$\underline{c}^1 = \underline{c}^0 + \underline{e} \tag{8.47}$$

The new value of $\underline{c}$ is inserted in Eq. (8.42) and (8.43) again, and the process is repeated iteratively until $\underline{e}$ is sufficiently small.

In order to use the method outlined above y in Eq. (8.42) is replaced by measured temperatures $T_j(\tau_i,x_j)$ and weighted measured moisture contents $w{\cdot}u_i(\tau_i,x_i)$. Furhtermore, f in Eq. (8.42) and (8.43) is replaced by calculated temperatures $T_j'(\tau_j,x_j,\underline{c})$ and weighted calculated moisture contents $w{\cdot}u_i'(\tau_i,x_i,\underline{c})$.

Finally, in order to ensure convergence of the iterative procedure, it can be necessary to reduce size of the iteration step $\underline{e}$ by a factor v ($0 < v < 1$), which turns Eq. (8.47) into

$$\underline{c}^1 = \underline{c}^0 + v\underline{e} \tag{8.48}$$

Of course, the functions describing the material properties are not restricted to polynomials but may be chosen in many ways as functions of the type f = f(u,T,$\underline{c}$).

The first derivatives of f with respect to the c_is is evaluated using finite differences as

$$\frac{\partial \mathrm{f}}{\partial c_i}(\underline{x},\underline{c}) \approx \frac{\mathrm{f}(\underline{x},\underline{c}+t\underline{e}_i) - \mathrm{f}(\underline{x},\underline{c})}{t} \tag{8.49}$$

where $\underline{e}_i$ is the ith basis vector (all vector elements are 0 except element i which is 1) and the factor t is given by

$$t = 10^{-4} \cdot \| \underline{c} \|_1 \tag{8.50}$$

8.5.1 Test of the estimation method on simulated data

In order to test the estimation method, a temperature and a moisture field in a sand specimen were simulated by solving the set of equations (6.16), (6.17) numerically. The functions describing the material properties (taken from Pedersen *et al.* [38]) were in order to simplify the problem restricted to

$$\lambda = \lambda(u) = c_1 + c_2 u + c_3 u^2 \tag{8.51}$$

$$\delta = \delta(u) = c_4 + c_5 u + c_6 u^2 \tag{8.52}$$

$$a_{\mathrm{m}} = a_{\mathrm{m}}(u) = c_7 u \tag{8.53}$$

$$\varepsilon = \varepsilon(u) = \frac{0.1348}{0.225+u}(\exp(-4379.2u^{2.8}) + 0.429) \tag{8.54}$$

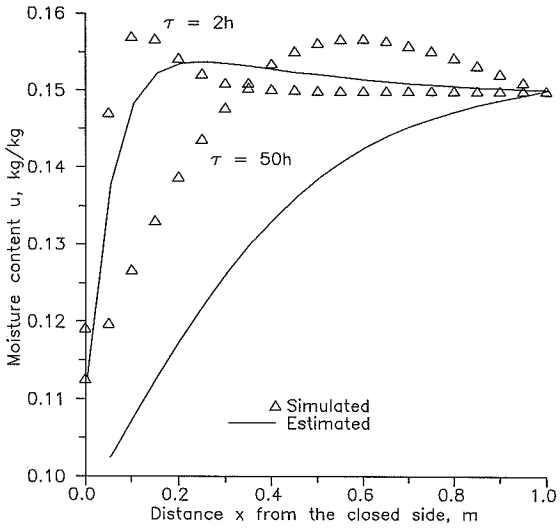

Figure 8.1a. **Moisture field in a sand specimen after 2 and 50 hours. Markers represent the moisture fields which were simulated. The solid curves are moisture contents calculated with the material properties estimated after 1 iteration.**

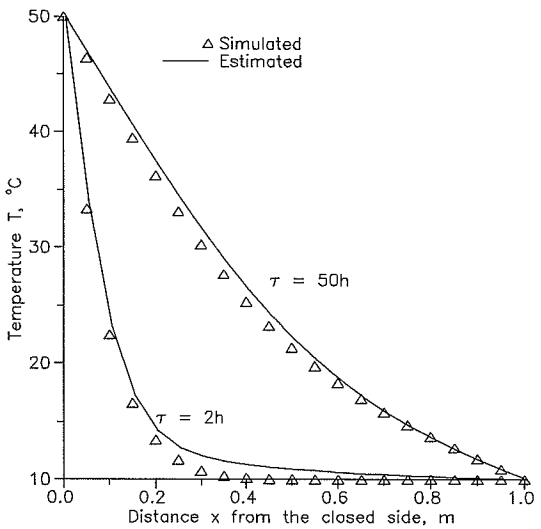

Figure 8.1b. **Temperature field in a sand specimen after 2 and 50 hours. Markers represent the temperature fields which were simulated. The solid curves ares temperatures calculated with the material properties estimated after 1 iteration.**

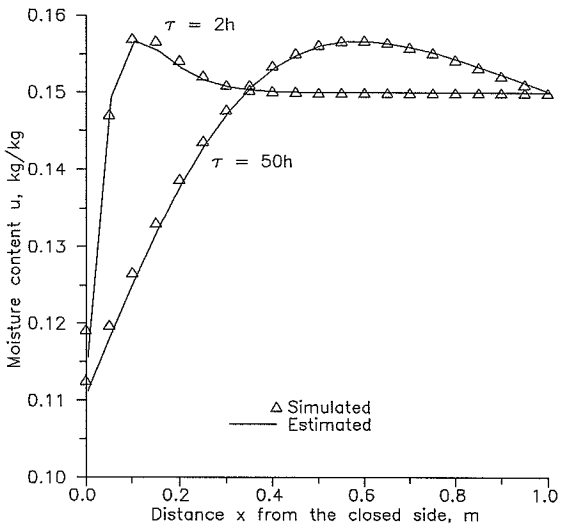

Figure 8.2a. **Moisture field in a sand specimen after 2 and 50 hours. Markers represent the moisture fields which were simulated. The solid curves are moisture contents calculated with the material properties estimated after 29 iterations.**

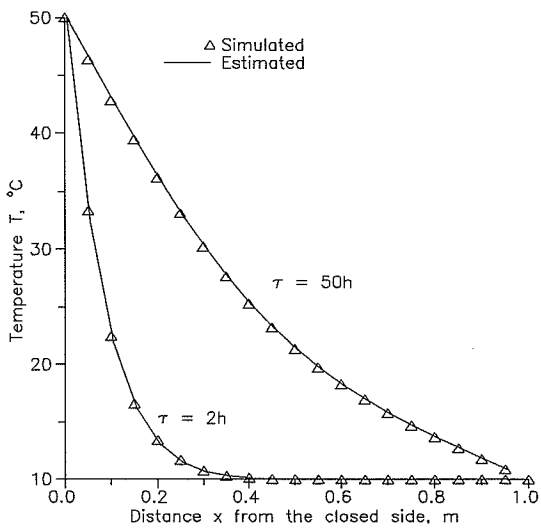

Figure 8.2b. **Temperature field in a sand specimen after 2 and 50 hours. Markers represent the temperature fields which were simulated. The solid curves are temperatures calculated with the material properties estimated after 29 iterations.**

Table 8.2. **Constants in the functions describing the material properties used in the simulation and the following estimation.**

Index	Simulation	Estimation		
		Initial guess	After 1 iteration	After 29 iterations
i	c_i	c_i	c_i	c_i
1	0.545	1.0	1.035	0.5452
2	5.6125	10.0	4.758	5.614
3	-28.1	-60.0	-27.07	-28.12
4	-0.0004	-0.0004	0.002404	0.0003892
5	0.042	0.04	0.07558	0.04169
6	-0.18	-0.2	-0.3555	-0.1784
7	0.000004027	0.0001	0.0001016	0.000004025
8		0.3	0.1229	0.2469
9		-1.5	-0.8784	-0.8086
10		3.6	6.975	1.268

$$a = \frac{\lambda}{\rho_0 c} \quad , \qquad \rho_0 = 1480 \text{ kg/m}^3 \quad , \qquad c_p = 837.5 \text{ J/kg K} \tag{8.55}$$

The initial conditions used in the simulation were

$$T(x,0) = 10 \text{ °C} \quad , \qquad u(x,0) = 0.15 \text{ kg/kg} \quad , \qquad 0 \le x \le 1 \text{ m} \tag{8.56}$$

and the boundary conditions were

$$T(0,\tau) = 50 \text{ °C} \quad , \qquad T(1,\tau) = 10 \text{ °C} \quad , \qquad \tau > 0 \tag{8.57}$$

$$\left(a_m \frac{\partial u}{\partial x} + a_m \delta \frac{\partial T}{\partial x} \right)(0,\tau) = 0 \quad , \qquad u(1,\tau) = 0.15 \text{ kg/kg} \quad , \qquad \tau > 0 \tag{8.58}$$

After the simulation, the material properties were estimated all over again on the basis of the simulated temperature and moisture fields, but this time a new function was used for the description of the condensation factor

$$\varepsilon = \varepsilon(u) = c_8 + c_9 u + c_{10} u^2 \tag{8.59}$$

In Table 8.2 the constants in the functions describing the material properties used in the simulation of the temperature and moisture fields in the sand specimen are tabulated along with the constants in the functions describing the material properties used in the estimation. The initial guess used in the estimation is tabulated together with the constants estimated after 1 and 29 iterations.

In Fig. 8.1 the simulated moisture and temperature fields are represented by triangles for τ = 2 hours and τ = 50 hours. In addition the temperature and moisture fields originating from the first iteration in the estimation are shown as solid curves.

In Fig. 8.2 the moisture and temperature fields calculated with the material properties estimated after 29 iterations are compared with those used in the simulation. In order to ensure convergence of the estimation the first 20 iteration steps were reduced by a factor of 10. 26 temperatures and 26 moisture contents of the form

$$T_i(\tau_i, x_i), \quad u_i(\tau_i, x_i), \quad i = 1, 2, \ldots, 26 \tag{8.60}$$

where

$$x_i \in \{0.1\ \text{m}, 0.2\ \text{m}, \ldots, 0.9\ \text{m}\}, \quad \tau_i \in \{6900\ \text{s}, 13800\ \text{s}, \ldots, 179400\ \text{s}\} \tag{8.61}$$

were used as goal for the estimation.

9 Experimental

Chapter 9 describes the measurements, which are the basis for the estimation of transfer coefficients in chapter 10.

9.1 Capillary suction measurements by Kielsgaard Hansen

Kielsgaard Hansen made a series of isothermal capillary suction experiments on bricks at the Building Materials Laboratory, The Technical University of Denmark in 1988. The measurements have not been published. This section gives a short description of the measurements.

The test specimens were ordinary bricks intended for use in brickwork. According to Danish Codes bricks are required to have the nominal dimensions 230 mm by 110 mm by 55 mm. This is of course not exactly true due to the differences caused by the firing process. Therefore, the overall dimensions and the mass of the bricks in the dry condition were individually measured and their dry densities were calculated. Table 9.1 gives a description of the types of bricks tested and their dry densities.

The capillary suction took place from one of the end surfaces of the bricks. All other sides of the bricks were covered with approximately three layers of water impermeable adhesive tape. During the experiments the moisture contents were measured with a gamma ray attenuation equipment. The moisture content was measured as a function of experimental time and distance from the open end placed in water. Nielsen [83] has previously reported gamma ray attenuation measurements made on the very same stones during capillary suction.

Figure 9.1 shows an example of how the moisture content varies with time at several distances from the open end surface during a capillary suction experiment.

Table 9.1. **Dry density of clay bricks. Calculated from dry mass and overall physical dimensions.**

Specimen	Type	Dry density kg/m^3
G362	Yellow	1786
G363	Yellow	1769
G465	Yellow	1890
G561	Yellow	1843
G565	Yellow	1732
R481	Red	1951
R486	Red	1895
R583	Red	1976
G1001	Yellow	1812
G1002	Yellow	1747
G1003	Yellow	1747
G1004	Yellow	1843
G1005	Yellow	1889

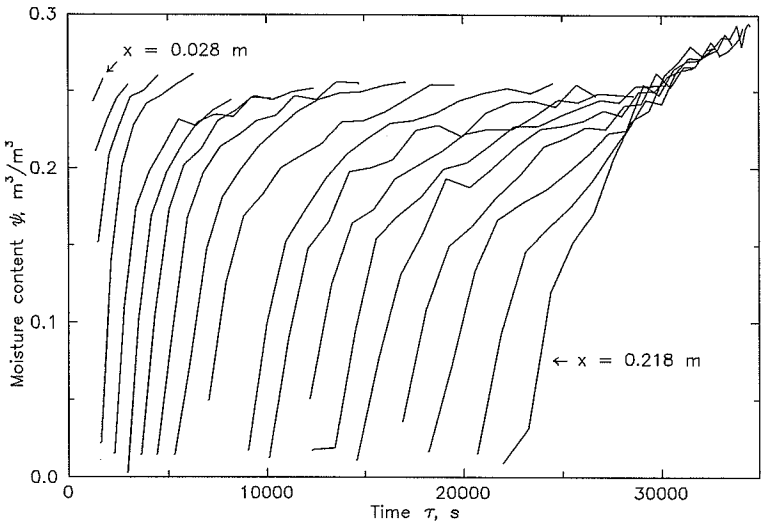

Figure 9.1. **Moisture content in brick G1001 as a function of time and distance from the open end during capillary suction. The moisture content is shown for the distances x from the open end placed in water, $x \in \{0.028\,\text{m}, 0.033\,\text{m}, ..., 0.218\,\text{m}\}$.** (Unpublished measurements by Kielsgaard Hansen, Building Materials Laboratory, the Technical University of Denmark).

9.2 Drying and condensation measurements by Nielsen

In a Ph.D. work carried out in the early 1970s at the Thermal Insulation Laboratory, the Technical University of Denmark, Nielsen [69] measured moisture and temperature profiles in specimens of cellular concrete during drying and condensation. The measurements were stored on computer tapes in order to make them accessible to other researchers. The temperature profiles shown in Fig. 9.6 are an example of the measurements originating from these tapes.

Unfortunately, the moisture measurements were lost so they have been digitized from graphs in Nielsen [69]. An example of the moisture profiles is shown in Fig. 9.2.

The measurements were made on cellular concrete cylindrical discs with diameter 121 mm diameter and 50 mm thickness. The cellular concrete was from the Danish manufacturer H+H Gasbeton. The average dry density of the specimens was $\rho_0 = 572.6$ kg/m^3 with standard deviation of 10.6 kg/m^3.

The specimens were, in order to assure one-dimensional moisture transport, covered on the cylinder surface and on one of the ends with a 5-layer foil containing a single layer of aluminium. The specimens were mounted in a plexiglass ring with 5 mm wall thickness in order to ensure the mechanical integrity of the specimens. Finally, a plexiglass disc with a thickness of 5 mm was glued onto the end covered with foil.

Table 9.2. **Drying conditions for cellular concrete specimens.**

Specimen	Environment	Air temperature °C	Dew point temperature °C	Air velocity m/s
188	Climate box	25.5	7	2
197	Laboratory	17	7-13	1.5
198	Climate box	22.5	7	0.1

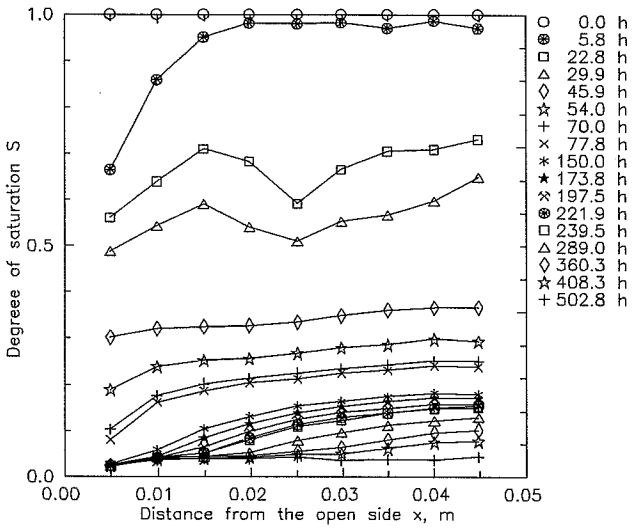

Figure 9.2. **Degree of moisture saturation in cellular concrete during isothermal drying experiment as a function of time and space coordinate. Specimen no. 188.** (Measurements by Nielsen [69]).

9.2.1 Isothermal drying experiments

Nielsen conducted a series of drying experiments. In this work, three of the drying experiments made on the specimens, numbered by Nielsen as 188, 197 and 198, have been used. Prior to the drying, the specimens were vacuum saturated with water in a desiccator. Drying of the specimens took place in a climate chamber or at laboratory conditions. The drying conditions are presented in Table 9.2

The measured moisture profiles are shown in Fig. 9.2, 9.3 and 9.4. The measured moisture content has been transformed into the degree of vacuum saturation.

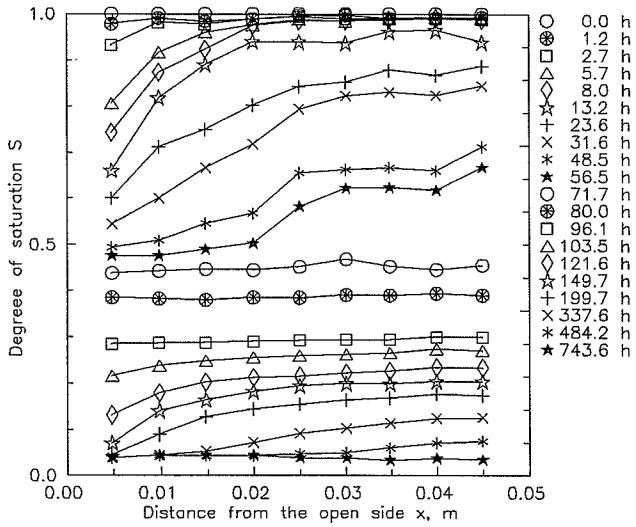

Figure 9.3. **Degree of moisture saturation in cellular concrete during isothermal drying experiment as a function of time and space coordinate. Specimen no. 197.** (Measurements by Nielsen [69]).

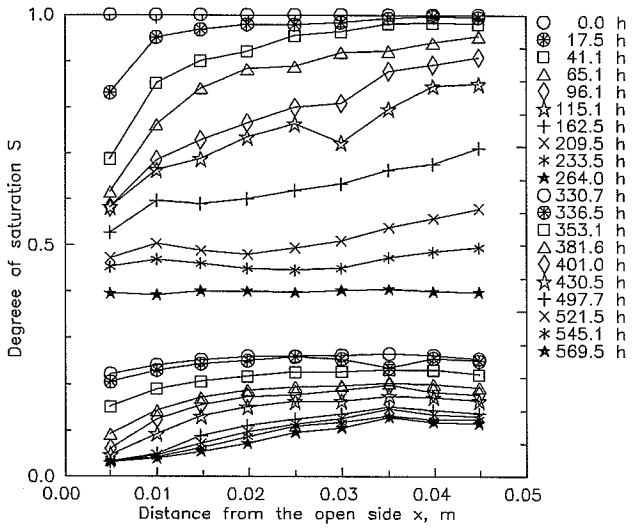

Figure 9.4. **Degree of moisture saturation in cellular concrete during isothermal drying experiment as a function of time and space coordinate. Specimen no. 198.** (Measurements by Nielsen [69]).

9.2.2 Coupled heat and moisture transfer

In addition to the drying experiments Nielsen also conducted a number of condensation experiments with cellular concrete. The specimens were similar to the ones described above except for the presence of 5 thermocouples placed 5 mm, 16 mm, 27 mm, 38 mm and 49 mm from the open end. The closed end of the specimens was cooled with a cooling plate while the open end was subjected to humid air in a climate chamber.

In this work, the measurements from one of the condensation experiments, which were made on specimen no. 170, has been used. Prior to the experiment the specimen was equibrilated with the air in the laboratory which lead to an average moisture content in the specimen of about 3.2 vol. %. The air temperature in the climate box was approximately 30 °C and the dew point temperature was approximately 17 °C. The cold plate temperature was 1 °C.

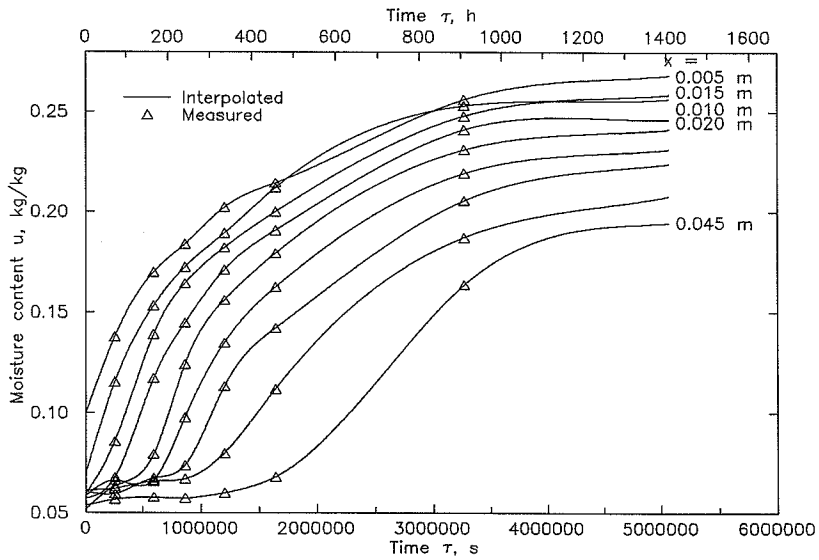

Figure 9.5. **Moisture content in cellular concrete specimen during condensation as a function of time and space coordinate. Specimen no. 170.** (Measurements by Nielsen [69]).

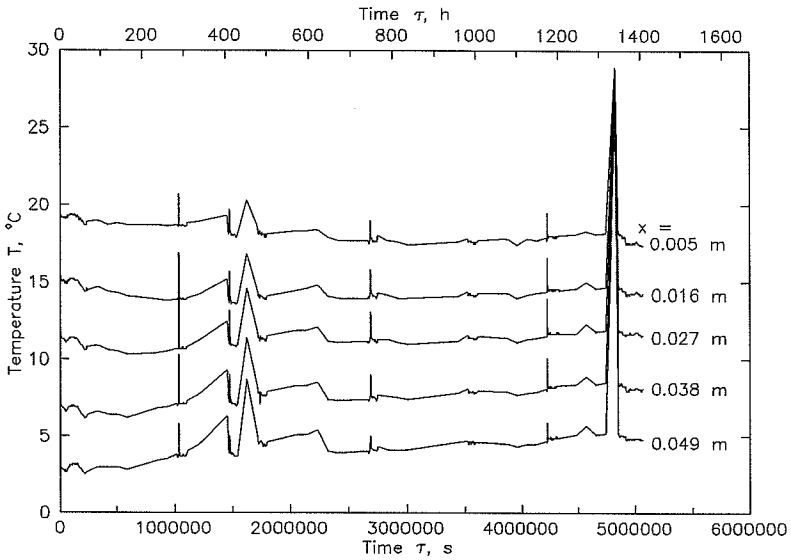

Figure 9.6. **Temperatures in cellular concrete specimen during condensation as a function of time and space coordinate. Specimen no. 170.** (Measurements by Nielsen [69]).

The moisture content and the temperature measured as a function of time is shown in Fig. 9.5 and 9.6 respectively.

10 Estimation of transfer coefficients from measurements

This chapter describes the transfer coefficients found by use of the methods described in chapters 7 and 8. The transfer coefficients are estimated on the basis of the measurements presented in chapters 7 and 9.

10.1 Boltzmann transformation

The Boltzmann transformation was presented in section 7.8.1. In this section the Boltzmann transformation is used on the isothermal suction experiments with brick described in section 9.1 and the isothermal suction experiment with cellular concrete presented in Fig. 7.21.

10.1.1 Liquid diffusivity of cellular concrete

In this section the Boltzmann transformation is used to calculate the liquid diffusivity of cellular concrete from the isothermal suction experiment made by Nielsen [69] and described in section 7.8.2, see Fig. 7.21. Only the measurements of moisture profiles made at experimental time 2.6 h, 19.1 h and 25.6 h were used.

The Boltzmann transformed moisture profiles are shown as triangles in Fig. 10.1. The solid line shows an approximation to the Boltzmann transformed moisture profile is given by

$$\lambda(u) = c_0 + c_1 u \tag{10.1}$$

with $c_0 = 526.495 \cdot 10^{-6}$ m $s^{-1/2}$ and $c_1 = -369.366 \cdot 10^{-6}$ m $s^{-1/2}$.

The liquid diffusivity is calculated from Eq. (7.31) and (10.1) as

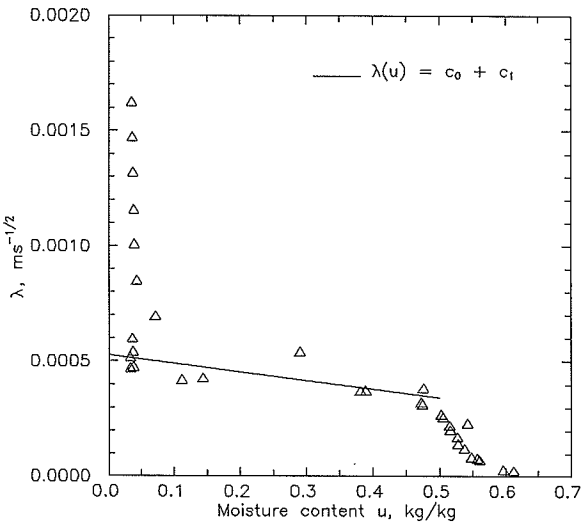

Figure 10.1. **Boltzmann transformed moisture profiles calculated from Fig. 7.21 Cellular concrete.** (Measurements by Nielsen [69]).

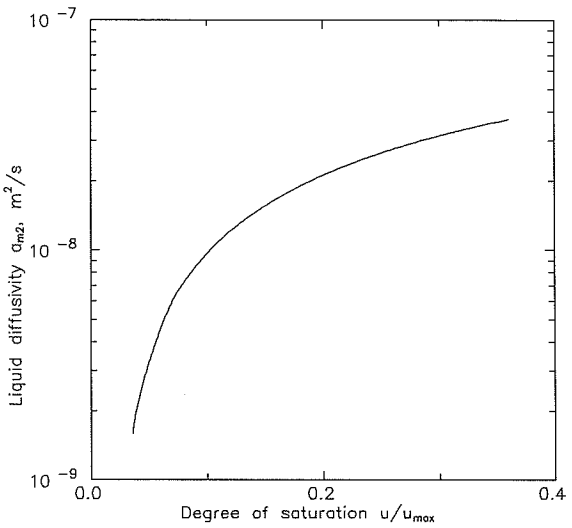

Figure 10.2. **Liquid diffusivity of cellular concrete as a function of the degree of saturation. Calculated with the Boltzmann transformation.** (Measurements by Nielsen [69]).

$$a_{m2}(u) = -\frac{c_1}{2}\left(\frac{c_1}{2}(u^2 - u_i^2) + c_0(u - u_i)\right) \tag{10.2}$$

with u_i=0.03267 kg/kg. The liquid diffusivity calculated with Eq. (10.2) is shown in Fig. 10.2 as a function of the degree of saturation (u_{max} = 1.3861 kg/kg).

10.1.2 Liquid diffusivity of brick

In this section the Boltzmann transformation is used on the isothermal suction experiments with brick described in section 9.1.

The third order polynomial given by Eq. (7.32) with the moisture content on weight basis replaced by the volumetric moisture content was used for fitting the Boltzmann transformed moisture profiles. The polynomial coefficients found by regression for the various bricks tested are presented in Table 10.1. From these coefficients the liquid diffusivity as a function of the volumetric moisture content is given by

$$a_{m2}(\psi) = -\left(\frac{c_1}{2} + c_2\psi + \frac{3}{2}c_3\psi^2\right) \cdot \left(c_0(\psi - \psi_i) + \frac{c_1}{2}(\psi^2 - \psi_i^2) + \frac{c_2}{3}(\psi^3 - \psi_i^3) + \frac{c_3}{4}(\psi^4 - \psi_i^4)\right) \quad \mathrm{m^2/s} \tag{10.3}$$

The liquid diffusivity of the bricks described in section 9.1 is seen in Fig. 10.3, 10.4 and 10.5.

In Fig. 10.6 the liquid diffusivities of three of the bricks is compared to the liquid diffusivities estimated from the measurements made by Nielsen [83]. The latter were estimated from Nielsen's gamma ray attenuation measurements with the method used in this section.

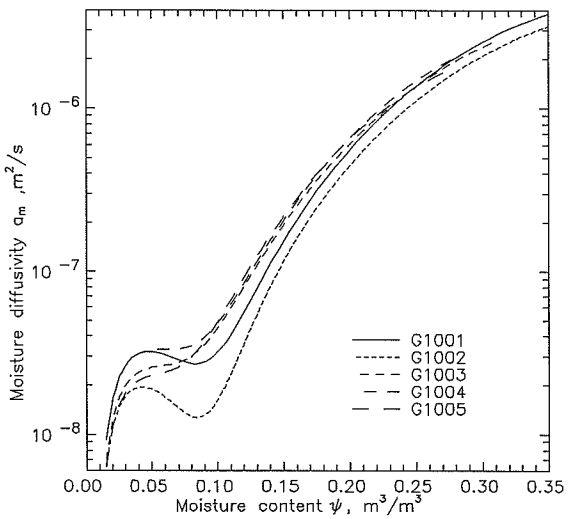

Figure 10.3. **Liquid diffusivity of brick as a function of moisture content. Calculated with the Boltzmann transformation.** (Measurements by Kielsgaard Hansen).

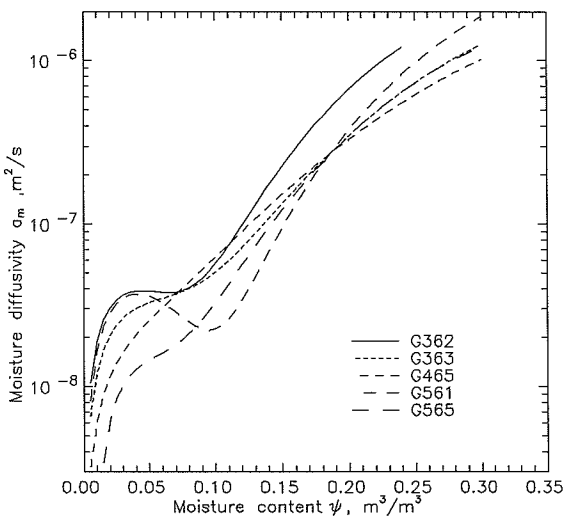

Figure 10.4. **Liquid diffusivity of brick as a function of moisture content. Calculated with the Boltzmann transformation.** (Measurements by Kielsgaard Hansen).

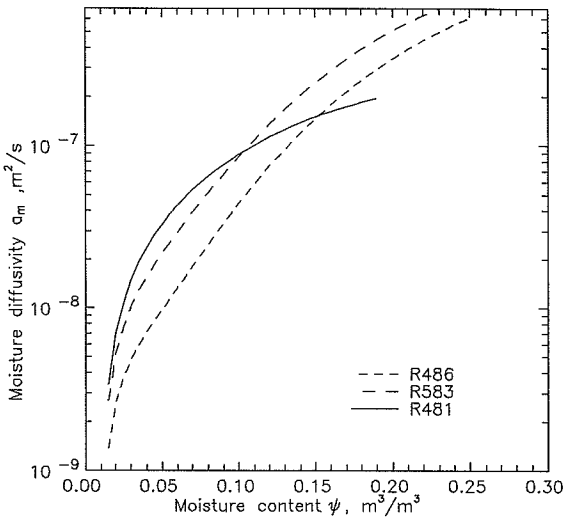

Figure 10.5. **Liquid diffusivity of brick as a function of moisture content. Calculated with the Boltzmann transformation.** (Measurements by Kielsgaard Hansen).

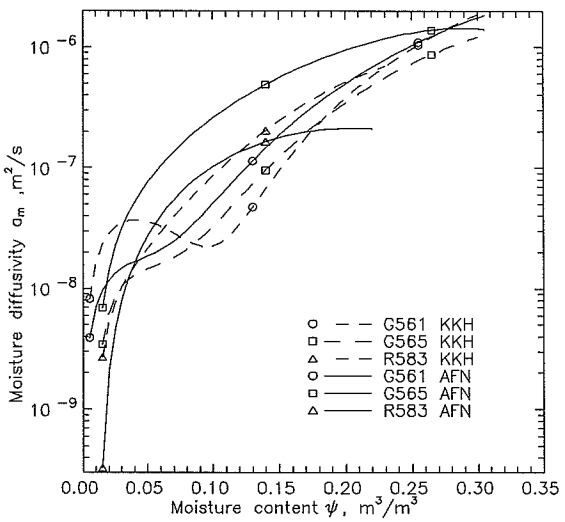

Figure 10.6. **Liquid diffusivity of brick as a function of moisture content. Calculated with the Boltzmann transformation.** (Measurements by Kielsgaard Hansen (KKH) and Nielsen (AFN) [83]).

Table 10.1. **Coefficients in polynomials describing liquid diffusivity of brick. Found from Boltzmann transformation of measurements by K. K. Hansen and A. F. Nielsen (AFN). An asterisk (*) in the duration column indicates that the only a part of the measured values has been used.**

Specimen	c_0	c_1	c_2	c_3	ψ_i m³/m³	$\psi = \lambda^{-1}(0)$ m³/m³	Duration h
G362	0.00105241	-0.00444631	0.0412416	-0.167909	0	0.24	15.64
G363	0.00108609	-0.00260074	0.0186947	-0.0716233	0	0.30	15.89
G465	0.00124049	-0.00110685	0.00505444	-0.0318287	0	0.36	11.84*
G561	0.00131795	-0.00342537	0.0299902	-0.0981834	0.001	0.30	11.91
G565	0.000984216	-0.00187636	0.016669	-0.0749683	0.01	0.30	15.82
R481	0.000746179	-0.00165469	-0.00733408	0	0.01	0.22	6.70
R486	0.000776127	-0.000901748	0.0072878	-0.0629009	0.01	0.25	25.32*
R583	0.000870997	-0.001432	0.0074012	-0.0810478	0.01	0.23	9.56
G1001	0.00151013	-0.00340924	0.0313621	-0.112235	0.01	0.35	7.91
G1002	0.0013912	-0.0025614	0.025642	-0.0946616	0.01	0.35	7.94
G1003	0.00139971	-0.00273715	0.0256757	-0.105237	0.01	0.31	7.66
G1004	0.00130008	-0.00390521	0.0359694	-0.139893	0.01	0.28	10.10
G1005	0.00112596	-0.00317834	0.0313268	-0.138256	0.01	0.28	8.02
G561AFN	0.00128436	-0.00133598	0.0123205	-0.0647232	0	0.32	9.14*
G565AFN	0.00136224	-0.0017911	0.0095122	-0.0434507	0	0.35	4.98
R583AFN	0.000795616	-0.000240917	-0.0114694	0	0	0.25	7.16

10.2 Use of the estimation method on experimental data

The estimation method previously described in chapter 8.5 is in this section applied on the experimental data on cellular concrete presented in chapter 9.2.

10.2.1 Isothermal drying experiments

This section describes the estimation of the moisture diffusivity from the isothermal drying experiments presented in section 9.2.1. The moisture diffusivity was estimated with the same program that was later on used to estimate the full set of transfer parameters in the Luikov model for coupled heat and moisture transfer presented in chapter 6.

For reasons of simplicity, the full model was used although the aim was only to estimate the isothermal moisture diffusivity. Simplicity shall is this context be seen as what concerns the programming effort not the computational work required by the estimation.

In order to have measurements of as well moisture content as temperature at the same space coordinate x and time τ it was necessary to interpolate the measured data. Interpolation was made with cubic splines in the x-direction for both moisture content and temperatures. Interpolation of the moisture content in the τ-direction was made with cubic splines. Linear interpolation was used for the interpolation of the temperatures in τ-direction.

The isothermal moisture diffusivity was modelled as a power function with a 6th order Chebyshev polynomial as argument, see Eq. (10.10). Chebyshev polynomials are often used in the interval $x \in [-1;1]$. Therefore, it is necessary to transform the moisture content as it is done in Eq. (10.4) - (10.6). The Chebyshev polynomials are defined recursively , see Eq. (10.7) - (10.9).

The following models for the material properties were applied in connection with the estimation method

$$u_{\min} = 0.0 \text{ kg/kg} \tag{10.4}$$

$$u_{\max} = 1.4 \text{ kg/kg} \tag{10.5}$$

$$x = \frac{2u - (u_{\min} + u_{\max})}{u_{\max} - u_{\min}} \tag{10.6}$$

$$\mathrm{T}_0(x) = 1 \tag{10.7}$$

$$\mathrm{T}_1(x) = x \tag{10.8}$$

$$\mathrm{T}_{n+1}(x) = 2x\mathrm{T}_n - \mathrm{T}_{n-1} \quad n \geq 1 \tag{10.9}$$

$$a_m(u) = 10^{-\frac{1}{2}c_0 + \sum_{k=0}^{k=6} c_k \mathrm{T}_k(x)} \text{ m}^2/\text{s} \tag{10.10}$$

$$\delta(u) = 10^{-7} \text{ K}^{-1} \tag{10.11}$$

$$\lambda(u) = 0.1 \text{ J/s m K} \tag{10.12}$$

$$\rho_0 = 572.6 \text{ kg/m}^3 \tag{10.13}$$

$$c_p = 960 \text{ J/kg K} \tag{10.14}$$

$$\varepsilon = 0 \tag{10.15}$$

$$\Delta_l H^{\theta}_{T,l \to g} = 2499940 \text{ J/kg} - 2370.94 \text{ J/kg K} \cdot t \tag{10.16}$$

Note that the temperature t is inserted in °C in Eq. (10.16).

The regression constants found with the estimation procedure are presented in Table 10.2.

Also in Table 10.2 the number of iterations used in the regression analysis are found. The first regression analysis performed was the one involving specimen 197. The huge number of iterations 2263 is explained by the fact that this first iteration was used a test case where the iteration step size was varied in order to see how it affected the convergence of the iteration, see also Eq. (8.48) in section 8.5.

In 999 of the 2263 iterations the iteration step size was reduced by a factor of 1000, which is equal to setting $\nu = 0.001$ in Eq. (8.48). In other 1258 of the iterations the step size was reduced by a factor of 100. In one iteration a reduction of the steps in the order of a factor of 10 was used while the full step taken in the remaining 5 iterations.

In the regression analysis made on the measurements from the experiments with specimens 188 and 198, the iteration step size was reduced by a factor of 10.

The moisture diffusivities calculated with Eq. (10.10) and the estimated constants in Table 10.2 are presented in Fig. 10.7.

Table 10.2. **Regression constants for specimens 188, 197 and 198 in the model used for the estimation of isothermal moisture diffusivity.**

Chebyshev index	188	188	197	197	198	198
	Initial guess	After 356 iterations	Initial guess	After 2263 iterations	Initial guess	After 213 iterations
k	c_i	c_i	c_i	c_i	c_i	c_i
0	-15.137066	-16.306822	-15.462100	-15.136882	-16.306822	-18.191531
1	-0.030218796	-0.21517636	0.92631785	-0.030080048	-0.21517645	-0.93102162
2	0.28197896	-0.58350136	0.38418168	0.28212321	-0.58350136	-1.2895411
3	0.71534653	0.061503286	-2.3699573	0.71546787	0.061503348	-0.56616975
4	0.85056418	0.43031844	1.8159709	0.85063485	0.43031836	-0.31690001
5	-0.16231303	-0.17615533	-0.18945715	-0.16226222	-0.17615532	-0.81149309
6	0.74273969	0.48644017	9.6856973	0.74275986	0.48644025	-0.23187148

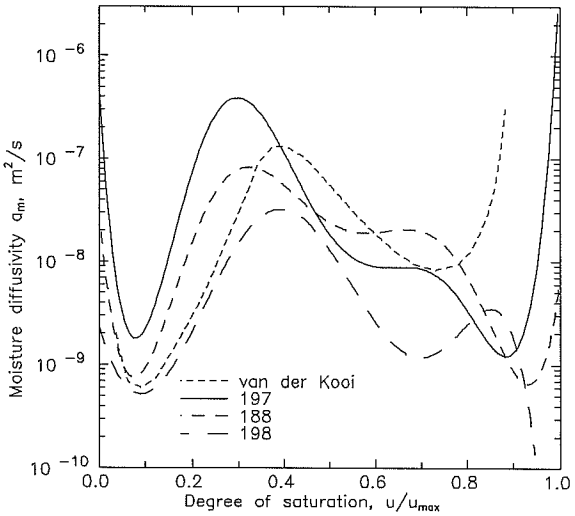

Figure 10.7. **Moisture diffusivity of cellular concrete as a function of the degree of saturation. Calculated with the inverse method described in section 8.5. 188, 197 and 198 are specimen numbers for measurements made by Nielsen [69]. Calculated diffusivities are compared to diffusivity measured by van der Kooi [72].**

10.2.2 Coupled heat and moisture transfer

This section describes the estimation of all 4 transfer coefficients in the Luikov model from measurements of moisture contents and temperature during coupled transfer. The measurements used for this estimation are from the condensation experiment presented in section 9.2.2. The measurements were interpolated in the same way as is described in section 10.2.1.

The temperature dependence of the 4 transfer coefficients was neglected. The same power model incorporating Chebyshev polynomials which was presented in section 10.2.1. was used for the description of all 4 transfer coefficients, see Eq. (10.23), (10.24), (10.25) and (10.28). The order of the Chebyshev polynomials is found in Table 10.3. A total of 19 constants was to be found from the estimation.

A first attempt was made to estimate all 4 transfer coefficients incorporating the 19 constants with the following model for the material properties

$$u_{\min} = 0.0537 \text{ kg/kg} \tag{10.17}$$

$$u_{\max} = 0.27 \text{ kg/kg} \tag{10.18}$$

$$x = \frac{2u - (u_{\min} + u_{\max})}{u_{\max} - u_{\min}} \tag{10.19}$$

$$T_0(x) = 1 \tag{10.20}$$

$$T_1(x) = x \tag{10.21}$$

Table 10.3. **Regression constants in the 19 constant model.**

Transfer coefficient	No. of constants	Chebyshev index k	Index i	Initial guess c_i	After 125 iterations c_i
		0	1	-1.4931273	-8.5168912
λ	3	1	2	0.14767672	0.33275567
		2	3	-0.012130432	-0.0097370175
		0	4	-4.8229041	-7.6838830
δ	4	1	5	-0.21865490	1.5780064
		2	6	-0.49809093	-1.3505817
		3	7	0.14714163	0.66796216
		0	8	-16.234135	-17.155145
		1	9	0.62790027	0.77891961
		2	10	0.37031149	0.20726574
a_m	7	3	11	-0.10785247	-0.17607905
		4	12	0.0019019595	0.039607743
		5	13	0.0034855545	-0.040802177
		6	14	0.012076460	-0.081358094
		0	15	-0.96761856	-28.692932
		1	16	-0.26504598	22.922072
ε	5	2	17	0.14282318	-14.463098
		3	18	-0.081777027	7.7851136
		4	19	0.034934598	-1.9281445

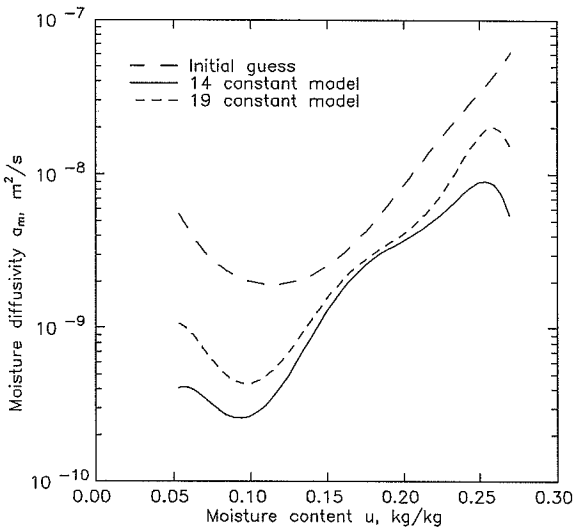

Figure 10.8. **Moisture diffusivity of cellular concrete as a function of moisture content. Calculated with the inverse method described in section 8.5. Specimen 170.**

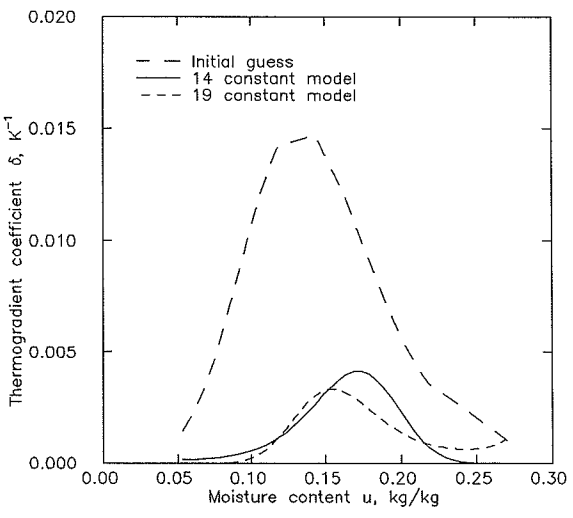

Figure 10.9. **Thermogradient coefficient of cellular concrete as a function of moisture content. Calculated with the inverse method described in section 8.5. Specimen 170.**

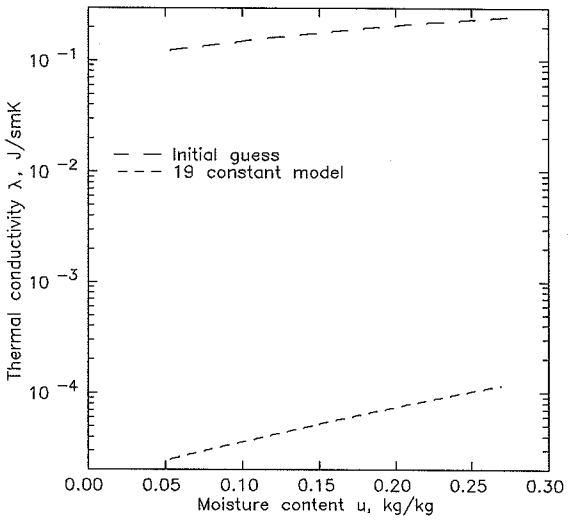

Figure 10.10. **Thermal conductivity of cellular concrete as a function of moisture content. Calculated with the inverse method described in section 8.5. Specimen 170. 19 constant model.**

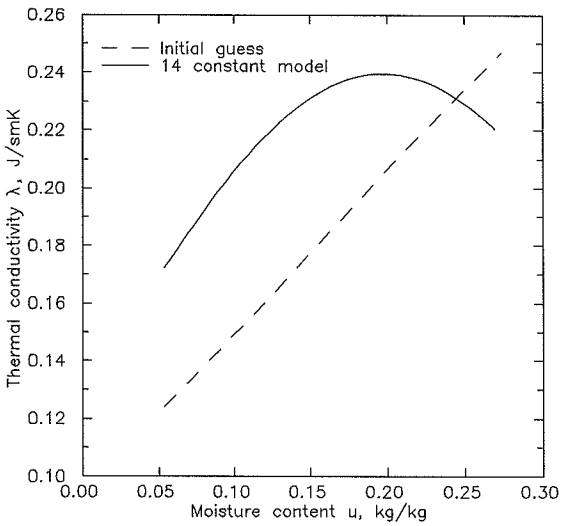

Figure 10.11. **Thermal conductivity of cellular concrete as a function of moisture content. Calculated with the inverse method described in section 8.5. Specimen 170. 14 constant model.**

$$T_{n+1}(x) = 2xT_n - T_{n-1} \quad n \geq 1 \tag{10.22}$$

$$a_m(u) = 10^{-\frac{1}{2}c_0 + \sum_{k=0}^{k=6} c_k T_k(x)} \quad \text{m}^2/\text{s} \tag{10.23}$$

$$\delta(u) = 10^{-\frac{1}{2}c_0 + \sum_{k=0}^{k=3} c_k T_k(x)} \quad \text{K}^{-1} \tag{10.24}$$

$$\lambda(u) = 10^{-\frac{1}{2}c_0 + \sum_{k=0}^{k=2} c_k T_k(x)} \quad \text{J/s m K} \tag{10.25}$$

$$\rho_0 = 572.6 \text{ kg/m}^3 \tag{10.26}$$

$$c_p = 960 \text{ J/kg K} \tag{10.27}$$

$$\varepsilon = 10^{-\frac{1}{2}c_0 + \sum_{k=0}^{k=4} c_k T_k(x)} \tag{10.28}$$

$$\Delta_l H^{\theta}_{T,l \to g} = 2499940 \text{ J/kg} - 2370.94 \text{ J/kg K} \cdot t \tag{10.29}$$

Note that the temperature t is inserted in °C in Eq. (10.29).

The result of the estimation made with this 19 constant model is found in Table 10.3. A total of 125 iterations were used. In 36 of the iterations the step was reduced by a factor of 1000, in 83 by a factor of 100 and in the remaining 6 by a factor of 10. This was done in order to see how it affected the convergence.

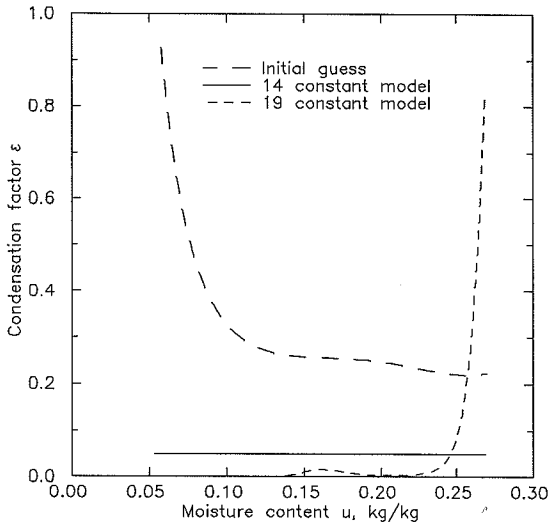

Figure 10.12. **Condensation factor of cellular concrete as a function of moisture content. Calculated with the inverse method described in section 8.5. Specimen 170.**

The estimated transfer coefficients are presented in Fig. 10.8 - 10.10 and Fig. 10.12. The initial guess was made with transfer coefficients for cellular concrete taken from literature. It is seen in Fig. 10.10 that the estimated thermal conductivity is almost factor of 10000 lower than the initial guess and it is so low that it has lost its physical meaning. The estimated condensation factor (Fig 10.12) is also behaving quit different from the initial guess and has similarly lost its physical meaning.

This, altogether, indicated problems with the estimation of the transfer coefficients belonging to the equation of continuity for energy in the Luikov model given by Eq. (6.19). Therefore, it was decided to make a new estimation with a reduced model where the condensation factor was set to a fixed value and see how it would affect the estimation.

This reduced model contained 14 constants in three transfer coefficients to be estimated. For these three transfer coefficients the same models as in the previous estimation were used giving the following total model for the material properties

$$u_{\min} = 0.0537 \text{ kg/kg} \tag{10.30}$$

$$u_{\max} = 0.27 \text{ kg/kg} \tag{10.31}$$

$$x = \frac{2u - (u_{\min} + u_{\max})}{u_{\max} - u_{\min}} \tag{10.32}$$

$$\mathrm{T}_0(x) = 1 \tag{10.33}$$

$$\mathrm{T}_1(x) = x \tag{10.34}$$

$$\mathrm{T}_{n+1}(x) = 2x\mathrm{T}_n - \mathrm{T}_{n-1} \quad n \geq 1 \tag{10.35}$$

$$a_{\mathrm{m}}(u) = 10^{-\frac{1}{2}c_0 + \sum_{k=0}^{k=6} c_k \mathrm{T}_k(x)} \quad \mathrm{m}^2/\mathrm{s} \tag{10.36}$$

Table 10.4. **Regression constants in the 14 constant model.**

Transfer coefficient	No. of constants	Chebyshev index k	Index i	Initial guess c_i	After 31 iterations c_i
		0	1	-8.5168912	-1.3399704
λ	3	1	2	0.33275567	0.052907891
		2	3	-0.0097370175	-0.040600721
		0	4	-7.6838830	-7.5236687
δ	4	1	5	1.5780064	-0.88224108
		2	6	-1.3505817	-1.3568018
		3	7	0.66796216	-0.47236869
		0	8	-17.155145	-17.635919
		1	9	0.77891961	0.78161186
		2	10	0.20726574	0.015582052
a_m	7	3	11	-0.17607905	-0.21637180
		4	12	0.039607743	0.033789990
		5	13	-0.040802177	-0.024813674
		6	14	-0.081358094	-0.081328619

$$\delta(u) = 10^{-\frac{1}{2}c_0 + \sum_{k=0}^{k=3} c_k T_k(x)} \quad \mathrm{K}^{-1} \tag{10.37}$$

$$\lambda(u) = 10^{-\frac{1}{2}c_0 + \sum_{k=0}^{k=2} c_k T_k(x)} \quad \mathrm{J/s\ m\ K} \tag{10.38}$$

$$\rho_0 = 572.6\ \mathrm{kg/m^3} \tag{10.39}$$

$$c_p = 960\ \mathrm{J/kg\ K} \tag{10.40}$$

$$\varepsilon = 0.05 \tag{10.41}$$

$$\Delta_r H^{\theta}_{T,l \to g} = 2499940\ \mathrm{J/kg} - 2370.94\ \mathrm{J/kg\ K} \cdot t \tag{10.42}$$

Note that the temperature t is inserted in °C in Eq. (10.42).

The result of the estimation with the 14 constant model is found in Table 10.4. A total of 31 iterations were used. 28 of the iteration steps were reduced by a factor of 10 while the full step was taken in the remaining 3 iterations.

The estimated transfer coefficients are presented in Fig. 10.8 - 10.9 and Fig. 10.11.

11 Discussion

In this chapter the results presented in the previous chapters are discussed.

11.1 Temperature dependence of transfer coefficients

In this section the temperature dependence some of the transfer coefficients in the Luikov model for coupled heat and mass transfer in porous media Eq. (6.16) and (6.17) is analysed.

In chapter 2 the thermodynamic and transport properties of water were presented. In chapter 3 the thermodynamic properties of porous materials and moist air were presented. This gave an opportunity to estimate the temperature dependence of the transfer coefficients in the Luikov model using the theories for the prediction of the behaviour of composite materials. This analysis has not been performed. In stead a simplified temperature dependence analysis is made in this section. The analysis is restricted to the temperature range from -20 °C to 60 °C which should cover most practical building physical purposes, at least in Denmark.

The discussion is restricted to the temperature dependence of the vapour diffusivity, the liquid diffusivity, the moisture diffusivity and the condensation factor. In the analysis, the value of the transfer coefficient relative to its value at a fixed standard temperature T_0 is taken as a measure of its sensitivity to temperature changes. The absolute temperature $T_0 = 298.15$ K is used as the fixed standard temperature.

An expression for the vapour diffusivity was presented in Eq. (4.14). This expression originates from Eq. (4.5) where the factor $\zeta(u)$ was introduced. It was tacitly assumed that this factor is independent of temperature. It is possible to imagine that this is not always true. The reason why is that it seems likely that the condensation might take place in the pores as a consequence of a temperature drop thereby causing obstruction of the vapour diffusion. If this assumption of $\zeta(u)$ being independent of temperature is maintained the relative temperature dependence of the vapour diffusivity can expressed as

$$\frac{a_{m1}(u,T)}{a_{m1}(u,T_0)} = \frac{T_0}{T}\frac{p_b - p_1(T_0)}{p_b - p_1(T)}\frac{D(T)}{D(T_0)}\frac{p_s(T)}{p_s(T_0)} \tag{11.1}$$

Furthermore, this requires that the change of the slope of the sorption isotherm with temperature is negligible.

It can be shown that the term

$$\frac{p_b - p_1(T_0)}{p_b - p_1(T)} \tag{11.2}$$

is restricted to the interval

$$0.97 \le \frac{p_b - p_1(T_0)}{p_b - p_1(T)} \le 1.21 \tag{11.3}$$

in the observed temperature range if a barometric pressure of 101325 Pa is assumed.

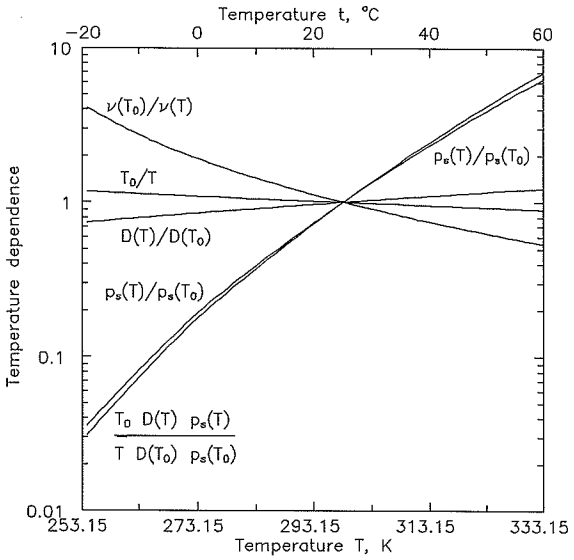

Figure 11.1. **Temperature dependence of the vapour and the liquid diffusivity.**

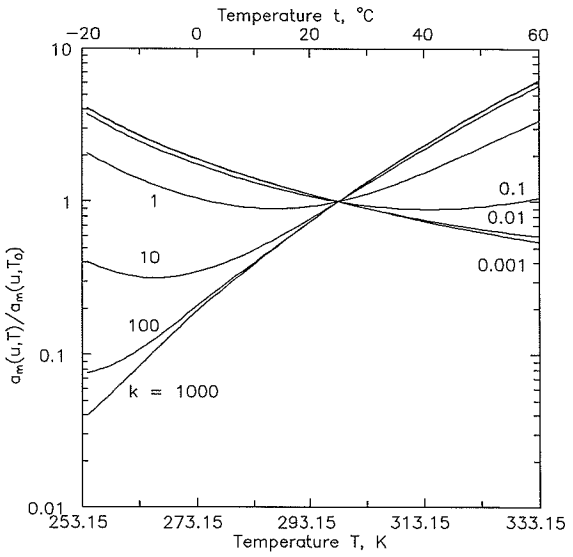

Figure 11.2. **Temperature dependence of the moisture diffusivity.**

The remaining three factors of the right hand side of Eq. (11.1) are plotted in Fig. 11.1. It is seen that the factor involving the saturation vapour pressure is the far most dominating. Furthermore, it is seen that this factor yields almost the same value as all three factors multiplied together. Therefore, it seems justifiable to approximate the temperature dependence of the vapour diffusivity from the change in the saturation vapour pressure.

Finally, it is seen that the change of the vapour diffusivity with temperature in the observed temperature range is so large that it necessary to take it into account. Therefore, the vapour diffusivity as a function of moisture content and temperature as an approximation can be calculated from the expression

$$\frac{a_{m1}(u,T)}{a_{m1}(u,T_0)} \approx \frac{p_s(T)}{p_s(T_0)} \tag{11.4}$$

where $a_{m1}(u,T_0)$ is the vapour diffusivity measured as a function of moisture content at constant temperature T_0.

From Eq. (4.19) and (4.22) it follows that the liquid diffusivity can be written as

$$a_{m2} = \frac{p(u)}{\nu(T)\rho_0}\left(\frac{\partial p_2}{\partial u}\right)_T \tag{11.5}$$

The use of the Eq. (4.19) which to some extent separates the temperature and moisture dependence of the liquid diffusivity might not always be strictly valid but it will nevertheless be used in the following. Furthermore, it is assumed that the change of the slope of the suction curve with temperature is negligible which gives the following expression for the temperature dependence of the liquid diffusivity

$$\frac{a_{m2}(u,T)}{a_{m2}(u,T_0)} = \frac{\nu(T_0)}{\nu(T)} \tag{11.6}$$

where $a_{m2}(u,T_0)$ is the liquid diffusivity measured as a function of moisture content at constant temperature T_0. The right hand side of Eq. (11.6) is shown in Fig. 11.1. It is seen that the temperature dependence of the liquid diffusivity over the observed temperature range is moderate.

The moisture diffusivity is the simple sum of the vapour diffusivity and the liquid diffusivity, see Eq. (6.11). In the following the temperature dependence of the moisture diffusivity is analysed from the temperature dependence of the vapour diffusivity and the liquid diffusivity. The analysis is performed at 7 different ratios between the vapour diffusivity and the liquid diffusivity given by

$$\frac{a_{m1}(u,T)}{a_{m2}(u,T)} = k \quad , \quad k = 0.001, 0.01, 0.1, 1, 10, 100, 1000 \tag{11.7}$$

From Eq. (6.11) and (11.7) it follows that

$$a_m(u,T_0) = a_{m1}(u,T_0) + a_{m2}(u,T_0) = (k+1)a_{m2}(u,T_0) \tag{11.8}$$

Combination of Eq. (6.11), (11.4), (11.6) and (11.7) gives

$$\begin{aligned} a_m(u,T) &\approx a_{m1}(u,T_0)\frac{p_s(T)}{p_s(T_0)} + a_{m2}(u,T_0)\frac{\nu(T_0)}{\nu(T)} \\ &= k a_{m2}(u,T_0)\frac{p_s(T)}{p_s(T_0)} + a_{m2}(u,T_0)\frac{\nu(T_0)}{\nu(T)} \end{aligned} \tag{11.9}$$

Finally Eq. (11.8) and (11.9) gives the following expression for the temperature dependence of the moisture diffusivity

$$\frac{a_m(u,T)}{a_m(u,T_0)} \approx \frac{k}{k+1}\frac{p_s(T)}{p_s(T_0)} + \frac{1}{k+1}\frac{\nu(T_0)}{\nu(T)} \tag{11.10}$$

where $a_m(u,T_0)$ is the moisture diffusivity measured as a function of moisture content at constant temperature T_0. The right hand side of Eq. (11.10) is plotted in Fig. 11.2 for different values of k. It is seen that the temperature dependence of the moisture diffusivity over the observed temperature range is very dependent of the ratio between the liquid diffusivity and the vapour diffusivity.

From the definition of the condensation factor given by Eq. (6.14) and from the expressions for the temperature dependence of the vapour diffusivity and the liquid diffusivity given by Eq. (11.4) and (11.6), respectively, it follows that

$$\varepsilon(u,T) \approx \frac{a_{m1}(u,T_0)\frac{p_s(T)}{p_s(T_0)}}{a_{m1}(u,T_0)\frac{p_s(T)}{p_s(T_0)} + a_{m2}(u,T_0)\frac{\nu(T_0)}{\nu(T)}} \tag{11.11}$$

which together with Eq. (11.7) gives

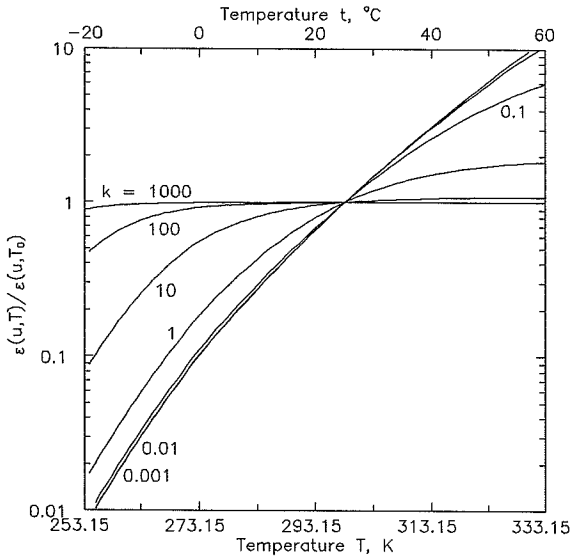

Figure 11.3. **Temperature dependence of the condensation factor.**

$$\frac{\varepsilon(u,T)}{\varepsilon(u,T_0)} \approx \frac{(k+1)\frac{p_s(T)}{p_s(T_0)}}{k\frac{p_s(T)}{p_s(T_0)}+\frac{\nu(T_0)}{\nu(T)}} \tag{11.12}$$

This expression is plotted in Fig. 11.3. It is seen that the temperature dependence of the condensation factor over the observed temperature range is strongly dependent on the ratio between the liquid diffusivity and the vapour diffusivity.

11.2 A model for the sorption isotherm as a function of u and T.

In section 3.3.7 a model for the sorption isotherm as a function of moisture content and temperature was presented as Eq. (3.44). The model is made on the basis of the thermodynamics of adsorption presented earlier in section 3.3. In order to use the model it is necessary to know the standard differential enthalpy of adsorption and the differential specific heat capacity of adsorption as functions of moisture content. Two empirical expressions given by Eq. (3.47) and Eq. (3.48) were introduced for this purpose.

The model was fitted to measurements of relative humidity as a function of moisture content and temperature for steam cured hardened cement paste and sitka spruce taken from literature. The fit was such that a cubic spline in advance was fitted to sorption isotherm at the reference temperature T_0 = 298.15 K. The cubic spline was used in stead of the models presented in section 3.3.6 (Langmuir, BET, modified BET by Nielsen) for two reasons.

Firstly, the Langmuir and the BET model did not cover the entire relative humidity range of interest.

Secondly, the modified BET model by Nielsen had troubles modelling the very pronounced "knee" of the sorption isotherm for steam cured hardened cement paste, see Fig. 3.3 for u = 0.01 kg/kg. The moisture content here was predicted too low by the modified BET model.

The result was that the regression procedure tried to level out this discrepancy at other temperatures by attributing even more physically unrealistic values to parameters in the empirical relations describing the standard differential enthalpy of adsorption and the differential specific heat of adsorption.

The result of the use of the model is seen in Fig. 3.15, 3.16 and 3.19 where measured values are compared to values calculated by the model. The difference between calculated and measured values is seen to be small. This indicates that the model provides a mean for the calculation the vapour pressure (or the relative humidity) when the moisture content is known. Admittedly, it is hard (read impossible) to explicitly find the moisture content from Eq. (3.44) when the relative humidity and the temperature are known.

The expressions used for the standard differential enthalpy of adsorption and the differential specific heat capacity of adsorption were introduced as empirical expressions. They are defined in such a way that they are exact in the limit, i.e. they are zero at saturation and equal to the value found when the first water molecule is adsorbed on the bare surface at zero moisture content. In between these extremes a power function interpolation is made.

There is no theoretical justification for the use of a power function for the interpolation. Nevertheless, the power function is able to fit the very few measurements of differential enthalpy and heat capacity found in literature.

It is possible to refine the model further if the differential specific heat capacity of adsorption is allowed to be a function of temperature.

Finally, the modelling capacity of the proposed model can be said to be fine seen in the light of it's theoretical justification from the thermodynamics of adsorption. The fineness of the model can be tuned to fit the users needs by adjustment. The adjustment can for instance be to make the differential specific heat capacity a function of temperature or on the contrary to omit it totally. Furthermore, the user is free to supply a model of own choice for the sorption isotherm at the reference temperature.

11.3 Evaluation of δ_p from cup measurements with a least squares method

In section 7.3.4 a method for the determination of the water vapour conductivity with a least squares method was presented. A small demonstration of the use of the method was given. Calculated versus measured water vapour flux from this demonstration example was presented in Fig. 7.8. It is seen that the accordance between the measured and the calculated values is quite good.

The method requires the use of an empirical expression which describes the water vapour conductivity as a function of relative humidity. No general guide-lines for the choice of this empirical expression can be given, which must be said to be a drawback of the method. Furthermore, it is recommendable that the cup measurements are organised in such a way that they are following the requirements of Bazant and Najjar's method.

If, due to practical circumstances, it is impossible to organise cup measurements according to Bazant and Najjar's method, the presented least squares offers a useful alternative for the evaluation of the relative humidity dependence of the water vapour conductivity.

11.4 Estimation of a_{m2} from sorptivity measurements

In section 7.8.2 two methods for the determination of constant isothermal liquid diffusivity from sorptivity measurements were presented. In the first method the validity of the expression given by Eq. (7.38) was assumed and led the expression for the liquid diffusivity given by Eq. (7.43). The liquid diffusivity found by this method is in the following part of this section denoted by $a_{m2}^{(1)}$.

In the second method it was assumed that the transfer of liquid takes place as a diffusion into semi-infinite media governed by Fick's second law with constant diffusivity. Thereby, the so-called error function solution given by Eq. (7.34) can be applied. This led to expression for the liquid diffusivity presented in Eq. (7.49).The liquid diffusivity found by this method is in the following part of this section denoted by $a_{m2}^{(2)}$.

The two expressions for finding the liquid diffusivity from sorptivity measurements, Eq. (7.43) and Eq. (7.49), are not identical. Mathematically seen the method given by Eq. (7.49) is to prefer because it is elucidated without approximations like the one required by Eq. (7.43), compare Eq. (7.37) and (7.39).

The ratio between the liquid diffusivities calculated with the two methods is found from Eq. (7.43) and (7.49) as

$$\frac{a_{m2}^{(1)}}{a_{m2}^{(2)}} = \frac{1}{4\pi} \tag{11.13}$$

under the assumption that the initial moisture content is zero ($u_i = 0$) and all the porosity is open.

This ratio implies that the two methods have different physical significance or that one of them is less trustworthy.

In Fig. 7.20 and 7.21 a sorptivity experiment made with cellular concrete by Nielsen [69] was presented. From the slope of the straight line to the left in Fig. 7.20 and the height of the specimen (0.15 cm, see Fig. 7.21) the sorptivity S can be determined. The liquid diffusivities calculated from the sorptivity calculated with the two methods are

$$a_{m2}^{(1)} = 9.7 \cdot 10^{-10} \text{ m}^2/\text{s}$$

$$a_{m2}^{(2)} = 1.3 \cdot 10^{-8} \text{ m}^2/\text{s}$$

when the values $u_{vac} = 1.37$ kg/kg, $u_i = 0.033$ kg/kg and $\rho_s = 2650$ kg/m^3 are used.

It is interesting to compare these liquid diffusivities with the moisture diffusivity found as a function of the degree of saturation. If the moisture diffusivity is known as a function of the degree of saturation, an average moisture diffusivity can be found as

$$< a_m >= \frac{1}{S_1 - S_2} \int_{S_1}^{S_2} a_m(S) \mathrm{d}S \tag{11.14}$$

In section 10.2.1 the isothermal moisture diffusivity of cellular concrete was determined as a function of the degree of saturation with the inverse method presented in chapter 8.5. The moisture diffusivity was found from measurements made by Nielsen [69] of the moisture content in test specimens as a function of time and space during isothermal drying, see section 9.2.1.

The average moisture diffusivity of the cellular concrete specimens 188, 197 and 198, can be found from the moisture diffusivities presented in Fig. 10.7, using S_1 = 0.033 kg/kg / 1.37 kg/kg = 0.024 and S_2 = 1. The average moisture diffusivities are

$$< a_m >_{188} = 2.2 \cdot 10^{-8} \text{ m}^2/\text{s}$$

$$< a_m >_{197} = 8.6 \cdot 10^{-8} \text{ m}^2/\text{s}$$

$$< a_m >_{198} = 7.2 \cdot 10^{-9} \text{ m}^2/\text{s}$$

These average moisture diffusivities approximates the liquid diffusivity $a_{m2}^{(2)}$ found from the sorptivity experiment better than $a_{m2}^{(1)}$. This cannot be seen as an authoritative proof of the superiority of Eq. (7.49) to Eq. (7.43). But it seems to be a piece of evidence on the positive side. The low value of the $<a_m>_{198}$ is due to the erroneous slope of the estimated moisture diffusivity of this specimen at degrees of saturation greater than 0.85. Therefore, there should not be paid too much attention to this value.

Another interesting feature is exhibited by the expression given by Eq. (7.49). The liquid diffusivity calculated from sorptivity experiments with this expression goes towards infinity when the initial moisture content u_i approaches the moisture content at saturation u_{vac}. The same is seen to be the case with the measured moisture diffusivities presented in Fig. 10.7. Theoretically this was to be expected because the slope of the suction curve is zero at saturation thereby causing the liquid diffusivity to become infinite (see Eq. (4.22).

It could be interesting to perform a series of sorptivity experiments where initial degree of saturation of the test specimens of the material under investigation are preconditioned to a number of different degrees of saturation, say $S \in \{0, 0.1, 0.2, ..., 1\}$. The degree of saturation must be constant throughout the specimens.

From the sorptivity curves the liquid diffusivity $a_{m2}^{(2)}$ is calculated with the expression given by Eq (7.49). A guess is made on a functional that is capable of modelling the moisture content dependence of the moisture diffusivity. The functional could for instance be an expression similar to Eq. (10.10). Finally, the moisture content dependence of the moisture diffusivity is evaluated by finding the unknown constant in the functional by fitting the average moisture diffusivities $<a_m>$ found from Eq. (11.14) to the liquid diffusivities $a_{m2}^{(2)}$ found from the determined sorptivities.

A first attempt to evaluate the possibilities of this procedure could be made numerically by calculating the moisture content profiles during a fictitious sorptivity experiment. In the calculations a moisture diffusivity with an a priori known moisture content dependence is used. Then from the calculated moisture content profiles the sorptivity is calculated and the above outlined procedure can be tested.

Admittedly this idea has not been theoretically validated. In it's present form it can merely be seen as an educated guess. Nevertheless, it is felt that in this way it might be possible to evaluate the moisture content dependence of the moisture diffusivity from simple sorptivity experiments.

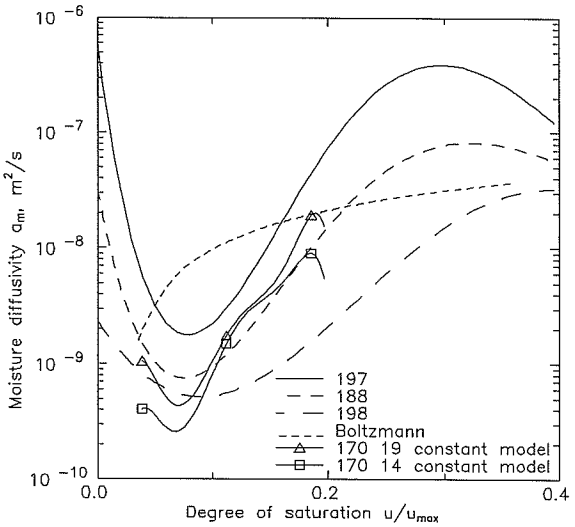

Figure 11.4. **Comparison of liquid and moisture diffusivity of cellular concrete as a function of the degree of saturation.**

Summarising, a method for the calculation the liquid diffusivity from sorptivity experiments has been presented. The method is based on the assumptions that the liquid diffusivity is constant, that the test specimen is semi-infinite and that the moisture concentration is uniform at the start of the sorptivity experiment. Based on few observation the method is found likely to yield values of the liquid diffusivity which correspond to the average moisture diffusivity in the area between total saturation and the initial degree of saturation.

11.5 Boltzmann transformation

In section 10.1 the Boltzmann transformation was used for the determination of the liquid diffusivity of cellular concrete and brick as a function of moisture content. The Boltzmann transformation was used on measurements made by Nielsen and K. K. Hansen. The measurements are presented in section 9.1.

The use the Boltzmann transformation on cellular concrete is described in section 10.1.1. A simple linear expression was used for the description of the Boltzmann transformed as a function of moisture content. Although this expression probably is too simple to describe the real shape of the Boltzmann transformed moisture profiles of cellular concrete during isothermal suction, the experimentally determined values are so few and scattered that they do not justify a more refined model, see Fig. 10.1.

In Fig. 11.4 the liquid diffusivity of cellular concrete calculated with the Boltzmann transformation is compared to the moisture diffusivity found in section 10.2 from isothermal drying (specimens 188, 197 and 198) and condensation experiments (specimen 170) with an inverse method.

As was to be expected from the theory the comparison does of course not yield identical results. This is due to the difference caused by hysteresis and the fact that liquid diffusivity is compared to moisture diffusivity.

In the degree of saturation range 0.04 to 0.16 the liquid diffusivity calculated with the Boltzmann transformation seems to be overestimated. At degrees of saturation greater than 0.16 the liquid diffusivity might be underestimated.

Furthermore, from comparison with the moisture diffusivities calculated from the drying experiments it is seen that the slope of the liquid diffusivity is too low. It was to be expected that it would have a slope similar to the slope of tangent of the moisture diffusivities between their minima (approximately at $u/u_{max} = 0.08$) and maxima (approximately at $u/u_{max} = 0.3$).

The deviations from what was to be expected is mainly attributed to the primitive linear model applied with the Boltzmann transformation. Despite of these deviations from the expected shape of the liquid diffusivity curve the order of magnitude seems to be acceptable.

The use of the Boltzmann on brick is described in section 10.1.2. The third order polynomial used to describe the Boltzmann transformed as a function of moisture content resulted in the 6th order polynomial expression given by Eq. (10.3) for the description of the liquid diffusivity as a function of moisture content. In two cases, that is for specimen R481 (measurements by K. K. Hansen) and specimen R583 (measurements by Nielsen) a second order polynomial was used in stead of the third order polynomial.

The liquid diffusivities of yellow bricks seen in Fig. 10.3 and 10.4 appears to be very similar. All except one (specimen G465) exhibit more or less pronounced maxima and minima or points of inflection at a moisture content around 0.06 m^3/m^3. The liquid diffusivities of the red bricks seen in Fig. 10.5 do not have these extrema but are simply monotonously increasing with moisture content.

The liquid diffusivities found with the Boltzmann transformation from measurements by K. K. Hansen are in Fig. 10.6 compared to the liquid diffusivities calculated from measurements made by Nielsen on the very same bricks. The results from the two sets of measurements are not identical. There is no reason to believe that one of the sets of measurements is better than the other. The differences must be attributed to the reproducibility of the moisture content measurements and probably also to the way the Boltzmann transformation has been used.

From Table 10.1 it is seen that with the use of the Boltzmann transformation it is possible to determine the liquid diffusivity of brick within 10 hours of experimental time.

If one has the access to equipment for the measurement of moisture content as a function of time and space during capillary suction, the Boltzmann transformation provides an effective tool for the evaluation of the liquid diffusivity as a function of moisture content.

11.6 Estimation method used in this work

In section 8.5 a so-called inverse method for the estimation of the transfer coefficients in the Luikov model was presented. Theoretically, inverse methods offer certain advantages over traditional methods, i.e. allow for the release of restrictions such as steady state conditions. Furthermore, the inverse methods have the possibility of yielding a mathematical, although empirical, expression for the transfer coefficients as functions of moisture content and temperature. The mathematical expression might afterwards be used for simulation purposes.

The use of the method was at first demonstrated in chapter 8.5.1 on simulated "measurements". The transfer coefficients were restricted to moisture content dependence. The method worked well on this demonstration problem. Convergence was obtained in the optimisation procedure after 29 iteration steps. The iteration step size was reduced by a factor of 10 in the first 20 steps to ensure convergence.

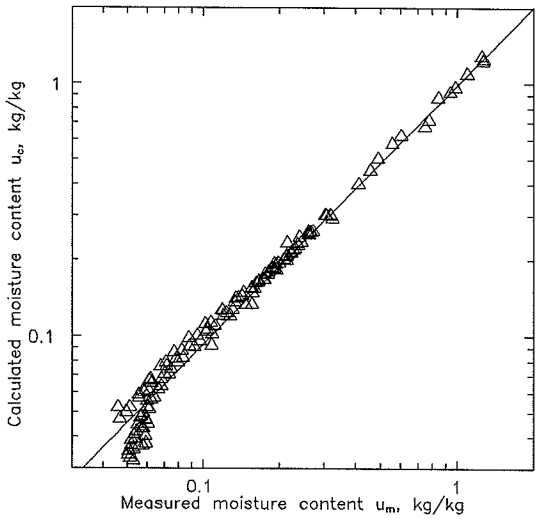

Figure 11.5. **Calculated versus measured moisture content. Specimen 188.**

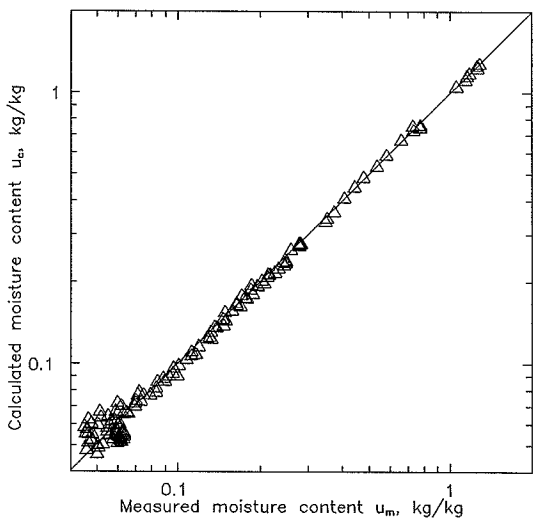

Figure 11.6. **Calculated versus measured moisture content. Specimen 197.**

In order to make things a little more difficult, the condensation factor was changed to a 2nd order polynomial in stead of the expression given by Eq. (8.35) which was used in the simulation of the "measured" data. This presented no difficulty to the estimation procedure.

The result of the estimation is presented in Fig. 8.2a and 8.2b. It is seen that difference between the estimated and the simulated ("measured") values is small. This gave the courage to test the method with real data measured during diffusive heat and mass transfer in porous media.

In section 10.2 the estimation method was tested on temperature and moisture content data measured during experiments made with cellular concrete. The data were taken from literature.

In section 10.2.1 the method was tested on isothermal drying experiments. The method was used on three different sets of data from tests made with three specimens. The estimated isothermal moisture diffusivity is presented in Fig. 10.7. Also shown in Fig. 10.7 is the moisture diffusivity of cellular concrete measured by van der Kooi. It is seen that the moisture diffusivity estimated in this work is very similar to the one measured by van der Kooi.

The diffusivities of the three specimens are not identical. They tend to exhibit the two minima and the maximum at degrees of saturation similar to those found in van der Kooi's measurements. The diffusivity of specimen 198 is obviously wrong at degrees of saturation greater than 0.85, where it goes towards zero instead of going towards infinity like the diffusivity of specimens 188 and 197.

It is hard to tell whether the horizontal inflection of the moisture diffusivity curve for specimens 188 and 197 round a degree of saturation of 0.6 are of physical nature or they merely are a result of the selected order of the Chebyshev polynomial. This might have been revealed by performing the estimation several times with Chebyshev polynomials of varying order.

Figure 11.5 shows how the moisture content calculated with the moisture diffusivity estimated for specimen 188 corresponds to the measured moisture content which was used as goal in the optimisation. A total of 140 moisture contents, all shown as triangles in Fig. 11.5, at varying experimental hours and varying space coordinate were used. There is a slight tendency of the calculated moisture content at low values to lie a little below the line $u_c = u_m$ (*calculated = measured*). Although this tendency exists, the slope of the line is close to 1 (1.00458) and

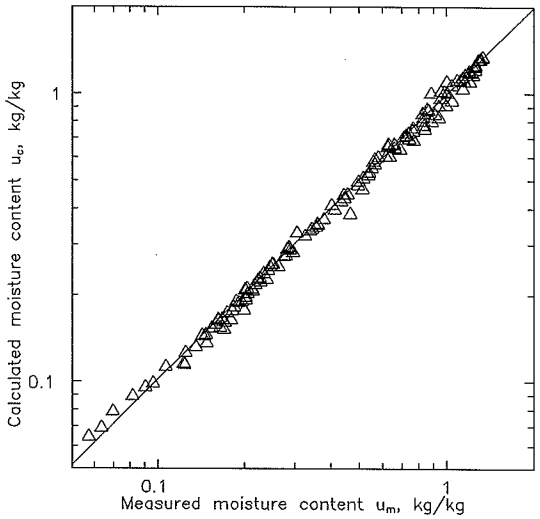

Figure 11.7. **Calculated versus measured moisture content. Specimen 198.**

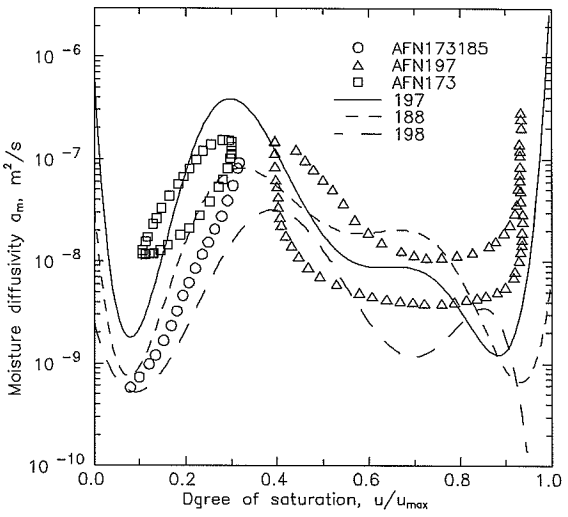

Figure 11.8. **Moisture diffusivity of cellular concrete. Comparison of diffusivities found by the inverse method (lines) to diffusivities found by Nielsen [69] (markers).**

the intercept with the u_c-axis is only -0.00035, so all in all it can be concluded that the estimation procedure has used the information in the input data (the measured moisture contents) satisfactorily.

Figure 11.6 and Fig. 11.7 shows the calculated moisture content as a function of the measured moisture content for specimens 197 and 198 respectively. The results are very similar to those obtained for specimen 188.

In Fig. 11.8 the isothermal moisture diffusivity found with the inverse method is compared to moisture diffusivity determined by Nielsen [69]. The comparison is interesting because the moisture diffusivity is determined from measurements made on very comparable specimens. In one case, that is for specimen 197, the moisture diffusivity is even calculated for the very same measurements made on the very same specimen but with two different methods which on one hand, are the estimation method discussed in this section and on the other, Krischer's method used by Nielsen, respectively.

Nielsen's measurements of moisture diffusivity of the specimens 173, 185, and 197 are represented by markers in Fig. 11.8 which are enclosing areas in which the diffusivities can be found. The moisture diffusivity of specimen 197 measured by Nielsen is seen in Fig. 11.8 as the area bounded by the triangles. The solid line represents the moisture diffusivity found with the inverse method discussed in this section. The latter matches Nielsen's measurements relatively well. Altogether, the diffusivities found with the inverse method compares reasonably well with Nielsen's measurements.

In section 10.2.2 two attempts were made to determine all four transfer coefficients in the Luikov model with the inverse method. In the first attempt the 19 constant model given by Eq. (10.17) - (10.29) was used.

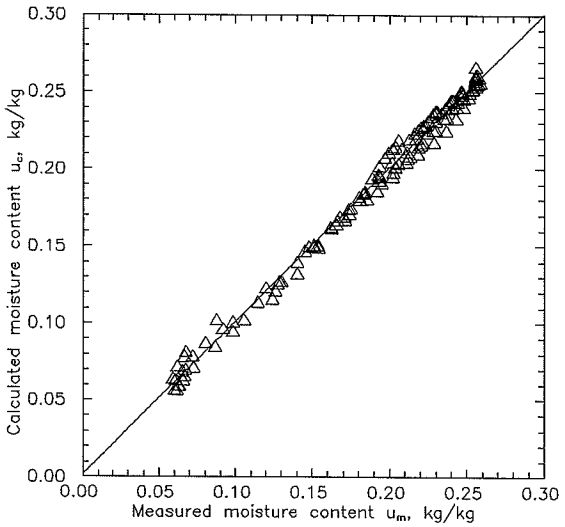

Figure 11.9. **Calculated versus measured moisture content. Specimen 170. 19 constant model.**

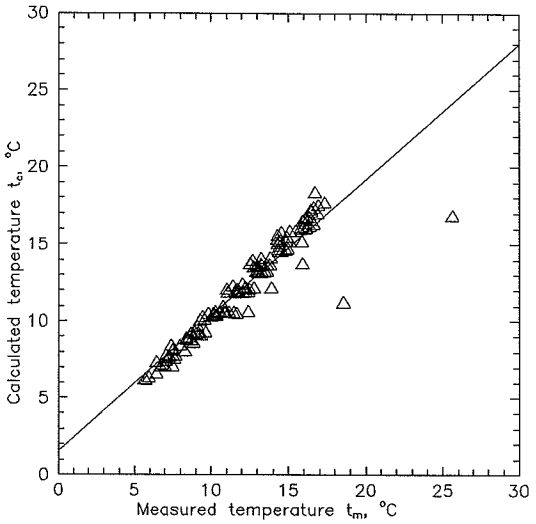

Figure 11.10. **Calculated versus measured temperature. Specimen 170. 19 constant model.**

In the 19 constant model all four transfer coefficients were functions of the moisture content but independent of temperature. After 125 iterations the estimation procedure was intentionally stopped. An examination of the material properties estimated after 125 iterations showed that the functions describing the thermal conductivity and the condensation factor yielded absolutely unrealistic values.

In Fig. 10.10 it is seen that the thermal conductivity estimated with the 19 constant model is almost 5 orders of magnitude lower than the initial guess. The initial guess was taken from literature and is representative for cellular concrete.

The condensation factor shown in Fig. 10.12 is also behaving strangely. As a matter a fact it has lost it's physical meaning by being small where it should have been large and vice versa.

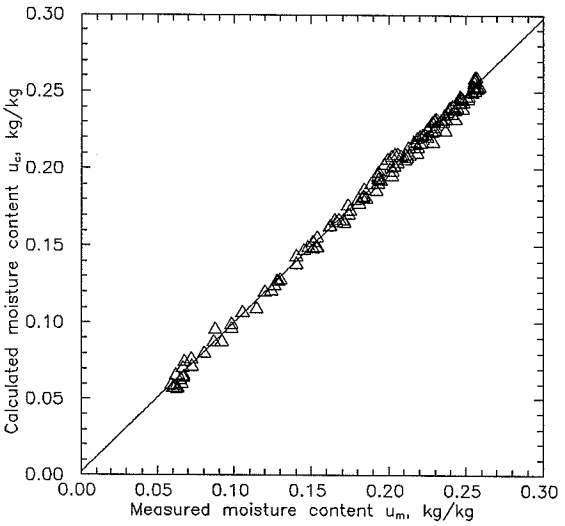

Figure 11.11. **Calculated versus measured moisture content. Specimen 170. 14 constant model.**

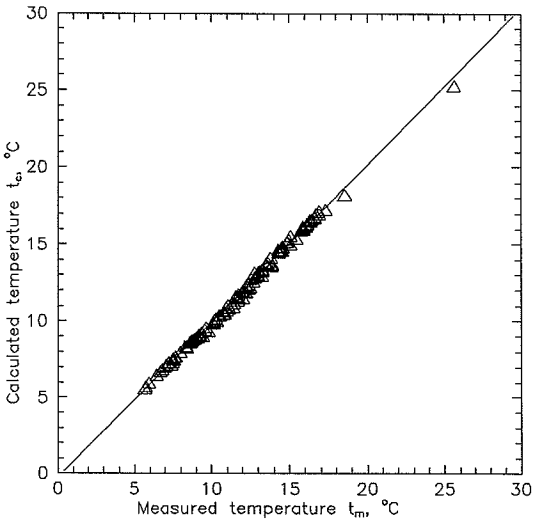

Figure 11.12. **Calculated versus measured temperature. Specimen 170. 14 constant model.**

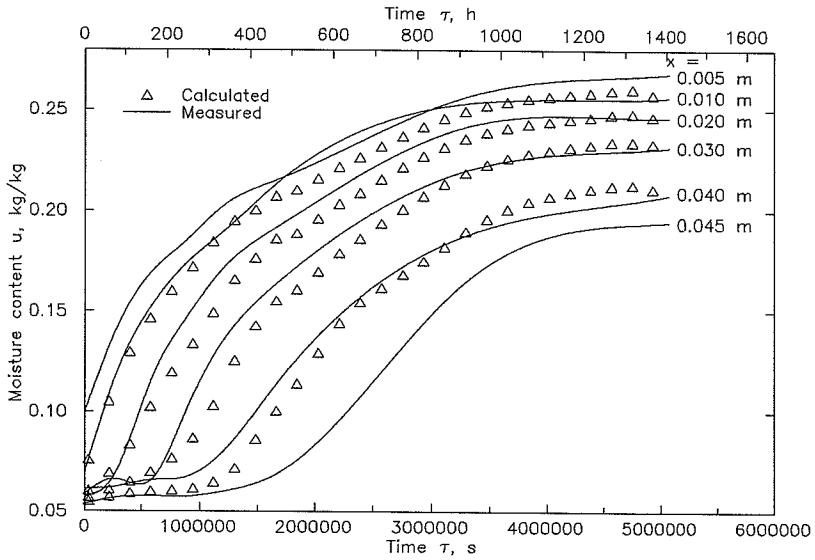

Figure 11.13. **Comparison of calculated and measured moisture content in cellular concrete specimen during condensation as a function of time and space coordinate. Specimen 170. 14 constant model.**

The effect of these two irregularities is not very pronounced in the comparison of the calculated versus measured moisture contents in Fig. 11.9. There tends to be a scatter around the line *calculated = measured*, but it is nicely distributed. Adversely, there are some substantial outliers seen in Fig. 11.10 where the calculated versus measured temperatures are shown.

These two irregularities led to the reduction of the 19 constant model to a 14 constant model where the condensation factor was kept at a constant value. This model behaved much more appropriately. The iteration was started off with the final iteration values from the 19 constant model and convergence was obtained after only 31 iterations.

The calculated versus measured values of moisture content and temperatures are shown in Fig. 11.11 and Fig. 11.12, respectively. In Fig. 11.11 it is seen that the scatter around the line *calculated = measured* has slightly diminished compared to 19 constant model. In Fig. 11.12 it is seen that the outliers now are much more close to line of equality.

The calculated versus measured moisture content as a function of space coordinate and experimental time is presented in Fig. 11.13. Observe that the measured values in Fig. 11.13 are interpolated, compare with Fig. 9.5. Furthermore, the temperatures for $x = 0.005$ m and $x = 0.045$ m are the boundary conditions used in the estimation. Therefore, no calculated values are shown for these. It is seen that difference between measured and calculated values is fairly tolerable.

In Fig. 11.14 the calculated versus measured temperatures are shown as a function of space coordinate and experimental time. Again, the measured values are interpolated, compare with Fig. 9.6. Furthermore, the temperatures for $x = 0.005$ m and $x = 0.045$ m are the boundary conditions used in the estimation. It is seen that the calculated temperature matches the measured temperatures quite well.

In Fig. 10.8 the moisture diffusivity estimated with the 14 constant model is compared to moisture diffusivity estimated with the 19 constant model and to the initial guess. It is seen that the moisture diffusivity estimated with the 14 constant model is a little lower than that estimated with the 19 constant model.

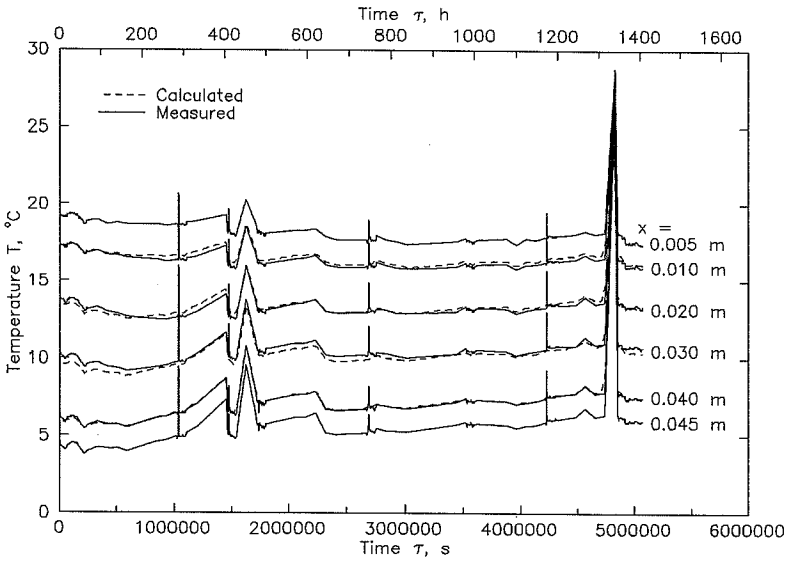

Figure 11.14. **Comparison of calculated and measured temperatures in cellular concrete specimen during condensation as a function of time and space coordinate. Specimen 170. 14 constant model.**

In Fig. 11.4 the moisture diffusivities estimated with the 14 and the 19 constant models from the condensation experiments are compared to the moisture diffusivities found from the drying experiments. The condensation experiment diffusivities are a little lower than the drying experiment diffusivities which was to be expected when hysteresis is considered.

In Fig. 10.9 The thermogradient coefficient estimated with the 14 constant model is compared to the thermogradient coefficient estimated with the 19 constant model and to the initial guess. The initial guess is quite close to one of the thermogradient coefficients found by Nielsen [69]. It seen that the estimated thermogradient coefficinets found in this work is a factor of 3 lower at the maximum value.

In Fig. 10.11 The thermal conductivity estimated with the 14 constant model is compared to the initial guess. It is seen that the estimated thermal conductivity is comparable to the initial guess. It is doubtful whether the shape of the thermal conductivity curve can be attributed to the physical properties of the cellular concrete because the estimated thermal conductivity depends on the chosen value of the thermogradient coefficient.

The concept of using inverse method leads to the idea that in the future it might be possible to determine the transfer coefficients in the Luikov model (or other models) from measurements of moisture content and temperature as a function of time and space in multi-layered structures in use. Before this vision becomes true, several difficulties have to be overcome. A rather long but probably incomplete list of these problem can be given:

A special feature used with the estimation procedure proved to be successful. As boundary conditions in the numerical solution of the Luikov equation set, temperatures and moisture content measured inside the test specimens were used. This eliminated the need for simulation of evaporation and or impermeable boundaries. Especially the simulation of evaporation might have added a substantial error to result of the estimation procedure.

1 It is necessary to possess an estimation method which makes use of a robust optimisation procedure. In this connection, robustness is seen as the ability of finding a solution to the inverse problem under investigation without it being necessary to make initial guesses on the constants in the functions describing the material properties which are very close to the ones obtained when convergence has ended the iteration procedure.

2 It requires the development of a model for the heat and mass transfer in a multi-layer structure. The development of such models has been demonstrated by several authors, see for instance Kohonen [66] or Pedersen [18].

3 It is necessary to have adequate functions for description of the heat and mass transfer coefficients. On one hand the functions must possess the necessary degrees of freedom that makes it possible to model the transfer coefficients without posing restrictions on them and on the other hand they must not contain too many parameters to estimate. The optimal solution would of course be to have mathematical expressions with physical significance and not just rely on empirical expressions. It is hard to put forward such physical meaningful expressions without posing to many restrictions on their generality.

4 It will be necessary to possess methods that are suitable for non-destructive measurement of temperatures and moisture content in the different layers of the structure as a function of time and space. The temperature measurements can be performed with relative ease by means of thermocouples. The problem is with the measurement of the moisture content as a function of time and space. So far no reliable non-destructive and easy-to-use in situ methods have been presented. Thermal probes like the one shown in Fig. 7.1 might be a possibility, but they require a lot of calibration work.

5 Using an inverse method on heat and mass transfer in a multi-layered in-situ structure would require excessive computational power. More layers means more coefficients to estimate in the functions describing the material properties. More coefficients means that more measurements have to be included in the penalty function which will cause additional computational work.

6 It will be necessary to have powerful tools for preprocessing the data measured in-situ. These tools would be used for setting up input data for the estimation procedure. A part of such a tool would probably be a two-dimensional interpolation procedure. Another part would be a correction module for the handling of errors in the measured data.

7 Finally, it must not be forgotten that so far we have only been dealing with diffusive transfer of heat and moisture transfer. If convection also takes place the much more sophisticated models must be used and the success of inverse methods would be enormously difficult to accomplish.

Robust optimisation procedures were mentioned above as a tool for improvement of the estimation procedure. A single robust optimisation procedure has been tried in this work. The procedure was the MINL2, kindly provided by Numerical Institute, The Technical University of Denmark.

Unfortunately this procedure was a little to investigative. In it's search for an optimum solution it tried to make look into the region of large negative thermal conductivities. This of course has no physical meaning. Nevertheless, it would have been totally harmless if it only was an iteration step on the way to a reasonable positive thermal conductivity.

It was never revealed whether this might have been the result. What happened was that the numerical finite difference procedure, which solves the Luikov model, became unstable and the calculation ended with an underflow exception. Therefore, one shall not expect that robust optimisation procedures are magic solutions to this kind of estimation problems. Nevertheless, it is the belief of the author that customised robust estimation procedures will be valuable tools in solving inverse problems like the one dealt with in this work.

12 Conclusion

The thermodynamic properties and the transport properties of water have been presented. On the basis of these properties approximations for the calculation of the temperature dependence of the vapour diffusivity, the liquid diffusivity, the moisture diffusivity and the condensation factor were made.

The thermodynamics of adsorption of porous materials has been presented as far as useful for building physics. On this basis a model for the sorption isotherm as a function of moisture content and temperature was elucidated. Two empirical expressions for the description of the standard differential enthalpy of adsorption and the differential specific heat capacity of adsorption as functions of moisture content were introduced.

Using these expressions and a cubic spline fit for the description of the sorption isotherm at a reference temperature the model was used to describe measurements of relative humidity of steam cured hardened cement paste and sitka spruce. The modelling covered the full relative humidity range (0 - 1) and the temperature range from 0 ° C to 100 °C. The differences between measured values and values predicted by the model were relatively small.

A least squares based method for the evaluation of the water vapour conductivity from cup measurements as a function of relative humidity has been proposed. The method is an alternative to Bazant and Najjar's method if the cup measurements are not fulfilling the requirement of this method.

A method for the calculation of the liquid diffusivity from the sorptivity determined in a capillary suction experiment has been presented. The method is based on the assumptions that the liquid diffusivity is constant, that the test specimen behaves like a semi-infinite media and that the moisture concentration is uniform at the start of the experiment. Liquid diffusivity calculated from a sorptivity experiment made with cellular concrete compared relatively well with average moisture diffusivity found from drying experiments.

A procedure for the use of the Boltzmann transformation for the determination of liquid diffusivity as a function of moisture content has been presented. The method was used to estimate the liquid diffusivity of cellular concrete and brick.

The use of inverse methods for the estimation of the transfer coefficients in the Luikov model for coupled heat and moisture transfer in porous media has been demonstrated. The use of the inverse method was demonstrated on simulated temperature and moisture fields. The method worked well on isothermal drying experiments.

It was tried to estimate all four transfer coefficients in the Luikov model as functions of moisture content using the inverse method on measured moisture and temperature fields. In this attempt a model incorporating 19 constants in the functions describing the material properties was used. While the estimated functions describing the moisture diffusivity and the thermogradient coefficient were acceptable, the estimated functions describing the thermal conductivity and the condensation factor had lost physical meaning.

The estimation of the moisture diffusivity, the thermogradient coefficient and the thermal conductivity using the inverse method with a fixed value of the condensation factor, from measured fields of moisture content and temperature, was successful. Moisture content and temperature calculated with the estimated functions as functions of space coordinate and experimental time compares well with the corresponding measured values.

References

1. Barin, I., *Thermochemical Data of Pure Substances*, VCH, Weinheim, 1989.

2. Eisenberg, D., and Kauzmann, W., *The Structure and Properties of Water*, Clarendon Press, Oxford, 1969.

3. *Handbook of Chemistry and Physics*, 64th edition, 1983-1984, CRC Press, Florida, 1984.

4. Haar, L., Gallagher, J. S., and Kell, G. S., *NBS/NRC Wasserdampftafeln*, Springer-Verlag, Berlin, 1988.

5. Keenan, J. H., Keyes, F. G., Hill, P. G., and Moore, J. G., *Steam Tables,* Wiley, New York, 1978.

6. Vos, B. H., and Tammes, E., Moisture and Moisture Transfer in Porous Materials, Institute TNO for Building Materials and Building Structures, Report No. BI-69-96, Delft, 1969.

7. Bird, R. B., Stewart, W. E., and Lightfoot, E. N., *Transport Phenomena*, Wiley, New York, 1960.

8. Krischer, O., and Kröll, K., *Die wissenschaftlichen Grundlagen der Trocknungstechnik*, 2nd edition, Springer-Verlag, Berlin, 1963.

9. de Vries, D. A., The theory of heat and moisture transfer in porous media revisited, *Int. J. Heat Mass Transfer*, Vol. 30, No. 7, pp. 1343-1350, 1987.

10. Lykow, A. W., *Transporterscheinungen in kapillarporösen Körpern*, Akademie-Verlag, Berlin, 1958.

11. Hütte, *Taschenbuch der Werkstoffkunde* (Stoffhütte), 4th edition, Berlin, 1967.

12. Condon, E. U., and Odishaw, H., *Handbook of Physics*, McGraw-Hill, New York, 1958.

13. Jakob, M., and Erk, S., Die Wärmeleitfähigkeit von Eis zwischen 0 und -125°, *Zeitschr. f. techn Physik*, Vol. 10, No. 12, pp. 623-624, 1929.

14. Bonacina, C., Comini, G., Fasano, A., and Primicerio, M., Numerical solution of phase-change problems, *Int. J. Heat Mass Transfer*, Vol. 16, No. 10, pp. 1825-1832, 1973.

15. Stamm, A. J., and Loughborough, W. K., Thermodynamics of the Swelling of Wood, *Journal of Physical Chemistry*, Vol. 39, No. 1, pp. 121-132, 1935.

16. Radjy, F., Thermodynamic Parameters for Sorption of Water by Hardened Cement Paste, Presented as paper no. 6, Cements Division, 77th Annual Meeting, The American Ceramic Society, May 3-8, Washington D.C., 1975.

17. Radjy, F., and Sellevold, E. J., Measurement of Isosteric P-T Data for Pore Water, Unpublished report, Building Materials Laboratory, The Technical University of Denmark, Lyngby, 197?.

18. Pedersen, C. R., Combined Heat and Moisture Transfer in Building Constructions, Report no. 214, Thermal Insulation Laboratory, The Technical University of Denmark, Ph.D. thesis, Lyngby, 1990.

19. Sandberg, P. I., Byggnadsdelars fuktbalans i naturligt klimat (in Swedish with summary in English; Moisture Balance in Building Elements exposed to Natural Conditions), Report 43, Division of Building Technology, Lund Institute of Technology, Tekn. Dr. thesis, Lund, 1973.

20. Kollmann, F., *Technologie des Holzes und der Holzwerkstoffe*, 2nd edition, Springer-Verlag, Berlin, 1982.

21. Flood, E. A. (Editor), *The Solid-Gas Interface*, Vol. 1-2, Marcel Dekker, Inc., New York, 1967.

22. Brunauer, S., Emmett, P. H., and Teller, Ex., Adsorption of Gases in Multimolecular Layers, *Journal of the American Chemical Society*, Vol. 60, pp. 309-319, 1938.

23. Nielsen, L. F., Moisture sorption in porous materials - A rational fit procedure, TR-200, Building Materials Laboratory, The Technical University of Denmark, Lyngby, 1989.

24. Bomberg, M., Moisture flow through porous building materials, Report 52, Division of Building Technology, Lund Institute of Technology, Tekn. Dr. thesis, Lund, 1974.

25. Sørensen, E. V., Water vapour permeability of hardened cement paste, Technical Report 83/80, Building Materials Laboratory, The Technical University of Denmark, Ph.D. thesis, Lyngby, 1980.

26. Fauconnier, R., Influence de l'humidite sur la consommation energetique d'un batiment en chauffage discontinu (modelage et copulage des phenomenes), in *L'humidite dans le batiment*, conseil international de la lanque francaise, pp. 147-186, Paris, 1984.

27. Fick, A., Ueber Diffusion, *Poggendorf Annalen der Physik und Chemie*, Vol. 94, No. 174, pp. 59-86, Leipzig, 1855.

28. Pitts, D. R., and Sissom, L. E., *Theory and problems of heat transfer*, Schaum's outline series in engineering, Addison Wesley, New York, 1977.

29. Gröber, H., Erk, S., and Grigull, U., *Die Grundgesetze der Wärmeübertragung*, Springer Verlag, Berlin, 1955.

30. Eckert, E. R. G., and Drake, R. M., *Analysis of heat and mass transfer*, McGraw-Hill, New York, 1959.

31. Carslaw, H. S., and Jaeger, J. C., *Conduction of heat in solids*, 2nd edition, Oxford University Press, Oxford, 1959.

32. Luikov, A. V., *Analytical Heat Diffusion Theory*, Academic Press, New York, 1968.

33. Lykov, A. V., and Mikhailov, Y. A., *Theory of energy and mass transfer*, Pergamon Press, Oxford, 1965.

34. Christiansen, C., Absolut Maaling af Udstraalings- og Indsugningsevne for Varme, (in Danish; Absolute Measurement of Emissivity and Absorptivity of Heat), *Oversigt over det Kongelige Danske Videnskabernes Selskabs Forhandlinger og dets Medlemmers Arbejder* i Aaret 1883, Bianco Lunos Kgl. Hof-Bogtrykkeri, Kjøbenhavn, pp. 20-57, 1883-1884.

35. Luikov, A. V., *Heat and Mass Transfer in Capillary-porous Bodies*, Pergamon Press, Oxford, 1966.

36. Luikov, A. V., Systems of Differential Equations of Heat and Mass Transfer in Capillary-Porous Bodies (Review), *Int. J. Heat Mass Transfer*, Vol. 18, No. 1-A, pp. 1-13, 1975.

37. Philip, J. R., and de Vries, D. A., Moisture Movement in Porous Materials under Temperature Gradients, *Transactions, American Geophysical Union*, Vol. 38, No. 2, pp. 222-232, 1957.

38. Pedersen, C. R., and Rasmussen, M. H., Kombineret fugt- og varmetransport i bygningsmaterialer (in Danish; Coupled moisture and heat transfer in building materials), M.Sc. thesis, Thermal Insulation Laboratory, The Technical University of Denmark, Lyngby, 1986.

39. Harmathy, T. Z., Simultaneous moisture and heat transfer in porous systems with particular respect to drying, *I&EC Fundamentals*, Vol. 8, No. 1, February, pp. 92-103, 1969.

40. Kiessl, K., Kapillarer und dampfförmiger Feuchtetransport in mehrschictigen Bauteilen, Universität-Gesamthocschule-Essen, Dr.-Ing. thesis, Essen, 1983.

41. Andersson, A.-C., Verification of calculation methods for moisture transport in porous building materials, report D6, Swedish Council for Building Research, Tekn. Dr. thesis, Stockholm, 1985.

42. Siang, H., Simultaneous heat and mass transfer in a porous medium, Department of Mechanical Engineering, Kansas State University, Ph.D. thesis, Manhattan, 1981.

43. ISO/DIS 8302 Thermal Insulation - Determination of steady-state areal thermal resistance and related properties - Guarded hot plate apparatus

44. ISO/DIS 8301 Thermal Insulation - Determination of steady-state specific thermal resistance and related properties - Heat flow meter method

45. ISO/DIS 10051 Thermal Insulation - Moisture effects on heat transfer - Determination of hygrothermal transmissivity

46. Perrin, B., and Javelas, R., Transferts couples de chaleur et de masse dans des matériaux consolides utilises en génie civil, *Int. J. Heat Mass Transfer*, Vol. 30, No. 22, pp. 297-309, 1987.

47. Foures, J. C., Javelas, R., and Perrin, B., Caractéristiques thermiques de matériaux de construction. Détermination. Variation en fonction de la teneur en eau, *Révue Génerale de Thermique. Fr,* No. 230, Février, 1981.

48. Foures, J. C., Javelas, R., and Perrin, B., Application d'une méthode impulsionelle à la détermination du coefficient de conductivité thermique des matériaux de construction, *Révue Génerale de Thermique. Fr,* No. 218, Février, 1980.

49. Jespersen, H. B., Bestemmelse af varmeledningstal for bygge- og isoleringsmaterialer ved varierende fugtindhold (in Danish; Determination of thermal conductivity of building and insulation materials at varying moisture contents), *Varme*, Vol. 14, No. 3-4, 1949.

50. West, G. P., and Hansen, K. K., Kopudstyr til måling af fugttransport (in Danish; Cup equipment for measurement of moisture transfer), Technical Report 179/88, Building Materials Laboratory, The Technical University of Denmark, Lyngby, 1988.

51. Bertelsen, N. H., Diffusionsmåling med kop-metoden på rødgran (in Danish; Diffusion measurement with the cup method on spruce), Technical Report 129/83, Building Materials Laboratory, The Technical University of Denmark, Ph.D. thesis, Lyngby, 1983.

52. Tveit, A., Measurements of moisture sorption and moisture permeability of porous materials, Rapport 45, Norwegian Building Research Institute, Oslo, 1966.

53. Bazant, Z. P., and Najjar, L. J., Nonlinear water diffusion in nonsaturated concrete, *Materials and Structures*, Vol. 5, No. 25, pp. 3-20, 1972.

54. Schou, J., Måling af betons vandtæthed (in Danish; Measurement of the water vapour tightness of concrete), in Proportionering af holdbar beton, Dansk Betonforening Publikation nr. 19, København, pp. 23-37, 1983.

55. Thorsen, T., "Inverted-cup" method, in Kronvall, J. (Editor), Symposium and day of building physics in Lund, Sweden, August 24-27 1987, Proceedings, Swedish Council for Building Research, Publication D13, pp. 380-385, Stockholm, 1988.

56. Wadsö, L., Inbjudan til nordiskt forskarsympoium, Beräkning av fukttransport och mätning av növendiga materialdata (in Swedish; Invitation to Nordic symposium, Calculation of moisture transfer and measurement of necessary material data) Ystad, Sweden 28-29th January 1991, Department of Building Materials, Lund Institute of Technology, Lund, 1990.

57. Bories, S., Crausse, P., Ghalleb, K., Lemarchand, D., and Uemure, Y., Thermomigration en milieu poreux. Évolution de la zone séche en système fermé, *Comtes Rendus hebd. Acad. Sci. Paris*, Série B, Vol. 280, 13 janvier,, pp. 29-32, 1975.

58. Bombaud, J.-P., Gaudu, R., Tan, H. N., and Thirriot, C., Étude experimentale et simulation numérique d'un écoulement unidimensionnel faisant intervenir l'effet d'hystérésis en milieu poreux non saturés, *Comtes Rendus hebd. Acad. Sci. Paris*, Série B, Vol. 282, 5 janvier, pp. 1-4, 1976.

59. Bories, S., Crausse, P., and Tan, H. N., Thermomigration en milieu poreux. Étude des coefficients de diffusion capillaire, *Comtes Rendus hebd. Acad. Sci. Paris*, Série B, Vol. 285, 12 septembre,, pp. 77-80, 1977.

60. Crausse, P., Bacon, G., and Bories, S., Etude fondamentale des transferts couples chaleur-masse en milieu poreux, *Int. J. Heat Mass Transfer*, Vol. 24, No. 6, pp. 991-1004, 1981.

61. Crausse, P., Bacon, G., and Zarcone, C., Diffusion de l'humidite dans les materiaux. Determination des coefficients de diffusion capillaire, in *L'humidite dans le batiment*, conseil international de la lanque francaise, pp. 33-52, Paris, 1984.

62. Crausse, P. Bacon, G., and Langlais, C., Experimental and Theoretical Study of Simultaneous Heat and Moisture Transfer in a Fibrous Insulant, *Journal of Thermal Insulation*, Vol. 9, July, pp. 46-67, 1985.

63. Fagerlund, G., Determination of pore size distributions by suction porosimetry, *Materials and Structures*, Vol. 6, No. 33, pp. 191-201, 1973.

64. Lund-Hansen, Fugttransport i byggematerialer, (in Danish; Moisture transport in building materials), meddelelse no. 15, Thermal Insulation Laboratory, The Technical University of Denmark, Ph.D. thesis, Lyngby, 1967.

65. Hall, C., Water sorptivity of mortars and concretes: a review; *Magazine of Concrete Research*, Vol. 41, No. 147, pp. 51-61, June 1989.

66. Kohonen, R., A method to analyze the transient hygrothermal behaviour of building materials and components, Dissertation, Publications 21, Technical Research Centre of Finland, Espoo, 1984.

67. Press, W. H., Flannery, B. P., Teukolsky, S. A., and Vetterling, W. A., *Numerical Recipes,* Cambridge University Press, Cambridge, 1988.

68. Madsen, K., Robust Data-fitting, in Thorbøll, P. (Editor), Symposion on applied statistics, UNI•C, Copenhagen, pp. 363-383, 1988.

69. Nielsen, A. F., Fugtfordelinger i gasbeton under varme- og fugttransport, (in Danish with summary in English; Moisture distributions in cellular concrete during heat- and moisture transfer), meddelelse no. 29, Thermal Insulation Laboratory, The Technical University of Denmark, Ph.D. thesis, Lyngby, 1974.

70. Beyer, W. H. (Editor), *CRC Standard Mathematical Tables*, 26th Edition, CRC Press Inc., Boca Raton, 1981.

71. Hedenblad, G. Determination of moisture permeability in concrete under high moisture conditions, *Nordic Concrete Research*, The Nordic Concrete Federation, No. 7, pp. 105-120, Oslo, 1988.

72. van der Kooi, J. Moisture transport in cellular concrete roofs, Dr. Tech. thesis, Uitgeverij Waltman, Delft, 1971.

73. Gaffner, D., Determination of moisture flow coefficients for porous materials by using "the moment method, in Kronvall, J. (Editor), Symposium and day of building physics in Lund, Sweden, August 24-27 1987, Proceedings, Swedish Council for Building Research, Publication D13, pp. 423-427, Stockholm, 1988.

74. Cunningham, M. J., Keey, R. B., and Kerdemelidis, C., Isothermal moisture transfer coefficients in *Pinus radiata* above the fiber-saturation point, using the moment method, *Wood and Fiber Science*, Vol. 21, No. 2, pp. 112-122, 1989.

75. Shah, D. J., Ramsey, J. W., and Wang, M., An experimental determination of the heat and mass transfer coefficients in moist, unsaturated soils, *Int. J. Heat Mass Transfer*, Vol. 27, No. 7, pp. 1075-1085, 1984.

76. Artyukhin, E. A., Determination of thermal diffusivity from experimental data, *Inzhenerno-Fizicheskii Zhurnal*, Vol. 29, No. 1, July, pp. 87-90, 1975.

77. Yankelev, L. F., and Guseva, L. I., Simultaneous determination of temperature-dependent thermal conductivity and volumetric heat capacity, *Inzhenerno-Fizicheskii Zhurnal*, Vol. 28, No. 4, April, pp. 653-656, 1975.

78. Ganoulis, J., Sur le problème inverse de thermomigration en milieu poreux, 7^{e} Symposium International de l'A.I.R.H. (A. Int. de Recherch. Hydral.), Toulouse, 8 pp, Aout 1980.

79. Salonvaara, M., Determination of moisture and heat transport coefficients using optimisation technique, Proceedings from the ICHMT symposium "Heat and mass transfer in building material and structure", Dubrovnik, September 4-8, 1989, Hemisphere Publishing Company, 1990.

80. Hansen, M. H., Estimation of transfer coefficients in a model for coupled heat and mass transfer in capillary-porous materials, Proceedings from the ICHMT symposium "Heat and mass transfer in building material and structure", Dubrovnik, September 4-8, 1989, Hemisphere Publishing Company, 1990.

81. Madsen, K., Curve-fitting (in Danish), Institute for Numerical Analysis, The Technical University of Denmark, Hæfte 20, pp. 17, Lyngby, Juli 1971.

82. Hansen, M. H., Matematisk modelbeskrivelse af opvarmningsanlæg, (in Danish; Mathematical modelling of heating plants), M.Sc. thesis, Thermal Insulation Laboratory, The Technical University of Denmark, pp. 52, Lyngby, Forår 1987.

83. Nielsen, A. F., Statusrapport over måling af fugttransport i teglsten, (in Danish; Status report on measurement of moisture transfer in bricks), Thermal Insulation Laboratory, The Technical University of Denmark, pp. 18, Lyngby, September 1976.